

PLATINUM AND PLATINUM-RUTHENIUM BASED CATALYSTS  
ON VARIOUS CARBON SUPPORTS PREPARED BY DIFFERENT  
METHODS FOR PEM FUEL CELL APPLICATIONS

A THESIS SUBMITTED TO  
THE GRADUATE SCHOOL OF NATURAL AND APPLIED SCIENCES  
OF  
MIDDLE EAST TECHNICAL UNIVERSITY

BY

AYŞE BAYRAKÇEKEN

IN PARTIAL FULFILLMENT OF THE REQUIREMENTS  
FOR  
THE DEGREE OF DOCTOR OF PHILOSOPHY  
IN  
CHEMICAL ENGINEERING

MARCH 2008

Approval of the Thesis

**PLATINUM AND PLATINUM-RUTHENIUM BASED CATALYSTS  
ON VARIOUS CARBON SUPPORTS PREPARED BY DIFFERENT  
METHODS FOR PEM FUEL CELL APPLICATIONS**

submitted by **AYŞE BAYRAKÇEKEN** in partial fulfillment of the requirements for the degree of **Doctor of Philosophy in Chemical Engineering Department, Middle East Technical University** by,

Prof. Dr. Canan Özgen  
Dean, Graduate School of **Natural and Applied Sciences** \_\_\_\_\_

Prof. Dr. Gürkan Karakaş  
Head of Department, **Chemical Engineering** \_\_\_\_\_

Prof. Dr. İnci Eroğlu  
Supervisor, **Chemical Engineering Dept., METU** \_\_\_\_\_

Prof. Dr. Lemi Türker  
Co-supervisor, **Chemistry Dept., METU** \_\_\_\_\_

**Examining Committee Members:**

Prof. Dr. Zeynep İlsen Önsan  
Chemical Engineering Dept., Boğaziçi University \_\_\_\_\_

Prof. Dr. İnci Eroğlu  
Chemical Engineering Dept., METU \_\_\_\_\_

Prof. Dr. Deniz Üner  
Chemical Engineering Dept., METU \_\_\_\_\_

Assoc. Prof. Dr. Gülsün Gökağaç  
Chemistry Dept., METU \_\_\_\_\_

Prof. Dr. Can Erkey  
Chemical and Biological Engineering,  
Koç University \_\_\_\_\_

**Date:** **17.03.2008**

**I hereby declare that all information in this document has been obtained and presented in accordance with academic rules and ethical conduct. I also declare that, as required by these rules and conduct, I have fully cited and referenced all material and results that are not original to this work.**

Name, Last name: AYŞE BAYRAKÇEKEN

Signature:

## ABSTRACT

### PLATINUM AND PLATINUM-RUTHENIUM BASED CATALYSTS ON VARIOUS CARBON SUPPORTS PREPARED BY DIFFERENT METHODS FOR PEM FUEL CELL APPLICATIONS

Bayrakçeken, Ayşe

Ph.D., Department of Chemical Engineering

Supervisor : Prof. Dr. İnci Eroğlu

Co-supervisor : Prof. Dr. Lemi Türker

March 2008, 165 pages

Proton exchange membrane fuel cells are one of the most promising hydrogen energy conversion devices for portable, mobile and stationary applications. For wide spread usage to produce electricity platinum loading has to be decreased by using highly active electrocatalysts. Even 10 ppm carbon monoxide or higher than 30% carbon dioxide cause performance losses via deactivation which can be diminished by using binary catalysts. The aim of this thesis is to develop new platinum based electrocatalysts with high catalytic activity and to overcome the problems due to the deactivation. platinum and platinum-ruthenium based catalysts on different carbon supports have been prepared by supercritical carbon dioxide deposition and microwave irradiation methods.

By using supercritical carbon dioxide deposition platinum on Vulcan XC72R (VXR), multi wall carbon nanotube (MWCNT) and Black Pearl 2000 (BP2000) catalysts were prepared and characterized by XRD, TEM and cyclic voltammetry (CV). XRD results showed that in catalysts prepared by using

supercritical carbon dioxide deposition method, the particle sizes as low as 1-2 nm can be obtained. From the CV results the electrochemical surface areas obtained were Platinum/VXR>Platinum/MWCNT>PlatinumBP2000. By means of the oxygen reduction reaction (ORR), the number of electrons transferred per oxygen molecule was calculated as 3.5, 3.6 and 3.7 for Platinum/BP2000, Platinum/VXR and Platinum/MWCNT, respectively.

The microwave irradiation was used to prepare platinum on VX, Regal and BP2000 and platinum-ruthenium on VX. The effects of microwave duration, base concentration, carbon support used and surfactant/precursor ratios were investigated. The particle sizes of the catalysts were ranging between 2-6 nm. The prepared catalysts were characterized by XRD, XPS, and then PEMFC tests were performed. The performance was ordered as Platinum/VX>Platinum/Regal>Platinum/BP2000. The power losses arising from carbon dioxide in hydrogen feed were decreased by using prepared platinum-ruthenium based catalysts.

Keywords: PEMFC, Supercritical carbon dioxide, Microwave irradiation, Electrocatalyst.

## ÖZ

### PEM YAKIT PİLİ UYGULAMALARI İÇİN ÇEŞİTLİ KARBON DESTEKLER ÜZERİNE PLATİN VE PLATİN-RUTENYUM BAZLI KATALİZÖRLERİN FARKLI YÖNTEMLERLE HAZIRLANMASI

Bayrakçeken, Ayşe

Doktora, Kimya Mühendisliği Bölümü

Tez Yöneticisi : Prof. Dr. İnci Eroğlu

Ortak Tez Yöneticisi : Prof. Dr. Lemi Türker

Mart 2008, 165 sayfa

Proton değişim zarlı yakıt pilleri portatif, hareketli ve sabit uygulamalar için en uygun alternatif enerji dönüşüm araçları olarak görülmektedir. Yaygın kullanımları için platin yükü azaltılmalıdır bu da daha aktif katalizörlerin kullanılmasını gerektirmektedir. Ortamdaki 10 ppm karbon monoksit veya %30'dan fazla karbon dioksit güç kayıplarına sebep olmaktadır, bu etki ikili katalizörler kullanılarak azaltılabilir. Bu tezin amacı yeni platin bazlı yüksek katalitik aktiviteli ve deaktivasyona dayanıklı katalizörler geliştirmektir. Platin ve platin-rutenyum bazlı katalizörler farklı karbon destekler üzerine süperkritik karbon dioksit ve mikrodalga ısıtma yöntemleri kullanılarak hazırlanmıştır.

Süperkritik karbondioksit yöntemi kullanılarak platin Vulcan XC72R (VXR), çok duvarlı karbon nanotüp ve Black Pearl 2000 (BP2000) destekleri üzerine hazırlanmış ve XRD, TEM ve döner disk elektrot ile karakterize edilmiştir. Bu yöntemle 1-2 nm boyutunda parçacıklar elde edilmiştir. Elektrokimyasal yüzey alanları Platin/VXR>Platin/MWCNT>Platin/BP2000 olarak bulunmuştur.

Oksijen indirgenme reaksiyonundan oksijen molekülü başına transfer edilen electron sayıları Platin/BP2000, Platin/VXR ve Platin/MWCNT katalizörleri için sırasıyla 3.5, 3.6 ve 3.7 olarak bulunmuştur.

Mikrodalga ısıtma yöntemi kullanılarak platin VX, Regal ve BP2000 ve platin-rutenyum da VX karbon destekleri üzerine hazırlanmıştır. Mikrodalgada kalma süreleri, baz konsantrasyonu, farklı karbon destekler ve sürfaktan/metal sağlayıcı oranlarının etkileri araştırılmıştır. Elde edilen katalizörlerin partikül boyutlarının 2-6 nm arasında olduğu saptanmıştır. Hazırlanan katalizörler XRD, XPS ile karakterize edilmiş ve sonra yakıt pilinde denenmiştir. Katalizörlerin performanslarının Platin/VX>Platin/Regal>Platin/BP2000 olduğu gözlenmiştir. Karbondioksit içeren hidrojen kullanıldığında meydana gelen güç kayıpları hazırlanan platin-rutenyum bazlı katalizörlerle azaltılmıştır.

Anahtar kelimeler: PEM yakıt pilleri, Süperkritik karbondioksit, Mikrodalga ısıtma yöntemi, Elektrokatalizörler.

*To my family*



## ACKNOWLEDGMENTS

I would like to express my deepest sincere gratitude to my supervisor Prof. Dr. İnci Erođlu for her scientific and academic guidance, suggestions, comments, encouragement, motivation and help during the course of this research. Also, I am thankful to her because of her kindly attitude not only related with the thesis but also in every occasion throughout this study.

Also, I would like to express my greatest appreciation to my co-supervisor Prof. Dr. Lemi Türker for his interest in my research, his guidance, valuable suggestions, comments and leading me to think for different aspects.

I also would like to thank Prof. Dr. Can Erkey for giving me opportunity to conduct my research in the laboratory in University of Connecticut for a while and for his guidance, help, financial support, suggestions, comments and encouragement during my stay in USA.

I am also thankful to Dr. Alevtina Smirnova for her guidance during the rotating disk electorde experiments that I conducted in Connecticut Global Fuel Cell Center.

The members of the PhD examining committee, Prof. Dr. Deniz Üner and Assoc. Prof. Dr. Gülsün Gökağaç are gratefully acknowledged for their critical and constructive comments that help the progress of the thesis.

Prof. Dr. Nurcan Baç is gratefully acknowledged for providing a commercial fuel cell hardware and his scientific contribution throughout the study.

Atatürk University is gratefully acknowledged for providing opportunity to me to conduct my PhD in METU by OYP program. Especially the Dean of the Engineering Faculty, Prof. Dr. Şahin Gülaboğlu, is kindly acknowledged for his academic guidance, encouragement and his valuable suggestions.

My special thanks go to my lab mate Serdar Erkan for sharing his advanced chemical engineering, computational, electronics knowledge with me, helping me in all stages of my study and his friendship. I learned many things during the brain-storming we made in the laboratory.

I am also thankful to the members of METU Fuel Cell Technology and Biohydrogen Research Groups especially Dr. Ela Eroğlu, Dr. Başar Uyar, Erce Şengül, Dr. R. Gültekin Akay, Berker Fiçıcılar and Dr. Yülser Devrim and from other groups Aytaç Kocabaş, Arzu Kanca, Hilal Demir Kıvrak, Mukaddes Can and Okan Komesli and all my friends for their encouragement and friendship throughout my study.

I also would like to thank my friends Fatma Geneli, Ayten Koç, Dr. Didem Sutay, Mihriban Yılmaz Civan for always being with me, their encouragement, and friendship.

I would like to thank to the technicians in the machine shop of METU Chemical Engineering Department. METU Central Laboratory is gratefully acknowledged for the XPS measurements.

I am very grateful to my family for their endless love and support and not leaving me alone although they were far away from me.

The Scientific and Research Council of Turkey (TUBİTAK) is kindly acknowledged for the project 104M364. The author is thankful for financial

support by METU Research Fund Projects (BAP-08-11-DPT.2002K120510)  
and (BAP-08-11-DPT.2005K120600) project from DPT.

## TABLE OF CONTENTS

ABSTRACT .....	iv
ÖZ.....	vi
DEDICATION.....	vii
ACKNOWLEDGMENTS .....	ix
LIST OF TABLES .....	xvi
LIST OF FIGURES.....	xviii
LIST OF SYMBOLS .....	xxiii
CHAPTER	
1. INTRODUCTION .....	1
2. PROTON EXCHANGE MEMBRANE FUEL CELLS .....	7
2.1 Principles of Proton Exchange Membrane Fuel Cells .....	7
2.2 PEMFC components.....	9
2.3 Fuel cell irreversibilities .....	13
2.3.1 Activation losses .....	16
2.3.2 Fuel crossover and internal currents.....	17
2.3.3 Ohmic losses.....	17
2.3.4 Mass transport or concentration losses.....	18
2.4 Electrocatalysis in Proton Exchange Membrane Fuel Cells .....	18
2.4.1 Hydrogen oxidation reaction.....	19
2.4.2 Oxygen reduction reaction.....	20
2.5 Catalyst preparation techniques.....	23
2.6 Deactivation of the catalyst by CO and CO <sub>2</sub> .....	25
2.6.1 The significance of CO and CO <sub>2</sub> contents in H <sub>2</sub> .....	25
2.6.2 CO and CO <sub>2</sub> tolerance of the catalysts .....	27

2.6.3 Improvements in CO and CO <sub>2</sub> tolerance of the catalysts.....	30
3. METHODS FOR CATALYST PREPARATION IN SUPERCRITICAL	
CARBON DIOXIDE .....	35
3.1 Supercritical fluid properties .....	35
3.2 Supercritical carbon dioxide as a green solvent.....	37
3.3 Utilization of scCO <sub>2</sub> in catalyst preparation .....	39
4. MICROWAVE IRRADIATION.....	43
4.1 Microwave heating theory.....	43
4.2 Comparison of microwave heating and conventional heating.....	47
4.3 Catalyst preparation by microwave irradiation.....	49
5. EXPERIMENTAL STUDIES FOR SUPERCRITICAL CARBON	
DIOXIDE DEPOSITION.....	51
5.1 Catalyst preparation by scCO <sub>2</sub> deposition .....	52
5.1.1 Materials.....	52
5.1.2 Supercritical carbon dioxide deposition setup .....	52
5.1.3 Experimental procedure .....	53
5.2 Catalyst Characterization .....	55
5.2.1 X-ray diffraction .....	55
5.2.2 Transmission electron microscopy .....	55
5.2.3 Cyclic voltammetry .....	56
5.3 Scope of the experiments.....	57
6. EXPERIMENTAL STUDIES FOR MICROWAVE IRRADIATION .....	59
6.1 Catalyst preparation.....	60
6.1.1 Materials.....	60
6.1.2 Experimental procedure .....	60
6.2 Catalyst characterization .....	62
6.2.1 X-ray diffraction .....	62
6.2.2 X-ray photoelectron spectroscopy .....	62
6.3 PEM fuel cell tests.....	62
6.3.1 Catalyst ink preparation.....	63
6.3.2 Membrane Electrode Assembly Preparation.....	63
6.3.3 Single PEM Fuel Cell Construction .....	65

6.3.4 Fuel Cell Test Station .....	65
6.4 Scope of the experiments.....	67
7. RESULTS AND DISCUSSION OF THE CATALYSTS PREPARED BY SUPERCRITICAL CARBON DIOXIDE DEPOSITION .....	69
7.1 Adsorption kinetics of Pt and Ru organometallic precursors on different carbon supports .....	69
7.2 XRD and TEM results .....	78
7.3 CV results .....	82
8. RESULTS AND DISCUSSION OF THE CATALYSTS PREPARED BY MICROWAVE IRRADIATION .....	94
8.1 Characterization of the catalysts .....	95
8.1.1 Characterization by XRD .....	95
8.1.2 Characterization by XPS .....	101
8.2 PEMFC tests .....	109
8.2.1 Effect of base concentration on PEMFC performance .....	109
8.2.2 Effect of microwave duration on PEMFC performance .....	111
8.2.3 Effect of carbon support on PEMFC performance .....	113
8.2.4 Effect of surfactant/Pt precursor ratio on PEMFC performance .....	115
8.2.5 Effect of catalyst properties on PEMFC performance.....	117
8.3 PEMFC operated with CO <sub>2</sub> containing H <sub>2</sub> .....	118
8.3.1 Effect of N <sub>2</sub> on PEMFC performance .....	119
8.3.2 Effect of CO <sub>2</sub> on PEMFC performance .....	120
8.3.3 Effect of 30% CO <sub>2</sub> on PEMFC performance when commercial PtRu/C anode (ETEK) is used.....	122
8.3.4 Effect of 30% CO <sub>2</sub> on PEMFC performance when PtRu/VX anode is used ..	125
8.4 Comparison of the PEMFC performances of the prepared and commercial Pt and PtRu based catalysts .....	127
9. CONCLUSION AND RECOMMENDATION.....	131
REFERENCES .....	136
APPENDICES	
A. Sample calculations.....	149
A.1 Calculation of particle size.....	149

<i>A.2 Calculation of metal total surface area (SA)</i> .....	150
<i>A.3 Calculation of electrochemical surface area (ESA)</i> .....	151
<i>A.4 Calculation of Pt utilization</i> .....	152
<i>A.5 Calculation of Tafel slope</i> .....	153
B. MEA preparation protocol.....	154
C. Cyclic voltammetry .....	156
D. Fuel cell operating protocol.....	160
E. Reproducibility .....	161
CURRICULUM VITAE.....	162

## LIST OF TABLES

### TABLES

Table 2.1 H <sub>2</sub> and CO adsorption enthalpies of some metals .....	34
Table 3.1 Physical properties of gas, liquid, and supercritical fluid of typical organic fluid (order of magnitude).....	36
Table 3.2 Critical constants of typical molecules used as SCF solvents.....	37
Table 4.1 Relaxation times (20°C) and dielectric properties of some organic solvents .....	46
Table 5.1 Catalyst preparation conditions and tests performed to the catalysts prepared by scCO <sub>2</sub> .....	58
Table 6.1 Catalysts prepared by microwave irradiation.....	67
Table 7.1 Surface area properties of carbon supports used in the experiments and previous studies .....	70
Table 7.2 Langmuir equilibrium constants for CODPtMe <sub>2</sub> on different carbon supports obtained in scCO <sub>2</sub> at 343 K and 24.2 MPa .....	73
Table 7.3 Langmuir equilibrium constants for Ru(COD)(Tmhd) <sub>2</sub> on different carbon supports in scCO <sub>2</sub> at 343 K and 24.2 MPa.....	74
Table 7.4 Area covered by Pt or Ru organometallic precursors on different carbon supports .....	77
Table 7.5 Langmuir equilibrium constants for Ru(COD)(Tmhd) <sub>2</sub> , scCO <sub>2</sub> and Pt/BP2000, Pt/MWCNT .....	77
Table 7.6 Electrochemical and total surface areas of the synthesized and commercial catalysts .....	84
Table 7.7 Electrochemical and total surface areas of the prepared high Pt loading catalysts.....	88
Table 8.1 Pt/VX (20%) catalyst prepared for different microwave durations..	96
Table 8.2 Particle sizes calculated for the commercial ETEK and the prepared catalysts by using XRD patterns .....	101



Table 8.3 Results of the fits of the XPS spectra for carbon oxidation states (%) .....	106
Table 8.5 Percent power losses of the commercial and prepared PtRu/C catalysts with 30% CO <sub>2</sub> .....	112
Table C.1 Potentials for Ag/AgCl reference electrode.....	159

## LIST OF FIGURES

### FIGURES

Figure 2.1 Operational principle of PEMFCs.....	8
Figure 2.2 PEMFC components.....	9
Figure 2.3 Typical fuel cell polarization curve .....	15
Figure 2.4 Schematic representation for the contact between Pt/C and Nafion in PEMFCs.....	19
Figure 2.5 Cyclic voltammetric current potential curve for a platinum electrode in contact with a 0.5 M H <sub>2</sub> SO <sub>4</sub> solution (mercury sulfate reference electrode was used, MSE) .....	22
Figure 2.6 Global hydrogen production in 1999.....	25
Figure 3.1 Schematic pressure–temperature phase diagram for a pure component showing the supercritical fluid (SCF) region.....	35
Figure 3.2 Schematic phase diagram for pure CO <sub>2</sub> .....	38
Figure 3.3 The scheme of using SCF as processing solvent to synthesize supported nanoparticles via deposition or impregnation.....	41
Figure 4.1 Differences in the temperature-time profiles for conventional and microwave dielectric heating .....	47
Figure 5.1 Experimental setup for supercritical deposition.....	53
Figure 6.1 Schematic representations of (a) Pt and PtRu based catalyst preparation without surfactant (b) Pt and PtRu based catalyst preparation with surfactant .....	61
Figure 6.2 Flow chart for MEA preparation techniques .....	64
Figure 6.3 Flow chart for the fuel cell test station .....	66
Figure 7.1 Equilibrium curve for Pt/VXR.....	72
Figure 7.2 Adsorption isotherms of CODPtMe <sub>2</sub> , scCO <sub>2</sub> on different carbon supports in scCO <sub>2</sub> (lines represents Langmuir (Eqn 7.1) fits for the corresponding catalysts) .....	72

Figure 7.3 Adsorption isotherms for Ru(COD)(Tmhd) <sub>2</sub> , scCO <sub>2</sub> on different carbon supports at 343 K and 24.2 MPa (lines represents Langmuir (Eqn 7.1) fits for the corresponding catalysts) .....	74
Figure 7.4 Uptake of Pt or Ru precursors on carbon supports with different mesoporous and macroporous surface area .....	75
Figure 7.5 Uptake of Pt or Ru precursors on carbon supports with different total surface area .....	75
Figure 7.6 Adsorption isotherm for Ru precursor at 343 K and 24.2 MPa on Pt/C catalysts (lines represents Langmuir (Eqn 7.1) fits for the corresponding catalysts) .....	77
Figure 7.7 XRD patterns for the prepared and commercial catalysts a) whole scan for all catalysts b) narrow scan for Pt/MWCNT, Pt/C (Tanaka), Pt/C (EOTEK) c) narrow scan for Pt/VXR and Pt/BP2000.....	79
Figure 7.8 Bright field and HRTEM images for catalysts (a) and (b) Pt/MWCNT, (c) and (d) Pt/VXR, (e) and (f) Pt/BP2000 .....	80
Figure 7.9 Bright field and HRTEM images for catalysts (a)-(d) Pt/C-EOTEK	81
Figure 7.10 CV results for Pt/BP2000 catalysts with different Pt loadings .....	82
Figure 7.11 Cyclic voltammogram for the prepared catalysts in 0.1 M HClO <sub>4</sub> in H <sub>2</sub> atmosphere at a scan rate of 50 mV/s .....	84
Figure 7.12 XRD pattern for high Pt loading Pt/VXR catalysts.....	86
Figure 7.13 TEM images for 15% Pt/VXR .....	87
Figure 7.14 CV for high Pt loading Pt/VXR catalysts .....	88
Figure 7.15 Hydrodynamic voltammograms of positive scans of Pt/VXR for O <sub>2</sub> reduction in O <sub>2</sub> saturated 0.1 M HClO <sub>4</sub> (a) Koutecky-Levich plot at 0.2 V ....	90
Figure 7.16 Hydrodynamic voltammograms of positive scans of Pt/MWCNT for O <sub>2</sub> reduction in O <sub>2</sub> saturated 0.1 M HClO <sub>4</sub> (a) Koutecky-Levich plot at 0.2 V .....	91
Figure 7.17 Hydrodynamic voltammograms of positive scans of for Pt/BP2000 O <sub>2</sub> reduction in O <sub>2</sub> saturated 0.1 M HClO <sub>4</sub> (a) Koutecky-Levich plot at 0.2 V.....	91

Figure 7.18 Tafel plots of $i_k$ for $O_2$ reduction in positive scans for synthesized catalysts in $O_2$ saturated 0.1 M $HClO_4$ for intermediate segment (0.85-0.75 V) .....	93
Figure 8.1 XRD pattern for the Pt/VX (20%) catalyst at base concentration of 0.14 g/l with different microwave durations.....	96
Figure 8.2 XRD pattern for the Pt/VX (20%) catalyst with different base concentrations (BCs), 50 s microwave duration.....	98
Figure 8.3 XRD pattern for the catalyst prepared with different carbon supports, 50 s microwave duration, Base concentration is 0.54 g/l.....	99
Figure 8.4 XRD pattern for the catalysts prepared with different SB12/H <sub>2</sub> PtCl <sub>6</sub> (S/Pt) molar ratios, 50 s microwave duration, BC=0.54 g/l .....	99
Figure 8.5 XRD pattern for PtRu/VX (30%) catalyst prepared with or without SB12 surfactant.....	100
Figure 8.6 XRD pattern for binary commercial catalysts of PtRu/C 20 and 40% .....	100
Figure 8.7 XPS core level spectra for Pt 4f for Pt/C (EOTEK) catalyst.....	102
Figure 8.8 XPS core level spectra for Pt 4f for Pt/VX catalyst .....	103
Figure 8.9 XPS core level spectra for Pt 4f for Pt/Regal catalyst.....	104
Figure 8.10 XPS core level spectra for Pt 4f for Pt/BP2000 catalyst .....	105
Figure 8.11 Survey XPS spectra for commercial and prepared catalysts .....	105
Figure 8.12 XPS core level spectra for C1s for Pt/C (EOTEK) catalyst .....	106
Figure 8.13 XPS core level spectra for C1s for Pt/VX catalyst.....	107
Figure 8.14 XPS core level spectra for C1s for Pt/Regal catalyst .....	107
Figure 8.15 XPS core level spectra for C1s for Pt/BP2000 catalyst.....	108
Figure 8.16 XPS for (a) whole and (b) core level spectra for Ru3p for PtRu based catalysts.....	109
Figure 8.17 Effect of base concentration (BC) on PEMFC performance (Pt/VX, 20%, 50 s microwave duration) .....	110
Figure 8.18 Effect of microwave duration on PEMFC performance (Pt/VX, 20%, Base concentration=0.14 g/l) .....	112

Figure 8.19 Effect of different carbon supports on PEMFC performance (50 s microwave duration, base concentration=0.54 g/l).....	113
Figure 8.20 Effect of surfactant/Pt precursor (S/Pt) ratio on PEMFC performance (Base concentration=0.54 g/l, 50 s microwave duration) .....	116
Figure 8.21 Current density versus the particle size for Pt/VX (20% ) with different conditions .....	117
Figure 8.22 Current density versus the particle size for Pt/VX, Pt/Regal and Pt/BP2000 catalysts.....	118
Figure 8.23 Effect of N <sub>2</sub> percentage in the H <sub>2</sub> gas fed to the fuel cell on PEMFC performance with commercial MEA (Electrochem) .....	119
Figure 8.24 Effect of CO <sub>2</sub> percentage in the H <sub>2</sub> gas fed to the fuel cell on PEMFC performance with commercial MEA (Electrochem) .....	121
Figure 8.25 Effect of CO <sub>2</sub> cut off on PEMFC performance.....	122
Figure 8.26 Effect of CO <sub>2</sub> on PEMFC performance (home made MEA with anode 20% Pt/C (E TEK), cathode 20% Pt/C (E TEK)).....	123
Figure 8.27 Effect of CO <sub>2</sub> on PEMFC performance (home made MEA with anode PtRu/C (E TEK, 40%), cathode 20% Pt/C (E TEK)).....	124
Figure 8.28 Effect of CO <sub>2</sub> on PEMFC performance (home made MEA with anode PtRu/C (E TEK, 20%), cathode 20% Pt/C (E TEK)).....	124
Figure 8.29 Effect of CO <sub>2</sub> on PEMFC performance (home made MEA with anode PtRu/VX (microwave, 30% PtRu), cathode 20% Pt/C (E TEK)).....	126
Figure 8.30 Effect of CO <sub>2</sub> on PEMFC performance (home made MEA with anode PtRu/VX (microwave with SB12, 30% PtRu), cathode 20% Pt/C (E TEK) .....	126
Figure 8.31 Comparison of PEMFC performances for commercial ETEK catalysts and the microwave irradiated catalysts with similar particle size and best performance .....	128
Figure 8.32 Comparison of commercial and microwave PtRu based catalysts .....	129
Figure 8.32 Current density versus the particle size for PtRu based catalysts	130

Figure A.1 XRD pattern .....	149
Figure A.2 Sample ESA graph for Pt/MWCNT .....	152
Figure A.3 Tafel slope for Pt/Regal .....	153
Figure C.1 Three electrode cell configuration .....	158
Figure E.1 Reproducibility of the catalyst of Pt/VX (20%) .....	161

## LIST OF SYMBOLS

A	Area under the curve for H <sub>2</sub> reduction part excluding double layer capacitance
B	Levich constant
BET	Brunauer-Emmett-Teller
c <sub>0</sub>	Oxygen bulk concentration, mol/cm <sup>3</sup>
CV	Cyclic voltammetry
D	O <sub>2</sub> diffusion coefficient, cm <sup>2</sup> /s
E	Voltage of the fuel cell
ESA	Electrochemical surface area
F	Faraday constant
fcc	Face cubic centered
GC	Glassy carbon
GDL	Gas diffusion layer
ID	Inner diameter
i <sub>k</sub>	Kinetic current density, mA/cm <sup>2</sup>
K	Charge corresponds to a fully covered monolayer for a polycrystalline Pt surface, 0.21 mC/cm <sup>2</sup>
L	Pt loading on glassy carbon electrode
MEA	Membrane electrode assembly
N	Avogadro's number
n	Number of electrons per O <sub>2</sub> molecule
OD	Outer diameter
PEMFC	Proton exchange membrane fuel cell
RDE	Rotating disk electrode
S	Scan rate, mV/s
SA	Surface area

scCO <sub>2</sub>	Supercritical carbon dioxide
TEM	Transmission electron microscopy
VX	Vulcan XC72
VXR	Vulcan XC72R
XPS	X-ray photoelectron spectroscopy
XRD	X-ray Diffraction
$\nu$	Viscosity of the electrolyte, cm <sup>2</sup> /s
$\Delta G_{\text{rxn}}^{\circ}$	Gibbs' Free Energy Change on Reaction at STP, kJ/mol
$\Delta G^{\circ}$	Gibbs' Free Energy of Formation, J/mol
$\Delta G_{0\text{rxn}}$	Gibbs' Free Energy Change on Reaction at STP, kJ/mol
$\Delta G_{\text{rxn}}$	Gibbs' Free Energy Change on Reaction, kJ/mol
$\Delta H^{\circ}$	Enthalpy of Formation, kJ/mol
$\Delta H_{0\text{rxn}}$	Enthalpy Change on Reaction at STP, kJ/mol
$\Delta H_{\text{rxn}}$	Enthalpy Change on Reaction, kJ/mol
$\Delta H_{\text{c}}^{\circ}$	Standard Heat of Combustion, kJ/mol



## **CHAPTER 1**

### **INTRODUCTION**

Rapid technological developments and increase in the world population accelerated the consumption of the fossil-fuel-based energy sources which resulted in the increase of the harmful gases released to the environment. From this aspect, global warming is becoming a big threat for human beings that threatens the future of the world. Therefore, a lot of efforts have been recently devoted to find renewable, clean and sustainable energy sources to reduce the dependency on fossil-fuel-based energy sources. The problem with fossil fuels is not only their harmful effects but they may also run out because of excessive utilization. Also the main reason for the commencement of wars in this century is the inequality in distribution of energy sources. So, energy technologists have been searching for new renewable, sustainable and clean energy sources, because of not only for clean energy sources but also for the peace of the world. If new renewable energy sources are found, the dependence of the energy source-deprived countries to other foreign countries will be decreased and they will be self reliant.

One of the most promising alternative energy carriers is hydrogen if some drawbacks such as storage, infrastructure and high production cost are solved. Hydrogen is not available in nature but it can be produced from the primary energy sources including natural gas, coal, biomass, nuclear, wind, solar, wastes etc. Producing electricity by using fuel cells may lead the way through the new energy era.

Fuel cells are electrochemical devices that directly convert the chemical energy of the fuel into electrical energy. Fuel cells, invented by Sir William Grove in 1839, have been still under investigation by the scientists in different fields of the science including chemical engineers, mechanical engineers, chemists, electrical and material engineers, physicists and so on. All these multidisciplinary studies are made to eliminate the lacking parts of the fuel cells for commercialization. The main problems that the researchers are trying to solve for the commercialization of the fuel cells are high cost of the fuel cell components, durability, life time and the poisoning effects of the gases coming from the reformat or biologically produced hydrogen. The cost of the fuel cell components can be reduced by using alternative low cost materials and developing suitable techniques for manufacturing.

Especially for portable and mobile applications proton exchange membrane fuel cell (PEMFC) seems to be the most reliable ones because of its low operating temperature, high power density, and clean emissions. The heart of a PEMFC is the membrane electrode assembly (MEA) which consists of an anode and a cathode electrode and membrane. The half cell reactions and proton conduction occurs in this part. When hydrogen is fed to the anode side of the fuel cell, hydrogen splits its proton and electron by the help of the platinum metal in the electrode. The membrane only allows the protons to pass through it and the electrons are directed to an external circuit. Then these electrons are sent to the cathode electrode and are reacted with the oxygen gas fed to the cathode side and with the protons that pass through the membrane and finally water is formed by this reaction.

During the master thesis (Bayrakçeken, 2004) a home made fuel cell test station was developed for PEMFC tests. Also, the operating conditions of the fuel cell such as anode and cathode humidification temperatures were optimized. A membrane electrode assembly preparation technique was developed by optimizing the preparation conditions. Furthermore the effects of

construction materials such as gas diffusion layer, membranes with different thicknesses and sealing material were also investigated. The evaluation of the performances was made by comparing the voltage-current data obtained from these fuel cells by using the home made test station.

Platinum (Pt) supported on carbon support catalysts are used as the anode and the cathode electrodes. Although a lot of studies were made to replace the Pt with non-precious metals, no catalyst has been found that would give a better performance than that of Pt. Pt is unique for both oxidation and reduction reactions. But, it is important to emphasize that the Pt reserves are limited, so the Pt loadings have to be decreased and the activity of the Pt metal on the support has to be increased.

The PEMFC is very sensitive to carbon monoxide. Even at concentrations as low as 10 ppm in the hydrogen feed, the performance of the PEMFC decreases drastically because of the poisoning effect of the CO on Pt catalyst. High CO<sub>2</sub> concentrations (30-50%) have an indirect CO effect because of either electroreduction of CO<sub>2</sub> or reverse water gas shift reaction. To compensate this corrupting effect another metal, usually Ru, Mo, or W can be added near Pt particles and these new binary or ternary catalysts may be CO and CO<sub>2</sub> tolerant.

There are several ways to deposit Pt onto the carbon support such as impregnation, microemulsion, sequential and co-precipitation, supercritical carbon dioxide (scCO<sub>2</sub>) deposition, microwave irradiation, ion exchange, sol-gel, ultrasonication. In this thesis by using scCO<sub>2</sub> deposition and microwave irradiation methods, it is aimed to increase the Pt utilization that is deposited onto the carbon support.

scCO<sub>2</sub> deposition method is gaining an increasing attention because scCO<sub>2</sub> is a green solvent with non-toxic, non-flammable, chemically inert and inexpensive

properties. It can be removed from the system only by depressurization and there no residue is left on the catalyst surface. Besides its environmental benefits supercritical carbon dioxide has also desirable physical and chemical properties such as relatively chemical inertness, readily accessible critical point ( $T_{cr}=31.1^{\circ}\text{C}$ ,  $P_{cr}=7.4\text{ MPa}$ ), excellent wetting characteristics, low viscosity, highly tunable solvent behavior, facilitating easy separation. Especially highly tunable solvent properties and leaving no residue characteristics are very important in catalyst preparation.

Another catalyst preparation method used in the experiments was microwave irradiation. In microwave processes heat is generated internally within the material instead of originating from external sources. Briefly, the solvent or the reagent has to be capable of absorbing the microwave energy and convert it into heat. In conventional heating the material is heated only the outside surface, but in case of microwave heating the microwaves can penetrate materials and heat on the inside and also the outside. Since microwave heating depends on the absorption ability of the materials, it will provide a selective heating for different materials. Also, the heating time is shortened by using this method.

In the present study, Pt and PtRu based catalysts are prepared by using  $\text{scCO}_2$  deposition and microwave irradiation methods. It is aimed to increase the performance of the fuel cell for the main reactions by changing the catalyst properties including particle size, metal distribution and also to increase the  $\text{CO}_2$  tolerance of the fuel cell.

In case of Pt based catalysts, Pt was decorated on different carbon supports which have different surface areas. The Pt based catalysts prepared by  $\text{scCO}_2$  deposition method were electrochemically characterized with CV by means of hydrogen oxidation and reduction and also oxygen reduction reaction mechanisms were investigated. The Pt based catalysts, prepared by the

microwave irradiation method, were tested in PEMFC test system as cathode electrode to see the oxygen reduction reaction performance. Various PtRu based catalysts, used as anode electrode, were prepared to increase the carbon dioxide tolerance of the PEMFC.

In Chapter 2, general information about PEMFCs including the principle, components, irreversibilities, electrocatalysis and the poisoning effects of either carbon monoxide or carbon dioxide gases on PEMFC performance are summarized.

In Chapter 3, a brief summary is given related with the properties of  $scCO_2$  and its applications. The literature summary of the catalyst preparation with  $scCO_2$  is also included in this chapter.

In Chapter 4, comparison of the microwave irradiation to conventional heating systems is given. The literature summary of the catalyst preparation with microwave irradiation is also included in this chapter.

In Chapter 5, experimental procedures of Pt based catalyst preparation with  $scCO_2$  deposition, physicochemical and electrochemical characterization of the catalysts which includes XRD, TEM and cyclic voltammetry (CV) are given.

In Chapter 6, experimental procedures of Pt and PtRu based catalyst preparation with microwave irradiation, physicochemical XRD, XPS and PEMFC tests of the catalysts are given.

In Chapter 7, the results for the catalysts prepared by  $scCO_2$  deposition are given which includes the XRD, TEM and CV results.

In Chapter 8, the results for the catalysts prepared by microwave irradiation are given which includes the XRD, XPS and PEMFC test results.

In Chapter 9, conclusion and recommendation part is summarized.

## CHAPTER 2

### PROTON EXCHANGE MEMBRANE FUEL CELLS

#### 2.1 Principles of Proton Exchange Membrane Fuel Cells

The proton exchange membrane fuel cell (PEMFC), also called the solid polymer fuel cell (SPFC), was first developed by General Electric company in the United States in 1960s for the first manned space vehicles used by NASA (Larminie and Dicks, 2003).

Proton exchange membrane fuel cells are considered as promising alternatives to internal combustion engines for transportation because of their high efficiency, high power density, low emissions, low operating temperature, and low noise (Lee et al, 2004) PEMFCs have further advantages such as elimination of electrolyte leakage, lower corrosion, simplification of stack design and increased ruggedness. These promising attributes have stimulated applications in areas such as military, aerospace and transportation (Lee et al, 1998).

A single PEM fuel cell consists of a solid polymer electrolyte sandwiched between two thin electrodes, a porous anode and cathode. Hydrogen, is fed to the anode, in which oxidation reaction occurs, where Pt catalyst separates hydrogen's negatively charged electrons from positively charged ions (protons). At the cathode, oxygen/air combines with electrons and produce water. The protons pass through anode to cathode with the help of a proton conducting membrane (which allows only H<sup>+</sup> ions, not electrons), and

electrons pass through the cathode via an external circuit and electricity produced. Figure 2.1 ([www.udomi.de/images/fcm.gif](http://www.udomi.de/images/fcm.gif) last accessed at 13.01.2008) illustrates the operational principle of a PEM fuel cell.

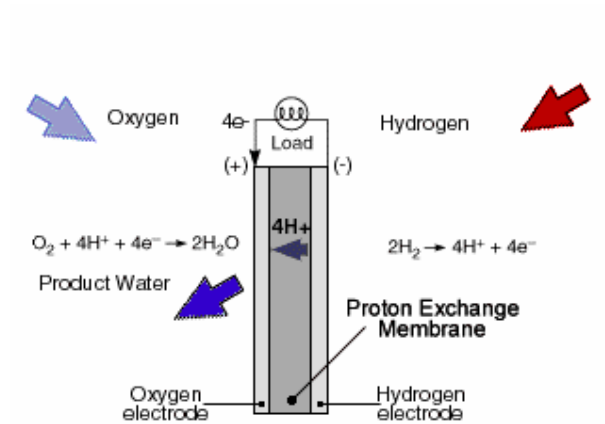
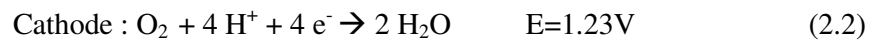


Figure 2.1 Operational principle of PEMFCs

In a PEM fuel cell; anode-cathode half cell and overall electrochemical reactions are given in Eqns 1, 2 and 3 as follows:





The heat of reaction and the Gibbs Free Energy change is as follows:

$$\Delta H_f^\circ (\text{H}_2\text{O}_{(l)}) = -285.8 \text{ kJ/mol and } \Delta H_f^\circ (\text{H}_2\text{O}_{(g)}) = -241.8 \text{ kJ/mol}$$

$$\Delta G_f^\circ (\text{H}_2\text{O}_{(l)}) = -237.1 \text{ kJ/mol and } \Delta G_f^\circ (\text{H}_2\text{O}_{(g)}) = -228.6 \text{ kJ/mol}$$

These values indicate that the overall reaction is an exothermic and spontaneous reaction (Larminie and Dicks, 2003).

## 2.2 PEMFC components

A PEMFC consists of the parts given in Figure 2.2 ([http://www.kemi.dtu.dk/forskning/rg\\_materials/projekter/fuelcells.aspx](http://www.kemi.dtu.dk/forskning/rg_materials/projekter/fuelcells.aspx) last accessed at 13.01.2008) in which each component is very critical for the fuel cell to be operated with high performance.

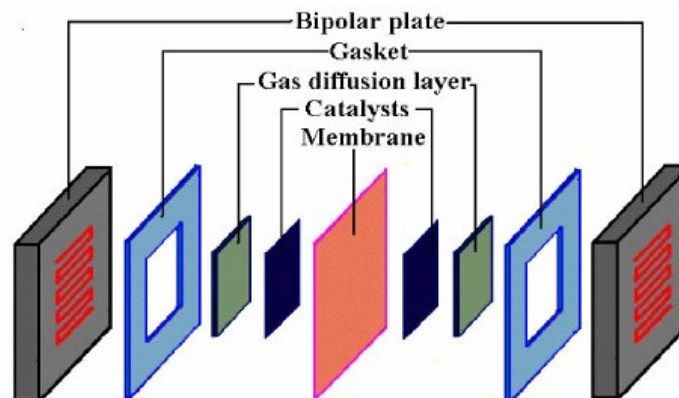


Figure 2.2 PEMFC components

*Electrolyte*, the heart of the PEMFC is in the form of a proton conducting membrane, and its thickness varies typically between 50 and 175 microns. Its functions are: conductance of protons, separation of hydrogen and air, and electronic isolation. The most frequently used PEM is made of Nafion produced by DuPont, which consists of Teflon-like chains with a fluorocarbon backbone and sulfonic acid groups,  $\text{SO}_3^-$ , permanently attached to the side chains. When the membrane is hydrated by absorbing water, protons initially attached to the  $\text{SO}_3^-$  groups combine with water molecules to form hydronium ions. Hydronium ions are quite mobile and hop from one  $\text{SO}_3^-$  site to another within the membrane making the hydrated solid electrolytes, like Nafion, as excellent conductors of the hydrogen ions (Grujicic et al, 2004). The proton conduction mechanisms in hydrated PEMs may be understood by considering dissociation of the proton from the acidic site, subsequent transfer of the proton to the aqueous medium, screening of the hydrated proton from the conjugate base by water (e.g., the sulfonate anion), and finally diffusion of the proton in the confined water within the polymer matrix (Paddison, 2003). Nafion proton conduction is so very susceptible to membrane hydration. Sridhar et al. (2001) observed that the fuel cell membrane always picks up water from the hydrogen stream even under no load conditions, which further strengthens the need for improved humidification. To provide 100% humidity for fuel cell operational conditions, (including cell temperature, humidification temperatures, flow rates and pressures) have to be optimized (Williams et al., 2004; Passos and Ticianelli, 2002; Wang et al. 2003). Nafion is suitable for low temperatures ( $\sim 80^\circ\text{C}$ ), so nowadays a lot of study is devoted to increase the operating temperature of the fuel cell by replacing Nafion with high temperature resistant membrane such as polybenzimidazole (PBI) (Korsgaard et al., 2006; Yurdakul, 2007; Şengül, 2007) or sulfonated polyethersulphone (PES) or polyetherether ketone (PEEK) membranes (Akay, 2008; Erdener, 2007). By increasing the temperature not only the kinetics of the electrodes will be improved but also the carbon monoxide poisoning effect will be mitigated.

A PEMFC contains two *electrodes*, an anode and a cathode. At the anode, hydrogen is oxidized to protons, while at the cathode oxygen (from air) is reduced to water. The state-of-the-art electrodes contain carbon supported platinum catalysts. The platinum loading is generally in the order of 0.2-0.4 mg platinum per cm<sup>2</sup> electrode area. Current state of the art of catalyst layers for gas diffusion electrodes utilizes carbon supported Pt as the catalyst for oxygen reduction at the cathode. The primary role of the carbon support is to provide electrical conduction between the widely dispersed Pt catalyst particles and the porous current collector (carbon cloth or paper) (Qi et al, 1998).

In order to facilitate transport of protons into the catalyst layer, a proton conducting polymer (e.g.Nafion) is mixed with the catalyst. Nafion impregnation is extending the three-dimensional reaction zone. A Nafion content of about 33% of the total electrode weight appeared to be optimal to minimize both ohmic and transport losses (Passalacqua et al, 2001).

The use of solid polymer as an electrolyte engenders the problem of non-active catalysts in the electrode. Therefore, as an ionic conductor Nafion solution is impregnated on the electrode surface to extend the catalytic reaction area by forming passages of ionic transfer (Lee et al, 2004). Methods for fabricating electrodes for PEMFCs include the silk printing, brushing and rolling techniques (Choi et al, 1998; Yazaydin, 2003).

The *electrode backing (gas diffusion layer)* serves as current collector, gas distributor and improves water management in the cell. Both carbon cloths and carbon papers are used, with a typical thickness of 300 microns. The carbon cloths generally contain one or two gas diffusion layers, having a thin (20-30 microns) microporous hydrophobic layer.

The gas diffusion layer in a PEMFC consists of a thin layer of carbon black mixed with polytetrafluoroethylene (PTFE) that is coated onto a sheet of

macro-porous carbon backing (Lee et al, 2004). These layers are porous enough to allow the distribution of the gases to unexposed areas of the flow channel whereby this distribution permits the complete utilization of the electrode area. The electrical conductivity of these layers may affect the transport of electrons to the current collector from the electrode. The hydrophobicity of these layers may compete with the hydrophilicity of water available for hydration at the membrane. The performance variations may also be due to changes in the porosity, the electrical contact resistance, and the excluded water at the membrane ( Lee et al, 1999; Bayrakçeken, 2004).

It has been shown that a fuel cell embedded with a GDL with a larger averaged porosity consumes a greater amount of oxygen, so that a higher current density is generated and a better fuel cell performance is obtained. This explains partly why fuel cell performance deteriorates significantly as the cathode is flooded with water (i.e. to give a lower effective porosity in the GDL) (Chu et al, 2003).

Also gas diffusion layer thickness is a parameter that affects the performance. A thin layer improves the gas supply and facilitates the removal of the produced water, but it has high electronic resistance and does not give a non-permeable support for coating with the catalyst layer during electrode fabrication. Therefore, permeation of the catalyst layer into the diffusion layer makes poor ionic contact with the Nafion membrane. On the other hand, a thick layer hampers the accessibility of gas due to the lengthened path in the layer and has poor gas diffusivity. Hence, an intermediate thickness enhances the electrode performance best (Lee et al, 2004; Şengül et al, 2007).

The *gaskets* not only prevent the leakage of gases from the cell to the exterior but also prevent the direct contact between the acidic electrolyte and the bipolar plate. The materials used as gasket can be any plastic material which is resistant to the conditions within a fuel cell. Teflon is often used.

The *bipolar plates* serve as gas separator between adjacent cells, contain flow channels that distribute the reactant gases and conduct the current to the adjacent cells. The materials used for bipolar plates need to have low electrical resistivity (bulk and surface), be corrosion resistant, and light weight. Graphite plates, composite materials and metals such as stainless steel, copper etc. can be used as bipolar plates.

The main tasks of a flow field plate are current conduction, heat conduction, control of gas flow and product water removal (Hoogers, 2003).

### 2.3 Fuel cell irreversibilities

In fuel cells, ‘Gibbs free energy’ is important because Gibbs free energy of formation,  $\Delta G_f$ , gives us the energy released and given as Eqn (4).

$$\sum G_f = \sum G_{f(\text{products})} - \sum G_{f(\text{reactants})} \quad (2.4)$$

For the hydrogen fuel cell, two electrons pass round the external circuit for each water molecule produced and each molecule of hydrogen consumed. So, for one mole of hydrogen used,  $2N$  electrons pass round the external circuit—where  $N$  is Avogadro’s number. If  $-e$  is the charge on one electron, then the charge that flows is,

$$-2NE = -2F \quad (2.5)$$

where  $F$  being the Faraday constant, or the charge on one mole electrons. If  $E$  is the voltage of the fuel cell, then the electrical work done for ( $W_e$ , Joules) moving this charge round the circuit is equal to charge times voltage:

$$W_e = -2FE \quad (2.6)$$

If the system is reversible (or has no losses), then this electrical work done will be equal to the Gibbs free energy released. So,

$$\Delta G_f = -2FE \quad (2.7)$$

$$E = \frac{-\Delta G_f}{2F} \quad (2.8)$$

This fundamental equation (Eqn 2.8) gives the electromotive force (EMF) or reversible open circuit voltage of the hydrogen fuel cell (Larminie and Dicks, 2003). Voltage-current density curve of a fuel cell is the performance indicator of the fuel cells. It is important to obtain higher current densities at higher voltages. These performance curves indicate which type of resistance is dominated and where the problem is in the fuel cell. A typical polarization curve for the fuel cell is given in Figure 2.3.

It can be obviously seen from the Figure 2.3 (Cooper et al., 2005) that there are some voltage losses while operating the fuel cell. An evaluation of deviation of operating voltage level from ideal operational case may provide information on the extent of improving efficiency and energy efficiency of a fuel cell (Ghadamian and Saboohi, 2004). The irreversibilities of a fuel cell is caused by activation losses, fuel crossover and internal currents, ohmic losses and mass transport or concentration losses.

The cell voltage including all cell reversibilities can be given as in Eqn (2.9):

$$V = E - \Delta V_{act} - \Delta V_{ohm} - \Delta V_{trans} \quad (2.9)$$

where

$$\Delta V_{act} = A \cdot \ln\left(\frac{i}{i_0}\right) \quad (2.10)$$

$$\Delta V_{ohm} = ir \quad (2.11)$$

$$\Delta V_{trans} = m \exp(n.i) \quad (2.12)$$

in which  $E$  is the reversible open cell voltage,  $A$  is Tafel slope,  $i_0$  is the exchange current density,  $r$  is the resistance and  $m$  and  $n$  are empirical coefficients (Larminie and Dicks, 2003).

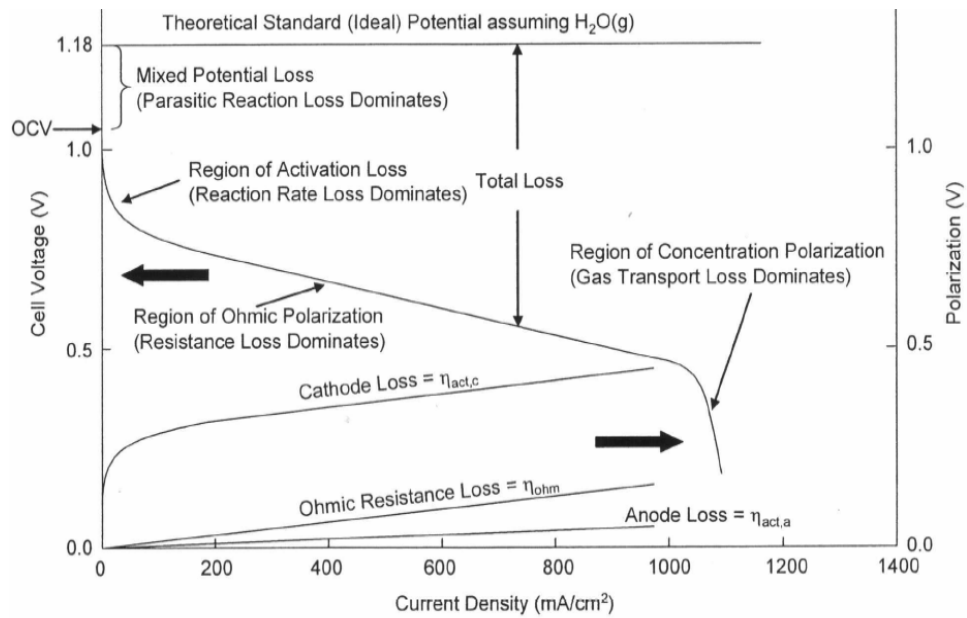


Figure 2.3 Typical fuel cell polarization curve

### 2.3.1 Activation losses

The overvoltage arising from the activation losses is given by the equation that was reported by Tafel in 1905 and given by the Eqn (13):

$$\Delta V_{\text{act}} = a \cdot \log\left(\frac{i}{i_0}\right) \text{ or } \Delta V_{\text{act}} = A \cdot \ln\left(\frac{i}{i_0}\right) \quad (2.13)$$

A is higher for an electrochemical reaction that is slow. The faster the reaction is the higher the constant  $i_0$ . Exchange current density ( $i_0$ ) can be considered as the current density at which the overvoltage begins to move from zero. It is important to remember that the Tafel equation only holds when  $i$  is greater than  $i_0$ .

From a theoretical basis, for a hydrogen fuel cell with two electrons transferred per mole, the constant A in the Tafel equation is given by;

$$A = \frac{RT}{2\alpha F} \quad (2.14)$$

The constant  $\alpha$  is called the charge transfer coefficient and it is the proportion of the electrical energy applied that is harnessed in changing the rate of an electrochemical reaction. Its value depends on the reaction involved and the type of electrode material, but it must be in the range of 0 to 1. For the hydrogen electrode, its value is about 0.5 for a wide variety of electrode materials. At the oxygen electrode the charge transfer coefficient shows more variation, but is still between 0.1 and 0.5 in most circumstances (Larminie and Dicks, 2003). Activation losses are caused by the slowness of the reactions taking place on the surface of the electrodes. A proportion of the voltage generated is lost in driving the chemical reaction that transfers the electrons to or from the electrode.  $i_0$  at the oxygen electrode (the cathode) is much smaller



than that at the hydrogen anode, sometimes  $10^5$  times smaller. Indeed, it is generally supposed that the overvoltage at the anode is negligible compared to that of the cathode, at least in the case of hydrogen fuel cells. A crucial factor in improving fuel cell performance is, therefore, to increase the value of  $i_0$ , especially at the cathode. This can be done in the following ways raising the cell temperature, using a more effective catalyst, increasing the roughness of the electrodes, increasing reactant concentration, for example, using pure  $O_2$  instead of air or increasing the pressure (Larminie and Dicks, 2003).

### *2.3.2 Fuel crossover and internal currents*

The membrane in PEMFC has to be only proton conducting. If some fuel and electron conduction occurs through the membrane, this will cause some energy loss. Fuel crossover is known as the migration of the fuel through the electrolyte.

### *2.3.3 Ohmic losses*

Ohmic losses in fuel cell include all resistances such as resistance to the electron flow through the material of the electrodes, various interconnections, and the resistance to the flow of ions through the electrolyte. Electronic resistances are located in a number of fuel cell stack components and, inside the MEA, in the electrode substrates and the two catalyst layers. Ionic resistances occur where proton transport takes place, i.e., inside the membrane electrolyte and inside the catalyst layers (Hoogers, 2003).

#### *2.3.4 Mass transport or concentration losses*

Mass transport or concentration losses result from the change in concentration of the reactants at the surface of the electrodes as the fuel is used. For both anode and cathode sides, the consumption of the feed gases will result in the decrease in the pressure which will reduce the voltage. Also, the flooding that occurs because of the excess water in fuel cell can hinder the gas transport.

### **2.4 Electrocatalysis in Proton Exchange Membrane Fuel Cells**

Platinum is the basic metal that is used for anode and cathode electrodes of PEMFCs because of its high catalytic activity for both oxidation and reduction reactions (Costamagna and Srinivasan, 2001). However, platinum is an expensive metal which causes the price of MEAs to be prohibitively high for commercialization and widespread usage of fuel cells (Xiong and Manthiram, 2005). For both anode and cathode sides, carbon supported Pt is used as the electrodes. Since, oxygen reduction reaction (ORR) on the cathode side is much slower than hydrogen oxidation reaction (HOR) at the anode side, the catalyst and the catalyst loading at the cathode side is gaining more importance. This sluggish ORR is the main contributor to the efficiency loss in PEMFCs. The catalytic activity of the catalyst and the utilization depends on the contact between the electrolyte and the Pt particles (Pan et al., 2005) as well as the size of the platinum particles. Figure 2.4 shows the schematic representation for the contact between Pt/C and Nafion in PEMFCs. To provide proton conduction between the catalyst and the electrolyte, the Nafion solution plays a network role.

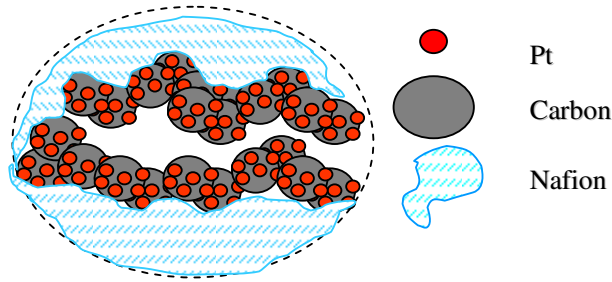
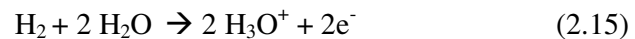


Figure 2.4 Schematic representation for the contact between Pt/C and Nafion in PEMFCs

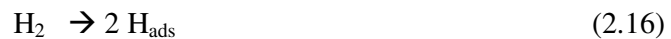
#### 2.4.1 Hydrogen oxidation reaction

Hydrogen oxidation reaction (HOR) takes place at the anode side of the fuel cell. The net reaction for the hydrogen oxidation is supposed to be with two different pathways, i. e. via Tafel-Volmer mechanism or the Heyrovsky-Volmer mechanism (Larminie and Dicks, 2003).

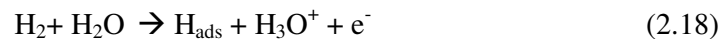
Overall half cell reaction



Tafel-Volmer mechanism



Heyrovsky-Volmer mechanism





The favored mechanism depends not only the electrolyte medium but also the catalyst used. Since the reaction at the anode side is very fast, the catalyst loading at the anode side can be lower than the cathode side. At the anode side of the fuel cell, it is important to prevent the poisoning effects of some gases including especially carbon monoxide since it is a by-product of reforming processes. So, many efforts have been devoted to find alternative catalysts to eliminate the CO poisoning.

#### 2.4.2 Oxygen reduction reaction

Oxygen reduction reaction (ORR) occurs at the cathode side of the fuel cell. For ORR, two reactions pathways are assumed depending on the pH of the electrolyte (Hamann et al, 1998):

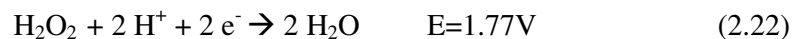
Direct reduction



Indirect reduction



followed by a further reduction via



or a chemical decomposition via



The target reaction is direct reduction, in the latter case hydrogen peroxide is formed which may accumulate and affect the fuel cell performance in a bad way by forming the radicals from the hydrogen peroxide with the help of the catalyst which causes membrane to deteriorate (Kunimoto et al, 2006).

Platinum bulk metal forms a face-cubic-centered (fcc) crystal structure, generally with 110, 100 or 111 crystal planes in which every plane shows different electrochemical behavior. The role of the local symmetry of surface atoms in electrocatalysis is on the kinetics of the oxygen reduction reaction and of the hydrogen evolution/oxidation reactions on single Pt crystals (Marković et al., 1999). Figure 2.5 shows the cyclic voltammetric current potential curve for a platinum electrode in contact with a 0.5 M H<sub>2</sub>SO<sub>4</sub> solution (mercury sulfate reference electrode was used, MSE) (Rodríguez et al, 2000). Since in Figure 2.5 the reference electrode used was MSE the electrode potentials can be converted to normal hydrogen electrode (NHE) referenced potentials by adding 680 mV (Rodríguez et al, 2000).

The equilibrium potential for the hydrogen evolution/oxidation reaction is to be -680 mV (0 V vs NHE) for any case. From the figure it is seen that below -300 mV (0.4 V vs NHE) hydrogen adsorption and desorption peaks appear. The areas under the curves are used to determine the electrochemical surface areas of the Pt that are active for the reactions. A fully covered monolayer is supposed to correspond to a charge of 210  $\mu\text{C}/\text{cm}^2$  for a polycrystalline Pt surface (Liu et al, 2005). At potentials higher than 100 mV (0.8 V vs NHE) Pt is oxidized. If potential is further increased to 700 mV (1.4 V vs NHE) oxygen evolution can be observed. Approximately, in anodic direction between -300 and 100 mV (0.35 and 0.8 V vs NHE) and in cathodic direction between 100 and -300 mV (0.65 and 0.35 V vs NHE) region (double layer region) only the current flow required to charge the electrochemical double layer can be observed where only capacitive processes take place. The hydrogen underpotentially deposited ( $\text{H}_{\text{upd}}$ ) region shows two well-resolved peaks. The

peak located around -600 mV (120 mV vs NHE) is related to the adsorption/desorption process of hydrogen on low coordinated Pt-surface atoms comparable to the H adsorption/desorption peak observed on Pt(110) single crystal surfaces. The second peak is located around -500 mV (240 mV vs NHE). At the same position a H adsorption/desorption peak can be observed on Pt (100) single crystal surfaces. This peak therefore points to the  $H_{\text{upd}}$  process taking place on 100 facets (Marković et al., 1995).

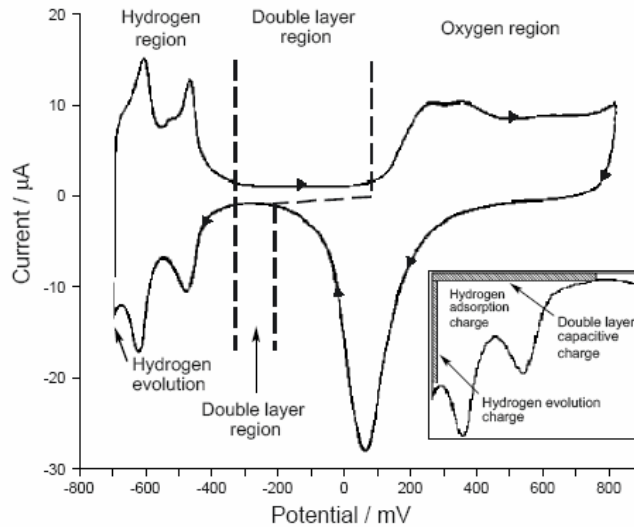


Figure 2.5 Cyclic voltammetric current potential curve for a platinum electrode in contact with a 0.5 M  $H_2SO_4$  solution (mercury sulfate reference electrode was used, MSE)

## 2.5 Catalyst preparation techniques

The catalytic activity of the catalysts depends on several parameters such as catalyst preparation technique, carbon support, precursor properties, accessibility of the metal on the support, conditions and so on. Several techniques were used to deposit platinum on different carbon supports, such as impregnation-reduction (Zhang et al, 2004; Kawaguchi et al, 2005), microemulsion based synthesis (Escudero et al, 2002) and ion exchange (Shao et al, 2006). By using different deposition methods, metals are decorated on different carbon supports such as Vulcan XC 72 R (Raghuveer and Manthiram, 2004), MWCNT (Liu et al, 2002; Li et al, 2003), carbon aerogel (Marie et al, 2004), activated carbon (Maruyama and Abe, 2003), BP2000 (Amine et al, 1998) and carbon cryogel (Babić et al, 2006). Carbon black is a widely used support because it has good electrical conductivity, high corrosion resistance (Gloaguen et al., 1997) and low cost. In all these techniques, it has been targeted to decrease the average size of Pt particles in order to increase the catalytic surface area per mass of Pt and also to disperse the Pt particles uniformly on the support.

Briefly, impregnation method includes the mixing of carbon support with a solution of metal salts and then drying this slurry to remove the solvent then to reduce the catalyst by heat treatment to obtain the desired catalyst (Hoogers, 2003). Compared to other catalyst preparation methods, the impregnation method has some drawbacks such as agglomeration which results in larger particle sizes (Hui et al, 2005).

The colloidal method contains the production of nanoscale catalysts in the homogeneous phase with the use of ligands, surfactants, or polymers as the stabilizer. Then the heterogeneous catalysts can be obtained by depositing the pre-prepared colloidal particles onto the supports. Therefore both the size and composition of the colloidal precursors may be tailored independent of support

(Hui et al, 2005). In microemulsion-based synthesis, removing the surfactant may be problematic (Yu et al, 2003).

Most of the patented Pt-based catalysts were prepared by using the precipitation method. This method includes the precipitation of a soluble species by chemical transformation. This is done by changing the pH (from acidic to basic) or the addition of a reducing agent (e.g., formaldehyde, hydrazine or any other reducing agent to precipitate metal) (Hoogers, 2003).

The supercritical deposition method involves the dissolution of an organometallic precursor in a supercritical fluid and the impregnation of the substrate by exposure to this solution. Subsequent treatment of the impregnated substrate results in metal/substrate nanocomposites. Because of its non-toxicity, non-reactivity, non-flammability and inexpensive properties the most commonly used fluid is CO<sub>2</sub> (Saquing et al, 2005). One of the most promising catalyst preparation techniques is the supercritical carbon dioxide (scCO<sub>2</sub>) deposition method (Leitner, 2002) which results in small particle sizes and homogeneous dispersion (Zhang et al, 2005). By using this method, the metal loading on the support can also be controlled thermodynamically (Saquing et al, 2005).

Microwave irradiation method is recently used for the heterogeneous catalyst preparation. In this method, reduction of the metal is achieved by using microwave heating (Liu et al., 2006).



## 2.6 Deactivation of the catalyst by CO and CO<sub>2</sub>

### 2.6.1 The significance of CO and CO<sub>2</sub> contents in H<sub>2</sub>

Molecular hydrogen is not naturally available so it has to be produced from the primary energy sources. The most commonly used ways for hydrogen production are electrolysis, coal gasification, biohydrogen and steam reforming. The gas output of the reforming systems contains carbon monoxide and carbon dioxide and biohydrogen processes only contain carbon dioxide besides hydrogen. Global hydrogen production in 1999 from different production methods is given in Figure 2.6 (Sperling and Cannon, 2004). The figure represents that most of the hydrogen is produced from hydrocarbon based fuel sources.

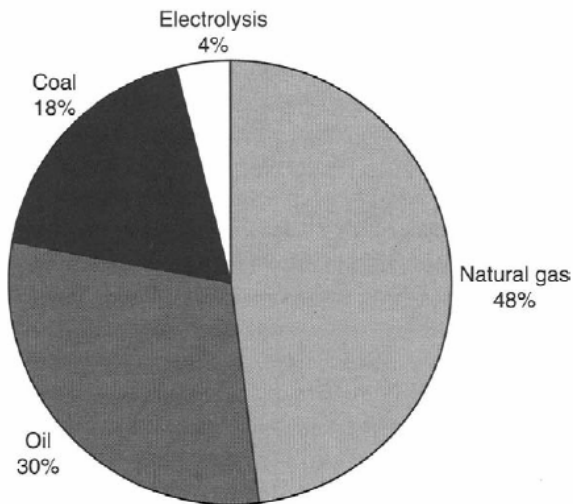


Figure 2.6 Global hydrogen production in 1999

Especially for mobile applications and also for residential applications on-board hydrogen produced by reforming systems seems to be the most suitable one. All hydrocarbon reforming methods, whether it be steam reforming, partial oxidation (Avcı et al, 2001a) or autothermal reforming (Avcı et al, 2001b), generate an effluent which is dilute in hydrogen and contains varying amounts of trace CO (Bhatia et al, 2004). Hydrogen can be generated on-board by reforming a liquid hydrocarbon, such as methanol, resulting in a fuel mixture consisting of approximately 74% hydrogen, 25% carbon dioxide and 1-2% carbon monoxide by volume (Baschuk et al, 2003). Currently, the most widely used method of hydrogen generation is via steam reforming of natural gas, because it is mainly composed of methane which has a higher hydrogen atoms per carbon atoms ratio close to 4:1 (Avcı et al, 2002).

Another hydrogen production method used is coal gasification. Coal is potentially a more economical source of hydrogen when compared to natural gas, because it is abundant and its delivery is safe (Sperling and Cannon, 2004).

Hydrogen production by electrolysis gives the purest hydrogen but it is not an energy efficient process. Most of the efforts are devoted to integrate the nuclear, solar or wind power with electrolyzers. So, by using sustainable energy sources the cost of the hydrogen production via electrolysis could be reduced.

Biological hydrogen production is also gaining increasing attention especially when the wastes of different factories such as olive oil are used as the hydrogen source (Eroğlu et al, 2006). By using this method carbon dioxide is produced with hydrogen in the range of 4-50%.

### 2.6.2 CO and CO<sub>2</sub> tolerance of the catalysts

The CO concentration must be reduced in a separate gas treatment unit down to <10 ppm if conventional carbon supported Pt is used as anode catalyst. Otherwise, CO molecules are adsorbed strongly on active sites of the catalyst and inhibit the hydrogen oxidation reaction at the anode (Divisek et al, 1998). Temporary deactivation occurs because CO binds strongly to Pt sites resulting in a high Pt surface coverage of CO at the operating temperature of PEFCs (Denis et al, 1999). Since, the electrodes in a PEM fuel cell contain platinum, only higher than 10 ppm CO and even higher percentages of CO<sub>2</sub> (20-50%) in the hydrogen poisons the catalyst. So the electrodes have to be improved for the tolerance of both CO and CO<sub>2</sub>. This improvement can be achieved by using binary or ternary catalyst combinations which help to reduce the platinum poisoning. Other poisons considered are H<sub>2</sub>S (Shi et al., 2007) and ammonia (Halseid et al., 2006).

The ways to overcome the performance loss due to the presence of CO are:

- advanced purification of reformat gas by fuel processor, but this will make the fuel cell system much more complex and expensive (Yu et al, 2002)
- electrodes poisoned by CO could be recovered quickly when fuels containing no CO was used (Qi et al, 2003)
- increasing the temperature (to decrease CO adsorption), but the operating temperature is limited to a maximum of about 120<sup>0</sup>C by the need for effective humidification of the membrane
- injecting a small amount of O<sub>2</sub> (up to about 2%), air bleeding, to oxidize CO chemically. However, the explosion threshold for H<sub>2</sub>/O<sub>2</sub> mixtures is 5% O<sub>2</sub> in H<sub>2</sub>. This limits the maximum level of CO that can be treated effectively by oxygen bleeding in PEFCs to about 100 ppm.

Furthermore, the chemical oxidation of CO by O<sub>2</sub> catalyzed by Pt at the anode reduces the amount of Pt available, for producing a current from the oxidation of hydrogen, and also the utilization of the fuel will certainly be decreased. Furthermore, only about 1 out of 400 oxygen molecules participates in the oxidation of CO, and the remaining oxygen chemically combusts with hydrogen. The combustion reaction not only lowers the fuel efficiency, but might also accelerate the sintering of catalyst particles which leads to a performance decline with time. In addition, the chemical combustion might also create pinholes in the electrolyte membrane, which could result in cell failure (Qi et al, 2003)

- the addition of H<sub>2</sub>O<sub>2</sub> shows comparable results to air bleeding. The decomposition of H<sub>2</sub>O<sub>2</sub> to active oxygen leads to CO oxidation and to enhanced cell performance. Addition of H<sub>2</sub>O<sub>2</sub> has advantages regarding the safety problem as compared to mixtures of hydrogen and oxygen. An alternative to the H<sub>2</sub>O<sub>2</sub> addition to the fuel gas could be a small electrolyzer which produces defined amounts of oxygen (Divisek et al, 1998).
- the usage of Pt alloy catalysts that are more tolerant towards CO poisoning than pure Pt. The use of Pt-Ru as oxidation catalyst for H<sub>2</sub> containing CO at the anode leads to a lowering of the CO oxidation potential (Denis et al, 1999). Search for an anode catalyst which oxidizes adsorbed CO at lower electrode potentials than Pt, showing at the same time a high activity for hydrogen oxidation (Divisek et al, 1998).

It is known that the higher percentages of CO<sub>2</sub> have an adverse effect on PEMFC performance. This effect is supposed to be due to either reverse water gas shift (RWGS) reaction or electroreduction.

The reverse water gas shift reaction



or electroreduction mechanism



The effect of either in terms of the effect of surface coverage and its effect on overpotentials will be the same (Urian et al, 2003). At low potentials, where Pt is covered by adsorbed hydrogen (Pt-H<sub>ads</sub>), CO forms both linear and bridge-bonded CO species. Moreover, the ratio of linear and higher coordinated forms (such as bridge-bonded) appears to be a function of electrode potential. Adsorption of CO<sub>2</sub> on the platinum surface is expected to occur mainly in the potential range where surface adsorbed hydrogen on Pt is present (hence in the low potential region) (Urian et al, 2003).

Nafion is used in the catalyst solution to provide a network between the Pt metal and the electrolyte. Uncovered platinum is likely to coexist with Nafion-covered platinum. Bruijn et al. (2002) found that the uncovered Pt metal affects the RWGS reaction. It is supposed to be this uncovered platinum (which is capable of catalyzing the RWGS reaction) exposed to hydrogen leads to adsorbed hydrogen atoms which cannot be removed electrochemically, due to the lack of electrolyte. The CO, formed on the surface by this RWGS reaction is in equilibrium with CO in the gas phase. On the Nafion-covered surface, adsorbed hydrogen is immediately oxidized to protons, the dissociative adsorption of molecular hydrogen being the rate determining step. By the low amount of adsorbed hydrogen, the RWGS reaction is strongly suppressed, and the influence of CO<sub>2</sub> is minor. Thin-film electrodes with high electrochemical utilization are much more tolerant towards CO<sub>2</sub>, irrespective of the noble metal composition of the anode (Bruijn et al, 2002).

Janssen (2004) modelled the CO<sub>2</sub> poisoning on PEMFC anodes. From this study it was found that RWGS reaction can in principle be the two sources of

anode poisoning in a fuel cell. There is the reduced  $\text{CO}_2$  that is in the form of CO or a related species which blocks the catalyst surface for hydrogen dissociation and oxidation. In addition, CO formed by  $\text{CO}_2$  reduction desorb from the surface, enter the gas flow and re-adsorb further down-stream. Apart from surface blocking, the dilution and utilization of hydrogen lead to a reduced partial hydrogen pressure and hence increased activation and Nernst losses. In this respect, the addition of  $\text{CO}_2$  is equivalent to the addition of  $\text{N}_2$ . At higher current density, the rate of  $\text{CO}_2$  reduction is reduced due to lower amount of H-adsorbed sites available for the  $\text{CO}_2$  reduction reaction, hence at higher current density the effects of 10 ppm CO become more significant than those of  $\text{CO}_2$ . Moreover, at high current densities the CO effect seems to prevail, whereas at low current densities the  $\text{CO}_2$  effect dominates. The most important conclusions are that increase of the rate constant of the RWGS reaction and reduction of the hydrogen dissociation rate enhances  $\text{CO}_2$  poisoning effects whereas CO desorption and CO electro-oxidation mitigate the effects (Janssen, 2004). Janssen (2004) has concluded that the performance loss due to  $\text{CO}_2$  is mainly caused by the indirect formation of CO (Eqns 2.24 or 2.25). So, it will be more meaningful to discuss the effect of CO on PEMFC performance. The active sites covered by CO lowers the performance. Bhatia et al (2004) found that while hydrogen dilution alone lowers the fractional coverage on the catalyst surface, it is only when CO is present that the coverage is lowered to a degree that effects cell voltage (Bhatia et al, 2004).

### *2.6.3 Improvements in CO and $\text{CO}_2$ tolerance of the catalysts*

A composite electrode structure was proposed by Yu et al (2002) for improving CO tolerance of PEMFCs. The electrode structure, as diffusion coefficients of  $\text{H}_2$  and CO are different, was designed to make the poisonous CO to react at a separate layer with CO active electrocatalyst in advance, and make the main

hydrogen to react at another layer with traditional electrocatalyst platinum. It is important for catalyst layer preparation that the inner catalyst layer should be rich in platinum and that the outer catalyst layer should be rich in CO tolerant electrocatalyst, e.g. PtRu/C. With the same catalyst loading, the new composite electrode has improved cell performance than traditional electrode with PtRu/C electrocatalyst for both pure hydrogen (since PtRu alloy is not as active as Pt when pure hydrogen is served as the fuel) and CO/H<sub>2</sub> (Yu et al, 2002).

For improving the CO tolerant, Yamada et al (2004) modified Pt/Cs by the addition of Y<sub>2</sub>O<sub>3</sub>, TiO<sub>2</sub>, Ga<sub>2</sub>O<sub>3</sub>, Nb<sub>2</sub>O<sub>5</sub>, La<sub>2</sub>O<sub>3</sub>, ZrO<sub>2</sub>, In<sub>2</sub>O<sub>3</sub>, Ta<sub>2</sub>O<sub>5</sub> or CeO<sub>2</sub>. The addition of Bi was less effective than the former metal oxide additions. The addition of vanadium and iridium shows no effect on the CO-tolerance. Among them, the Pt/C modified with niobium oxide and tantalum oxide was electrochemically tested by conventional cyclic voltammetry using a rotating electrode. With the addition of these metal oxides to Pt/C, the possibility of CO-tolerance improvement was also found in the CV measurements (Yamada et al, 2004).

Hou et al (2003) prepared a CO tolerant electrocatalyst of PtRu-H<sub>x</sub>MeO<sub>3</sub>/C. They found that such a structure promises better CO tolerance than PtRu/C for lowering the ignition potential to CO oxidation reaction (COOR) and improving the H<sub>2</sub> oxidation reaction current when active sites on noble metals are blocked by CO. The bifunctional mechanism of COOR is strengthened by the existence of active water bonded on the transitional metal oxides, and the anode polarization caused by CO poison is so diminished (Hou et al, 2003).

Papageorgopoulos et al (2002) incorporated Mo to PtRu catalyst and promising results were attained for PEMFC operation on methanol or reformat gas. The inclusion of 10wt% Mo in PtRu, led to an electrocatalyst with a higher activity than PtRu/C in the presence of CO. Also, they found that fuel cell anodes consisting of carbon supported PtMo (4:1) exhibit enhanced CO tolerance

compared to Pt/C and the other binary systems tested, but do not outperform PtRu/C (Papageorgopoulos et al, 2002).

Divisek et al (1998) showed that PtRu alloy catalysts are the most active ones to oxidize adsorbed CO and a detailed study on model catalysts with defined Pt to Ru surface compositions have shown that Pt<sub>0.5</sub>Ru<sub>0.5</sub> has the lowest overpotential in comparison to pure Pt. The maximum power density of a PEM single cell in H<sub>2</sub>/CO using such an anode catalyst is enhanced by a factor of four compared to Pt. Improved anode catalysts such as PtRu alloys supported on carbon showed an enhanced CO tolerance up to CO concentrations of 250 ppm (Divisek et al., 1998).

Different catalyst preparation techniques are used in the literature to prepare the PtRu based catalysts. Luna et al (2000) prepared carbon-supported Pt:Ru catalysts by using different methods and of all the preparation methods tested, the one originally proposed by Watanebe, via the formation of a sulfite complex, gives the best results, provided it is followed by a thermal treatment in hydrogen atmosphere (Luna et al, 2000). Denis et al (1999) used a ball milling (BM) process to obtain Pt-Ru unsupported catalyst. The best results were obtained by milling Pt, Ru and Al in a 1:1:8 atomic ratio. Equivalent hydrogen oxidation performance and CO tolerance results were obtained for prepared Pt<sub>0.5</sub>Ru<sub>0.5</sub> catalyst and commercially available catalysts (Denis et al, 1999).

Qi et al (2003) found that even trace amounts of CO in the fuel for a proton exchange membrane fuel cell (PEMFC) could poison not only the anode, which is directly exposed to the fuel, but also the cathode, which is separated from the fuel by a proton exchange membrane; and the performance decline of the cathode is sometimes more than that of the anode (Qi et al, 2003).



To reduce the CO level in the reformat gas a thin catalyst-sheet for PEMFC-integrated CO oxidation system was developed by Rohland et al (1999). If a PEMFC-stack is treated with catalyst-sheet in front of the Pt/Ru anode of each cell, it is enough to lower the CO content by an external CO cleaning device to 1000-2000 ppm CO. The advantage is a better dynamic and a simpler construction of the H<sub>2</sub> producing unit of the PEMFC-plant (Rohland et al, 1999).

Götz et al (1998) found that PtRuW exhibits a higher activity for oxidation of H<sub>2</sub>/CO and methanol than both a Pt/Ru catalyst synthesized by the colloid method and a Pt/Ru catalyst supplied by E-TEK. It is however, far from likely that ternary catalysts can be a factor of 10 better than binary Pt/Ru catalysts, which is necessary for commercialization of DMFCs (Götz et al, 1998).

Isono et al (2000) showed that the thickness of the catalyst layer has a significant effect on anode polarization. The CO tolerance of the PtRu alloy anode was improved by reducing its thickness from 40µm to 20 µm (Isono et al, 2000).

CO competes with H<sub>2</sub> adsorption on the anode surface. If Langmuir-Hinshelwood mechanism is assumed for the reactions given below:



where \* represents the active sites of the metal, coverages of CO and H<sub>2</sub> are as follows where,  $K_{\text{CO}} = k_{26} / k_{-26}$  and  $K_{\text{H}} = k_{27} / k_{-27}$  are the equilibrium constants. The ratio of the coverages is:

$$\theta_{CO} = \frac{K_{CO} P_{CO}}{1 + K_{CO} P_{CO} + (K_H P_{H_2})^{1/2}} \quad (2.28)$$

$$\theta_H = \frac{(K_H P_{H_2})^{1/2}}{1 + K_{CO} P_{CO} + (K_H P_{H_2})^{1/2}} \quad (2.29)$$

$$\frac{\text{coverage H}}{\text{coverage CO}} = \frac{\theta_H}{\theta_{CO}} = \frac{K_{ad,H}}{K_{ad,CO}} \approx \exp \left\{ \frac{- (\Delta H_{ad,H} - \Delta H_{ad,CO})}{RT} \right\} \quad (2.30)$$

The smaller the difference in the heats of adsorption of CO and hydrogen the less severe is the CO poisoning. H<sub>2</sub> and CO adsorption enthalpies of some metals are given in Table 2.1.

Table 2.1 H<sub>2</sub> and CO adsorption enthalpies of some metals

Metal	$\Delta H_{ad}(\text{CO})$ (kJ/mol)	$\Delta H_{ad}(\text{H}_2)$ (kJ/mol)
Ni	120 <sup>a</sup> (@303K)	85 <sup>a</sup> (@303K)
Pt	120 <sup>b</sup> (@300K)	90 <sup>c</sup> (@403 K)
Ru	120 <sup>d</sup> (@300K)	65 <sup>d</sup> (@300K)

<sup>a</sup> Spiewak and Dumesic, 1998

<sup>b</sup> King, 1997

<sup>c</sup> Spiewak et al., 1998

<sup>d</sup> Londhe and Gupta, 1997

## CHAPTER 3

### METHODS FOR CATALYST PREPARATION IN SUPERCRITICAL CARBON DIOXIDE

#### 3.1 Supercritical fluid properties

The relation between the temperature and the pressure of the pure substance is given in Figure 3.1. The states for the pure substance are solid, gas and liquid states. Between the boundaries of the two states, these two states are in equilibrium. At the triple point shown with “T” in the Figure 3.1 (<http://pubs.rsc.org/ej/jm/2000/a906486i/> last accessed at 13.01.2008), three states exist.

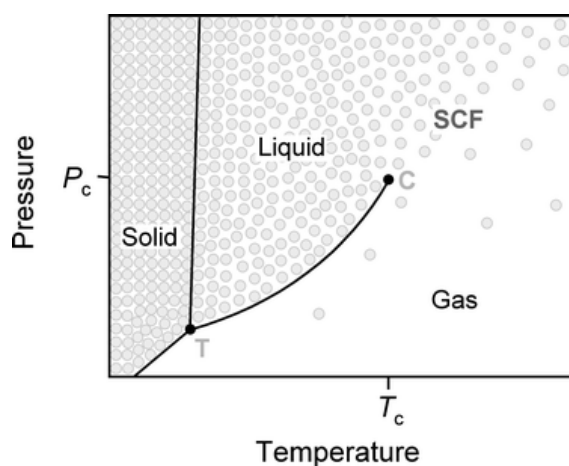


Figure 3.1 Schematic pressure–temperature phase diagram for a pure component showing the supercritical fluid (SCF) region

The critical point (C) defines the temperature and pressure at which the vapour and liquid phases existing in equilibrium have identical properties, so it is the upper boundary of the vapour-liquid region (Kıran and Brennecke, 1991). A supercritical fluid (SCF) is a fluid where it is heated and compressed above its critical point values ( $T_c$ ,  $P_c$ ). Close to the critical point, small changes in pressure or temperature result in large changes in density which allows many properties to be tuned. The properties are unique and include liquid-like densities, gas-like viscosities and kinematic viscosities, much higher diffusivities than liquids and zero surface tension. The physical properties of gas, liquid and supercritical fluid of a typical organic fluid are given in Table 3.1 (Weibel and Ober, 2003). High diffusivities in SCFs combined with their low viscosities result in enhanced mass transfer characteristics when compared to conventional liquid solvents. Better penetration and wetting of pores than liquid solvents do, is provided by the low surface tension of SCF.

Table 3.1 Physical properties of gas, liquid, and supercritical fluid of typical organic fluid (order of magnitude)

	Density (g/ml)	Diffusivity (cm <sup>2</sup> /s)	Dynamic viscosity (g/cm s)
Gas	$1.10^{-3}$	$1.10^{-1}$	$1.10^{-4}$
Liquid	1.0	$5.10^{-6}$	$1.10^{-2}$
Supercritical fluid	$3.10^{-1}$	$1.10^{-3}$	$1.10^{-4}$

One of the main differences between supercritical fluids and conventional solvents is their compressibility. Conventional solvents in the liquid phase require very large pressures to change the density, whereas for supercritical fluids, very significant changes in density and hence solvating properties can

be achieved by comparatively small pressure and/or temperature changes, particularly around the critical point (Erkey, 2000). In general, supercritical fluids are considerably less dense than conventional solvents. The critical constants of some typical molecules used as SCF solvents are given in Table 3.2 (Arai et al., 2002). As can be seen from the table, the compressibility factors of the supercritical fluids are close to each other and range between 0.235 and 0.296.

Table 3.2 Critical constants of typical molecules used as SCF solvents

Molecule	Critical temperature $T_c$ (K)	Critical pressure $P_c$ (atm)	Critical compressibility factor $Z_c = P_c V_c / RT_c$
Ar	151	49	0.296
CH <sub>4</sub>	191	45	0.287
Xe	290	58	0.287
CF <sub>3</sub> H	299	47	0.259
CO <sub>2</sub>	304	73	0.274
C <sub>2</sub> H <sub>6</sub>	305	48	0.285
C <sub>3</sub> H <sub>8</sub>	370	42	0.281
NH <sub>3</sub>	406	111	0.244
H <sub>2</sub> O	647	218	0.235

### 3.2 Supercritical carbon dioxide as a green solvent

Among other SCFs, supercritical carbon dioxide (scCO<sub>2</sub>) seems to be a promising green solvent because of being non-toxic, non-flammable, chemically inert and inexpensive. It can be removed from the system only by

depressurization and no residue is left in the system (Nalawade et al., 2005). The research on the utilization of scCO<sub>2</sub> as solvent in chemistry has been under investigation long ago. The phase diagram for pure CO<sub>2</sub> is given in Figure 3.2 (Kemmere and Meyer, 2005). Besides its environmental benefits supercritical carbon dioxide has also desirable physical and chemical properties such as relative chemical inertness, readily accessible critical point ( $T_{cr}=31.1^{\circ}\text{C}$ ,  $P_{cr}=7.4\text{ MPa}$ ), excellent wetting characteristics, low viscosity and highly tunable solvent behavior, facilitating easy separation. Although, scCO<sub>2</sub> has a lot of advantages its usage is limited by the ability of solving only the volatile and the relatively non-polar compounds as CO<sub>2</sub> is non-polar and has low polarizability and a low dielectric constant (Kemmere and Meyer, 2005).

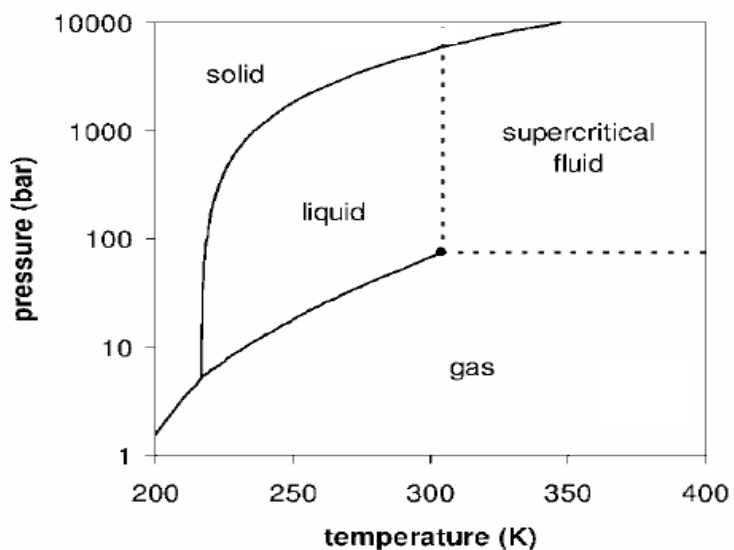


Figure 3.2 Schematic phase diagram for pure CO<sub>2</sub>

Hyatt (1984) searched for the use of either liquid or supercritical carbon dioxide as organic solvent and concluded that carbon dioxide exhibits

properties typical of hydrocarbon solvents. Leitner (2002), investigated the use of supercritical carbon dioxide instead of conventional organic solvents in the synthetic useful reactions and got similar or sometimes even better results with scCO<sub>2</sub>.

scCO<sub>2</sub> can be used in many fields of chemistry. Some applications can be given as: extraction (Cirimile et al., 1995; Mulcahey and Taylor, 1992), sterilization (White et al., 2006), pharmaceutical processing (Subramaniam et al., 1997), microelectronics (Weibel and Ober, 2003) and catalyst preparation (Lin et al., 2005) processes.

### **3.3 Utilization of scCO<sub>2</sub> in catalyst preparation**

Metal nanoparticles dispersed on high surface area substrates are used widely as catalysts for a variety of reactions. Carbon supported precious metals, such as platinum or ruthenium, are very important in fuel cells. There are several ways of deposition of the metal on carbon support. Among other catalyst preparation techniques, scCO<sub>2</sub> deposition method is also attracting increasing attention. There are a lot of parameters that affect the catalytic activity of the catalysts which arise from the catalyst preparation techniques. The impurities left from the solvent or precursor may influence the catalytic activity in a bad manner. The particle size of the metal deposited onto the carbon support also depends on the conditions of the reaction medium and so the preparation technique.

SC deposition involves the dissolution of an organometallic precursor in a SCF and the impregnation of the substrate by exposure to this solution. Subsequent treatment of the impregnated substrate results in metal/substrate nanocomposites (Saquing et al., 2005). As can be seen from the Figure 3.3

(Zhang and Erkey, 2006) there are two pathways to reduce the impregnated organometallic precursor in its metal form. In the first pathway after the impregnation the reaction medium depressurized and then the reduction method applied. In the latter case the reduction can be achieved in the reaction medium.

Many studies have been devoted to deposit Pt onto different carbon supports. Lin et al (2005) prepared Pt/CNT nanocomposites as electrocatalysts for low-temperature fuel cells. They obtained nanostructured and uniform particles and these particles possessed a higher catalytic activity both for methanol oxidation and oxygen reduction reaction.

Haji et al (2005) prepared Pt/Al<sub>2</sub>O<sub>3</sub> catalysts by using scCO<sub>2</sub> deposition method. The catalysts were found to be active for hydrodesulfurization of dibenzothiophene (DBT) dissolved in *n*-hexadecane (*n*-HD) without sulfiding the metal phase.

Different carbon supports such as carbon aerogel which has high surface area can also be produced by using scCO<sub>2</sub> deposition method. Saquing et al (2005) decorated carbon aerogels with platinum by using scCO<sub>2</sub> deposition method, and they showed that the reduction method for the organometallic precursor to its metal form also influences the metal loading and the particle size. The metal particle size and Pt loadings obtained ranged from 1 to 6 nm and 10 to 73 wt.% Pt, respectively, for different reduction methods.

Instead of organometallic precursors, metal salts dissolved in ethanol (or methanol) can also be used as the precursor in supercritical deposition method. With the aid of scCO<sub>2</sub>, Sun et al (2007) have extended the SCF deposition method to decorate CNTs with tin oxide using SnCl<sub>2</sub>·2H<sub>2</sub>O dissolved in ethanol as a precursor



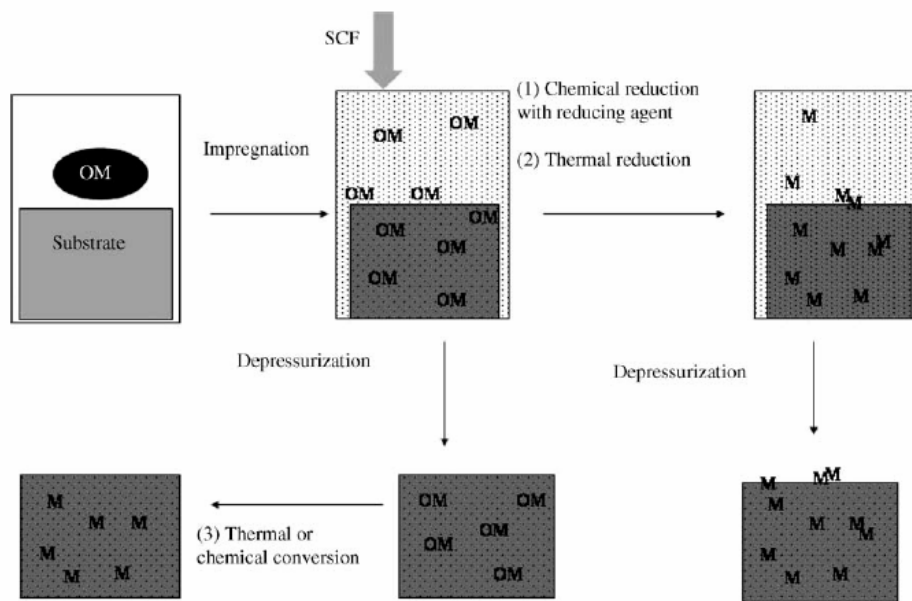


Figure 3.3 The scheme of using SCF as processing solvent to synthesize supported nanoparticles via deposition or impregnation

Besides being the proton conducting membrane, Nafion solution is also used for the proton conduction between the catalyst and the electrolyte. Zhang and Erkey (2005) synthesized the Nafion-platinum-carbon black nanocomposites by using supercritical deposition. The average particle size obtained was 2.6 nm. They showed that Pt-Nafion-carbon black nanocomposite displayed promising electroactivity as an electrocatalyst for fuel cells.

One of the most important parameters that affect the metal loading onto the substrate is the solubility of the metal precursor in the SCF. Zhang et al (2005) carried out their experiments by using two Ru precursors to deposit on carbon aerogel,  $\text{Ru}(\text{COD})(\text{tmhd})_2$  and  $\text{Ru}(\text{acac})_3$  which have solubilities of 0.0188 mol/l and 0.0025 mol/l, respectively. At the same conditions, the metal

loadings obtained were 10.7 and lower than 4% for the high and low solubility precursors, respectively.

Instead of using carbon supported precious metals, the metal can be deposited onto the membrane directly without any support. Jiang et al (2005) impregnated the Nafion membranes with Pd via a supercritical fluid route for use in direct methanol fuel cells (DMFCs). The fuel cell test results showed that this kind of impregnated membrane can lower the methanol crossover which is a main parameter that affects the performance of the DMFCs when compared to the pure Nafion membrane. Also the performance of the fuel cell was improved by the use of Pd impregnated membrane.

The adsorption of the precursor from  $\text{scCO}_2$  phase into the substrate phase is an important step in SCF impregnation. The equilibrium adsorption isotherm data of the organometallic precursor (OP)– $\text{scCO}_2$ –substrate system under impregnation conditions of constant temperature and pressure provide an understanding of the interaction between the components involved and how the metal precursor partitions between the SCF and substrate. The isotherm reflects the difference between the affinities or strength of interaction of the OP for the adsorbent and the fluid phases (Zhang and Erkey, 2005). For the definite temperature and pressure, the maximum metal loading on the substrate can be controlled thermodynamically by using adsorption isotherms.

## CHAPTER 4

### MICROWAVE IRRADIATION

#### 4.1 Microwave heating theory

Wavelengths of 1 cm to 1 m (300 GHz to 300 MHz) correspond to the microwave region of the electromagnetic spectrum, and by an international agreement only the frequencies 2.45 GHz (12.2 cm) and 900 MHz (33.3 cm) are available for dielectric heating (Tierney and Lidström, 2005). The improvement with microwave in chemistry is based on the efficient heating of materials by “microwave dielectric heating” effects (Kappe, 2004).

Microwave heating is fundamentally different from conventional heating. In microwave processes heat is generated internally within the material instead of originating from external sources. Briefly, the solvent or the reagent has to be capable of absorbing the microwave energy and convert it into heat. In conventional heating the material is heated only on the outside surface, but in case of microwave heating the microwaves can penetrate materials and heat the inside and also the outside. Since microwave heating depends on the absorption ability of the materials, it provides selective heating for different materials.

The conversion of the electromagnetic radiation to thermal energy can be explained at the molecular level. There are two principle mechanisms proposed for microwave interaction with matter: dipolar polarization and ionic conduction.

Polar molecules tend to align themselves and oscillate in step with the oscillating electric field of the microwaves and during this realignment energy is lost in the form of heat through molecular friction and dielectric loss. The more polar a molecule, the more effectively the molecule will couple with the microwave field. On the other hand, ions are charged species that can couple with the oscillating electrical field of the microwaves. The effectiveness or rate of microwave heating of an ionic solution is a function of the concentration of ions in solution. Therefore, rapid heating in a microwave field is caused by the ability of absorption of the radiation by a material that is placed in the field. The frequency of the applied field affects the amount of heat generated which is directly related to the ability of the matrix to align. If the dipole does not have enough time to realign, or reorients too quickly with the applied field, no heating occurs. But for the commercial systems where 2.45 GHz frequency is applied, such extreme cases have not been seen and it provides the molecular dipole time to align in the field (Kappe, 2004).

In the gas phase, the interaction of the small molecules with permanent dipole moments with microwave energy shows a well-defined spectrum that may be used to define the moment of inertia of the molecule. As long as the molecule has a permanent dipole moment, in this phase the rotation of molecules is quantized and the transition between the energy levels may be observed as sharp lines in the microwave spectrum. In liquids, the continuum of rotational states resulted in frequently interacting molecules and so the phenomenon loses its identity as a quantum mechanical description and rotational motions become less distinguishable from translational processes. The rotations at one center will influence the translational and rotational motions of neighbouring molecules via intermolecular interactions. The intermolecular perturbations will be greatest when the intermolecular forces arise from hydrogen bonding and strong dipole-dipole interactions. It is important to emphasize that microwave dielectric heating is not a quantum mechanical phenomenon localized at one molecular center, but is a collective property that occurs in a

semi-classical manner and involves aggregates of molecules” (Tierney and Lidström, 2005).

There are several important parameters related to microwave heating, such as dielectric loss, dielectric constant and penetration depth. The conversion capabilities for electromagnetic energy into heat of the materials at a given frequency and temperature are determined by their loss factors (loss tangent,  $\tan\delta$ ). Also an important parameter in deciding the extent of interaction between microwave radiation and a particular solvent is the average rotational frequency or its inverse, the average relaxation time. Debye first proposed that this relaxation time depends on the size of the molecule and the nature of the intermolecular forces. A dielectric material is one that contains permanent or induced dipoles, which when placed between two electrodes the whole assembly acts as a capacitor, that is if the electrodes are connected by a circuit the material allows charge to be stored and after the charging no d.c. conductivity is observed. The polarization of dielectrics results from the finite displacement of charges or rotation of dipoles in an electric field and must not be confused with conduction, which results from the translational motion of electric charges when a field is applied. At the molecular level, polarization may be associated either with a distortion of the distribution of the electron cloud of the molecule or the physical rotation dipoles. Dielectric heating in microwave region is strongly connected with the latter case. The permittivity of a material,  $\epsilon$ , is the property that defines the charge-storing ability of that material irrespective of the sample's dimensions. The dielectric constant or relative permittivity of a material is the permittivity of the material relative to free space. The angle,  $\delta$ , represents the angle between the vector for the magnitude of the total current and the charging current. In other words loss tangent represents the phase difference between the electric field and the polarization of the material. The loss tangent can be given by the equation as follows:

$$\tan\delta = \varepsilon''/\varepsilon' \quad (4.1)$$

where  $\varepsilon''$  and  $\varepsilon'$  represents the loss factor and dielectric constant, respectively (Copson, 1962).

The relaxation times and dielectric properties of some common organic solvents are given in Table 4.1 (Tierney and Lidström, 2005). The higher the loss tangent is the better the conversion of electromagnetic energy into heat.

Table 4.1 Relaxation times (20°C) and dielectric properties of some organic solvents

Solvent	Relaxation time $\tau$ (ps)	Loss tangent at 2.45 GHz
H <sub>2</sub> O	9.04	0.123
MeOH	51.5	0.659
EtOH	170	0.941
Propan-1-ol	332	0.757
Me <sub>2</sub> SO	20.5	0.825
HCONMe <sub>2</sub>	13.05	0.161
MeNO <sub>2</sub>	4.51	0.064
THF	3.49	0.047
CH <sub>2</sub> Cl <sub>2</sub>	3.12	0.042
CHCl <sub>3</sub>	8.94	0.091
MeCOMe	3.54	0.054
MeCO <sub>2</sub> Et	4.41	0.059
HCO <sub>2</sub> H	76.7 (25°C)	0.722
MeCO <sub>2</sub> H	177.4 (25°C)	0.174
MeCN	4.47	0.062
PhCN	33.5	0.459
Ethylene Glycol	113 (25°C)	1.35

## 4.2 Comparison of microwave heating and conventional heating

In conventional heating, heat can be transferred to the material by conduction, convection or radiation whereas in microwave heating energy is transferred to the materials through molecular interactions with the electromagnetic field. The difference between microwave and conventional heating is given in Figure 4.1 as below:

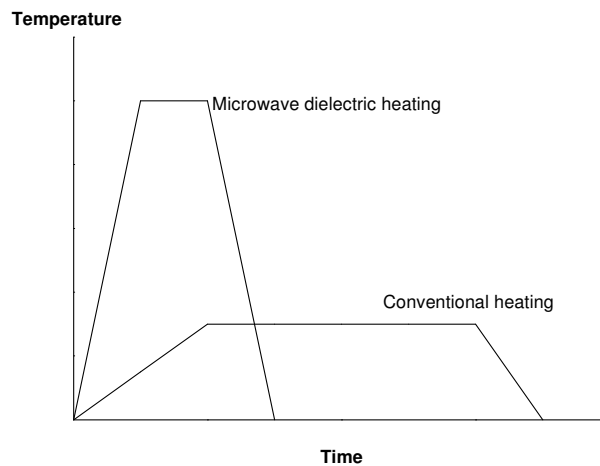


Figure 4.1 Differences in the temperature-time profiles for conventional and microwave dielectric heating (Tierney and Lidström, 2005)

The comparison between microwave and conventional heating is as follows:

- Heating rates in microwave are much higher than those can be achieved conventionally.
- In microwave heating, direct contact between the energy source and the sample undergoing heating is eliminated. With previous point, very different temperature-time profiles for the reaction can be achieved and

consequently may lead to an alternative distribution of chemical products in the reaction. Chemicals and the containment materials for chemical reaction do not interact equally with the commonly used microwave frequencies for dielectric heating and consequently selective heating may be achieved.

- Solvents heated under microwave conditions often boil at elevated temperatures even though they remain contained under 1 atmosphere pressure.
- In conventional heating, the heating rate is limited by the thermal conductivity, whereas in microwave heating individual heating of the molecules is provided. So, the heating times can be reduced to less than 1% of the conventional heating.
- In microwave heating, heat generation occurs in the product, not at walls or air, so the heat loss is decreased.
- Using the different absorption capacities of the materials selective heating can be achieved.
- Shutting on and off of the heating process can be achieved because of the electromagnetic waves.
- Microwave heating processes are time and energy saving (Tierney and Lidström, 2005; Robinson et al, 2007).

It is clear that due to the different heating phenomenon, in microwave heating in different reaction rates and product distributions may result. Metals are not used in microwave medium because of major sparking and arcing. But the metals can be used in microwave field as long as they are in powder form. The selection of the conditions such as low- microwave powers, high boiling point solvents, high pressures, non-aromatic solvents and small well-dispersed metal particles, is very crucial for low arcing for microwave synthesis in metal powder organic solvent system (Tierney and Lidström, 2005).



### 4.3 Catalyst preparation by microwave irradiation

Microwave irradiation has a wide variety of applications in chemistry. Many chemical reactions can be accelerated by the utilization of the microwave field which depends on the material having high dielectric constant.

For the supported catalysts the dispersion and the uniform distribution is very important for the particle size which will affect the catalyst activity. Highly active Fischer-Tropsch Co/SiO<sub>2</sub> catalyst was prepared by microwave irradiation with a uniform and better dispersion of the Co particles within the catalyst pellets, compared to that prepared by the conventional heating method (Reubroycharoen et al, 2007).

Microwave irradiation also can be used for the preparation of the fuel cell catalysts which require high quality catalyst properties. Tian et al (2006) synthesized carbon black supported polytetrafluoroethylene (PTFE/C) nanocomposites by an intermittent microwave irradiation for PEMFCs. They observed that with the incorporation of the PTFE/C nanocomposite into a Pt/C/Nafion catalyst, the mass transportation of the catalyst layer enhanced significantly without any adverse effect on the electrocatalytic activity of the Pt catalysts.

In microwave heating there are a lot of parameters which will affect the properties of the material in the microwave oven. Microwave irradiation duration is one of these parameters which affects the temperature. Wang et al (2007) varied the microwave irradiation duration between 30-120 s and they obtained the best electrocatalytic activity by using CV for 90 s with the particle sizes changing between 3-5 nm.

Microwave irradiation can also be used for the preparation of binary catalysts which is more suitable for the electrooxidation of methanol than the single Pt/C

catalysts. Liu et al (2004) synthesized PtRu nanoparticles supported on Vulcan XC72 with 2-6 nm particle sizes which showed more electrocatalytic activity for electro-oxidation of methanol. Also, PtSn/C catalysts with particle sizes of 2-7 nm were synthesized by microwave irradiation for methanol electro-oxidation (Liu et al, 2006).

To increase the carbon monoxide tolerance of the fuel cells not only binary but also ternary catalysts can be used which sometimes give better results. Carbon supported PtAuFe catalyst was prepared via a microwave-irradiated polyol process which enhanced the CO tolerance of the PEMFCs (Ma et al, 2007). PtRuIr/C catalyst prepared by microwave irradiation plus annealing synthesis strategy showed better CO tolerance when compared to the PtRu/C catalysts (Liang et al, 2006).

In colloidal catalyst preparation methods, a stabilizing agent is used to cover the metal particle to protect it from agglomeration. This process can also be used with the combination of the microwave irradiation. Zhao et al (2006) investigated the effect of addition of the sodium acetate solution as the stabilizing agent in the synthesis of carbon supported Pt nanoparticles with microwave irradiation. They demonstrated that the more the stabilizing agent added the smaller particle sizes were obtained.

Another important parameter for high catalytic activities in fuel cells is providing higher Pt loadings on the carbon support with small particle sizes. By using pulse-microwave assisted polyol synthesis Pt loadings as high as 50% on the carbon support with a small particle size of 2.7 nm was achieved (Song et al, 2007). Platinum and palladium supported on Vulcan XC72 carbon black were also prepared by a microwave-assisted polyol process for direct formic acid fuel cells and Pd/C catalyst gave better electrocatalytic activity (Liu et al, 2006).

## CHAPTER 5

### EXPERIMENTAL STUDIES FOR SUPERCRITICAL CARBON DIOXIDE DEPOSITION

The supercritical carbon dioxide (scCO<sub>2</sub>) deposition experiments were performed in the University of Connecticut Chemical Engineering Department and the cyclic voltammetry experiments were performed in Connecticut Global Fuel Cell Center in USA.

Cyclic voltammetry is a commonly used diagnostic tool for the electrocatalyst layer characterization. The active electrocatalyst layer in a PEM fuel cell consists of a mixture of carbon-supported Pt and a proton conductive ionomer such as Nafion. The carbon support provides electrical conduction and also dispersion of Pt metal and Nafion used as a binder and also it provides the proton conduction through the layer. The extent of formation of three phase boundary, where the reactants, ionomer and active catalyst sites are in contact with each other, affects the electrocatalytic activity of the catalysts. Electrocatalytic performance of the catalysts can be tested either with fuel cell or half cell experiments. Half cell experiments can be separated into two as ex situ or in situ voltammetry experiments. In ex situ experiments the electrodes were investigated by using a standard three electrode cell configuration with a liquid acid electrolyte. But in case of in situ experiments a two electrode cell configuration is used in fuel cell. To determine the ORR kinetics of fuel cell cathode, nitrogen is fed to the cathode (serves as counter electrode) and hydrogen fed to the anode (serves as counter/reference electrode). In the present study ex situ experiments were performed. Half cell experiments are a

convenient and relatively fast method of screening electrocatalysts. In this part of experiments the catalysts prepared by scCO<sub>2</sub> deposition were characterized by XRD, TEM and then tested with ex situ cyclic voltammetry.

## **5.1 Catalyst preparation by scCO<sub>2</sub> deposition**

### *5.1.1 Materials*

Carbon supports, Vulcan XC72R (VXR) and Black pearl 2000 (BP2000) (Cabot International) and multi wall carbon nanotube (MWCNT) (ID=1-3 nm, OD=3-10 nm, L=0.1-10µm >90%) (Aldrich) were impregnated with Pt and Ru using the scCO<sub>2</sub> deposition method. Dimethyl (cyclooctadiene) platinum (II) (99.9%) (STREM) (PtMe<sub>2</sub>COD) and bis (2,2,6,6-tetramethyl-3,5-heptanedionate) (1,5-cyclooctadiene) Ruthenium (II) (99%) (STREM) (Ru(COD)(Tmhd)<sub>2</sub>) were used as Pt and Ru precursors, respectively. Prior to impregnation all carbon supports were heat treated in a pyrolysis oven at 423 K for 4 hours in N<sub>2</sub> (99.999%, Airgas) atmosphere.

### *5.1.2 Supercritical carbon dioxide deposition setup*

A schematic diagram of the supercritical deposition setup is given in Figure 5.1. The deposition apparatus consists of a 54 ml custom-manufactured stainless steel vessel equipped with two sapphire windows, 25 mm in diameter, and sealed with poly ether ether ketone O-rings. A T-type thermocouple assembly (Omega Engineering, PX300-7.5KGV), a vent line and a rupture disk assembly (Autoclave Engineers) are also attached to the vessel.

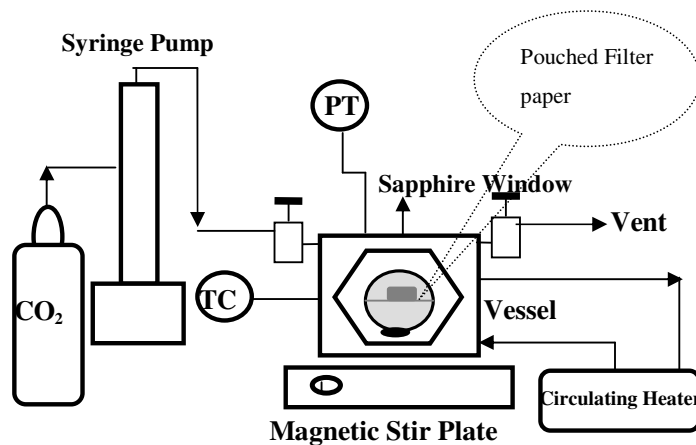


Figure 5.1 Experimental setup for supercritical deposition

### 5.1.3 Experimental procedure

Impregnation of the organometallic precursors depends on the dissolution of the precursor in scCO<sub>2</sub> and then exposure of this solution to the carbon support. Firstly, the heat-treated carbon support was placed into a pouch made of filter paper and placed into the vessel together with a certain amount of either PtMe<sub>2</sub>COD or Ru(COD)(Tmhd)<sub>2</sub> precursors, and a stirring bar. For the desired metal loading, the amounts of the corresponding precursors were determined by using the adsorption isotherm of the precursor onto the carbon support (Zhang et al., 2005). A stainless steel screen was used to separate the stirring bar from the filter paper pouch. The vessel was sealed and heated to 343 K using a circulating heater/cooler apparatus (Fisher Scientific Isotemp Refrigerated Circulator Model 80) and then charged slowly with carbon dioxide (99.998%, Airgas) to a pressure of 24.2 MPa using a syringe pump (ISCO, 260D). These conditions were maintained for a period of 6 h which was enough for the system to reach equilibrium and then the vessel was

depressurized. After allowing the vessel to cool, the pouch was removed and the impregnated carbon support was weighed to determine the amount of precursor adsorbed using an analytical balance (Adventure Model Ar 2140) accurate to  $\pm 0.1$  mg. Subsequently, the carbon support was placed in an alumina process tube in a tube furnace (Thermolyne 21100), and the Pt and Ru precursors were reduced thermally under flowing  $N_2$  ( $100 \text{ cm}^3 \text{ min}^{-1}$ ) for 4 h at 473 K and 673 K.

The kinetics data were obtained by dissolving 100 mg of the Pt precursor in 54 ml  $scCO_2$  and exposing this solution to the carbon support for various times ranging from 1 to 24 h. Adsorption isotherms were obtained by changing the amount of the organometallic precursor (either Pt or Ru precursor) dissolved in supercritical carbon dioxide where the carbon support amount was set to 0.1 g. The adsorption isotherm was obtained by determining the weight change of the plain supports before and after the exposure to the precursor dissolved in  $scCO_2$ . The adsorption data were collected until the saturation was reached. For all isotherms, temperature and the pressure were set to 343 K and 24.2 MPa. In case of single adsorption VXR, MWCNT and BP2000 carbon supports were used. In case of binary adsorption Ru precursor was impregnated onto the Pt/MWCNT and Pt/BP2000 catalysts at the same conditions as single adsorption.

Adsorption studies showed that the maximum Pt loading on the carbon support which could be achieved was 9%. In order to reach higher Pt loadings, another procedure was followed. The heat treated carbon black was also placed into a pouch made of a filter paper, and the pouch was placed into the vessel together with the theoretical amount of the required precursor, depending on the desired Pt loading. The vessel was heated to 343 K using a circulating heater/cooler apparatus and then charged slowly with carbon dioxide (99.998%, Airgas) to a pressure of 13.6 MPa using a syringe pump. These conditions were maintained overnight and then the temperature was increased to 413 K for 6 h for thermal

reduction which caused the pressure to increase 31 MPa. After allowing the vessel to cool, the pouch was removed and the impregnated carbon black was weighed to determine the amount of Pt adsorbed. This reduction method resulted in Pt/VXR (15%) and (35%) catalysts. Further reduction of the Pt/VXR catalysts taken from the vessel in a tube furnace under flowing N<sub>2</sub> did not make any significant change over the Pt loading.

## 5.2 Catalyst Characterization

By using scCO<sub>2</sub> deposition method Pt/MWCNT (9.9%), Pt/BP2000 (47.5%) and Pt/VXR (9%) catalysts were prepared and characterized by X-ray diffraction (XRD) and transmission electron microscopy (TEM) in the as-synthesized condition with no subsequent cleaning or purification steps and electrochemically characterized by cyclic voltammetry measurements. The prepared catalysts were compared with commercially available Pt/C (EOTEK, 10%) and Pt/C (Tanaka, 46.5%) catalysts.

### 5.2.1 X-ray diffraction

XRD measurements were recorded by using a Cu K $\alpha$  source in a SCINTAG XDS 2000 diffractometer. The diffractometer was operated in continuous scan mode at a scan rate of 0.6 deg/min in the range of 5-80° (2 $\theta$ ).

### 5.2.2 Transmission electron microscopy

TEM samples were produced by dispersing the material ultrasonically in ethanol, transferring a drop of this suspension onto a copper mesh grid coated

with a holey carbon film, and then allowing the ethanol to evaporate. The sample was examined in a UHR JEOL 2010 FasTEM operating at an accelerating voltage of 200 kV.

### *5.2.3 Cyclic voltammetry*

The electrochemical characterization of these catalysts was obtained by using cyclic voltammetry (CV) (Pine Instrument). CV measurements were carried out in a standard three-electrode electrochemical cell. A silver-silver chloride electrode (Ag/AgCl, Cl<sup>-</sup>) was used as the reference which was externally connected to the cell by a specially designed salt bridge filled with 0.1 M KCl solution and placed as close as possible to the working electrode to decrease the ohmic resistance. The possible leakage was checked by measuring the resistance of the salt bridge in 0.1 M KCl. The obtained value of 100 kOhm ensured the absence of leakage into the HClO<sub>4</sub> solution during the 2-3 hours necessary to complete the experiment. Pt wire and a glassy carbon (GC) electrode (5 mm in diameter) were used as the counter and working electrodes, respectively. The catalyst solutions were prepared by mixing measured amounts of either the commercial or the synthesized catalysts with 1 ml deionized water, 1 ml 1,2-propandiol and 400 μL % 5 wt Nafion solution (Ion Solutions Inc.). The amount of the catalyst in solution was in the range of 22-25 mg, which correlates to the Pt loading in the support. In all experiments the catalyst loading on the GC electrode was set to 28 μgPt cm<sup>-2</sup>. The suspension was homogenized for 1 h using an homogenizer (Ultra-Turrax® T25) followed by deposition of 5.8 μl of this solution onto the GC electrode and overnight drying.

CV data were collected in a 0.1 M HClO<sub>4</sub> electrolyte saturated with hydrogen for 30 min to remove the oxygen. Prior to the experiments the hydrogen supply



tube was taken out of the solution and placed on the top of the electrolyte solution. All the experiments were performed at room temperature. After 10 cycles between 0.0-0.8 V at a scan rate of  $50 \text{ mV s}^{-1}$ , the stabilized CV curves were recorded. In all the figures CV data are given with respect to normal hydrogen electrode (NHE). To determine the oxygen reduction reaction (ORR) kinetics, firstly the electrolyte was saturated with oxygen for 30 min and the rotation speed was varied between 100 and 2500 rpm. The hydrodynamic voltammograms were recorded in the range of 0.0-0.8 V at a scan rate of  $10 \text{ mV s}^{-1}$  in order to prevent the oxidation of the carbon support that usually occurs at 1.2 V (Gasteiger et al., 2004). Calculation of electrochemical surface area (ESA) was performed by using the area under the reduction part of the curve according to the equation given elsewhere (Smirnova et al., 2005).

### **5.3 Scope of the experiments**

Supercritical carbon dioxide deposition method was used to prepare Pt and PtRu based electrocatalysts which were then characterized by XRD, TEM and CV. Table 5.1 shows the catalyst preparation conditions and the tests performed to the catalysts prepared.

Table 5.1 Catalyst preparation conditions and tests performed to the catalysts prepared by scCO<sub>2</sub>

Support	Precursor	Catalyst	Tests performed	T (K)	P (MPa)
VXR	PtMe <sub>2</sub> COD	Pt/VXR (9%)	Adsorption kinetics, XRD, TEM, CV	343	24.3
VXR	PtMe <sub>2</sub> COD	Pt/VXR (15%)	XRD, TEM, CV	343 413	13.6 31.0
VXR	PtMe <sub>2</sub> COD	Pt/VXR (35%)	XRD, CV	343 413	13.6 31.0
MWCNT	PtMe <sub>2</sub> COD	Pt/MWCNT (15%)	Adsorption kinetics, XRD, TEM, CV	343	24.3
BP2000	PtMe <sub>2</sub> COD	Pt/BP2000 (47.5%)	Adsorption kinetics, XRD, TEM, CV	343	24.3
VXR	Ru(COD)(Tmhd) <sub>2</sub>	Ru/VXR	Adsorption kinetics	343	24.3
MWCNT	Ru(COD)(Tmhd) <sub>2</sub>	Ru/MWCNT	Adsorption kinetics	343	24.3
BP2000	Ru(COD)(Tmhd) <sub>2</sub>	Ru/BP2000	Adsorption kinetics	343	24.3
Pt/MWCNT	Ru(COD)(Tmhd) <sub>2</sub>	PtRu/MWCNT	Adsorption kinetics	343	24.3
Pt/BP2000	Ru(COD)(Tmhd) <sub>2</sub>	PtRu/BP2000	Adsorption kinetics	343	24.3

## CHAPTER 6

### EXPERIMENTAL STUDIES FOR MICROWAVE IRRADIATION

The microwave irradiation experiments were performed at METU Fuel Cell Research Laboratory. After the preparation of the catalysts, these catalysts were characterized by using XRD (METU, Metallurgical Engineering) and XPS (METU, Central Laboratory). The fuel cell tests were also performed in Fuel Cell Research Laboratory by using the home made test station.

The full fuel cell test which gives the voltage-current density relationship is the primary technique for the characterization of fuel cell performance. The performance of a fuel cell (geometry, catalyst/electrode characteristic, and electrolyte/membrane properties) under specified operating conditions (concentration, flow rate, pressure, temperature and relative humidity) is a function of the kinetic, ohmic and mass transfer resistances. The performance curve obtained gives information about the cell losses under the operating conditions. For better characterization of the fuel cell, the effects of both system components and operating conditions have to be analyzed by performance curves (Cooper et al., 2005). Because by using performance curves of fuel cells one can determine which performance loss dominates, and draw a new route to compensate the inverse effect.

## 6.1 Catalyst preparation

### 6.1.1 Materials

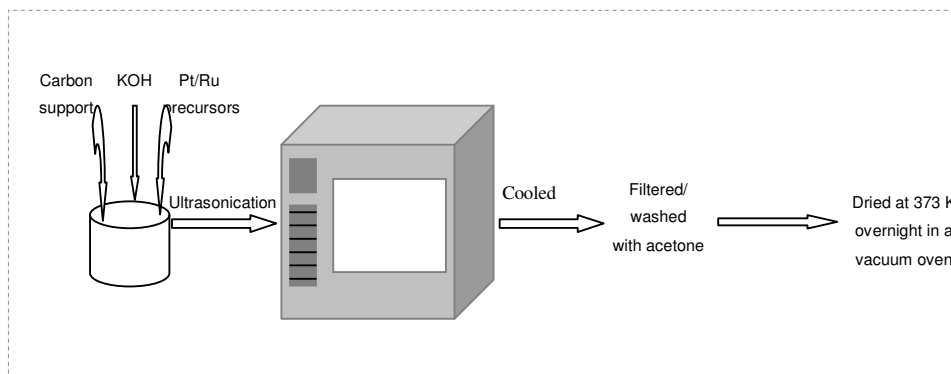
Carbon blacks (Cabot International); Black Pearl 2000 (BP2000), Regal 330 (Regal), Vulcan XC72 (pelleted, VX) which have different surface areas 1450, 94, 254 m<sup>2</sup>/g, respectively, were used as the carbon support material. As platinum and ruthenium precursors hexachloroplatinic acid (H<sub>2</sub>PtCl<sub>6</sub>) and ruthenium (III) chloride (RuCl<sub>3</sub>) (Aldrich) were used. As the surfactant, 3-N-N dimethyldodecylammonio-propanesulfonate (SB12) (Fluka) was used. KOH (Merck) was used as the base and ethylene glycol (Merck) was used as the reducing agent. All the materials were used as received, no further treatment was applied. In the catalyst preparation a domestic microwave oven (Akai, 2450 MHz, 800 W) was used. The commercial Pt (20% Pt/C, ETEK) and PtRu based (20 and 40% PtRu/C, ETEK) catalysts were selected for comparison.

### 6.1.2 Experimental procedure

Pt/VX, Pt/BP2000, Pt/Regal and PtRu/VX catalysts were prepared by using microwave heating of ethylene glycol solutions of the metal precursors. At first, 0.05 M aqueous solutions of metal precursors were prepared. A required volume of these solutions which corresponds to the desired Pt loading was mixed with 50 ml ethylene glycol (EG) in a 100 ml beaker. The base concentration of the solution was adjusted by using 0.4 M KOH solution. Then, 0.1 g carbon black was added to the solution. After ultrasonication for half an hour, the mixture was put in the center of the microwave oven and heated for 30-120 s by means of a 800 W microwave power. The resulting suspension was cooled immediately, and then filtered and the residue was washed with acetone. The solid product was dried at 373 K overnight in a vacuum oven. The

schematic representations of the single and binary catalyst preparations with and without surfactant-stabilized microwave irradiation are given in Figure 6.1.

(a)



(b)

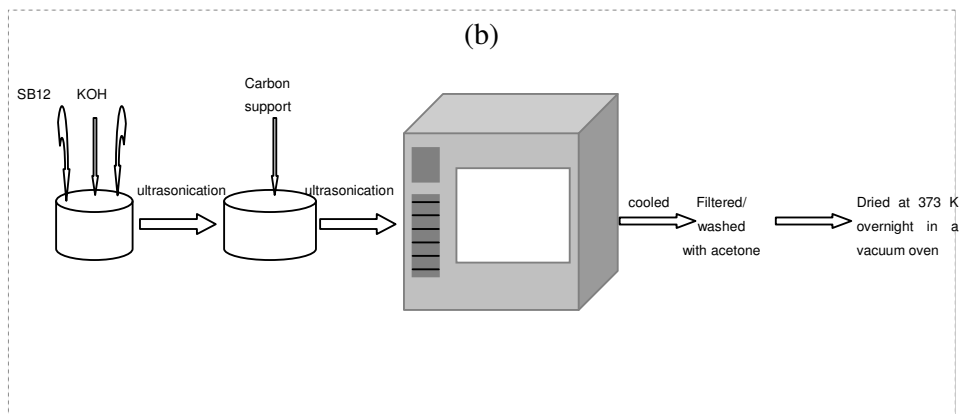


Figure 6.1 Schematic representations of (a) Pt and PtRu based catalyst preparation without surfactant (b) Pt and PtRu based catalyst preparation with the surfactant

## **6.2 Catalyst characterization**

### *6.2.1 X-ray diffraction*

In order to identify the crystalline phases, X-ray diffraction technique was used. The Rigaku D/MAX2200 diffractometer with a CuK $\alpha$  radiation source was used for the analysis. The scanning range of  $2\theta$  was set between 15° to 85° with a step size of 0.01°.

### *6.2.2 X-ray photoelectron spectroscopy*

The valence states of Pt and Ru were investigated in UNI-SPECS ESCA system (Specs GMBH., Germany) with monochromator, using Mg K $\alpha$  ( $\lambda=1253.6$  eV) as the X-ray source. A computer program (XPSPeak4.1) was used to analyze the XPS data by background subtraction (Shirley method) and curve fitting for the studied envelopes.

## **6.3 PEM fuel cell tests**

Before passing through the PEM fuel cell tests, the main part of the fuel cell consisting of the membrane electrode assembly was prepared. The procedure includes firstly the preparation of the catalyst ink and then MEAs were prepared by spraying method developed in the fuel cell laboratory. After the MEA preparation the single PEM fuel cell is constructed. The fuel cell tests were performed by using the home made fuel cell test station.

### 6.3.1 Catalyst ink preparation

The catalyst ink contains catalyst, 2-propanol, deionized water and Nafion solution. In the catalyst ink 2-propanol: deionized water ratio is 2:1. The platinum loading is  $0.4 \text{ mg Pt cm}^{-2}$ , (20% Pt/C, ETEK) whereas Nafion (5% Nafion solution, Ion Power) loading is 30% on a dry basis. In case of the binary catalysts, the PtRu loading is  $0.4 \text{ mg PtRu/cm}^2$ . The required amounts of these chemicals were weighed and then mixed together. After preparation of this mixture it was stirred in an ultrasonic stirrer for at least 1 hour. The Pt based catalysts prepared by microwave irradiation are used as cathode catalysts where the anode side catalyst was commercial Pt/C (ETEK, 20%) catalyst. The PtRu based catalysts prepared by microwave irradiation are used as anode catalysts where in this case the cathode side catalyst was commercial Pt/C (ETEK, 20%) catalyst. For comparison commercial binary PtRu/C (ETEK, 20% and 40%) catalysts are also used as anode electrode.

### 6.3.2 Membrane Electrode Assembly Preparation

In its simplest form, the membrane electrode assembly (MEA) consists of a membrane, two active catalyst layers, and two gas diffusion layers (GDL). Presently, two MEA preparation techniques have been used which are given in Figure 6.2. In Mode 1 the catalyst ink is directly applied on GDL. The prepared catalyst ink was sprayed directly on the treated GDL until the required Nafion and platinum loading was attained and then these catalyst coated GDLs were hot pressed at 403 K,  $172 \text{ N/cm}^2$  for 3 minutes onto the membrane and this is the method to obtain 5 layer MEA (Bayrakçeken et al., 2007).

Mode 2 is the application of catalyst directly on to the membrane. The prepared catalyst ink was sprayed onto the Teflon blanks which were as long as the size of electrode active area. After this application Teflon blanks were hot pressed

on the membrane at the conditions mentioned in Mode 1 and then cooled for 30 minutes (Yazaydin, 2003). The MEA obtained from this method was a 3 layer MEA which did not include GDLs. So GDLs were added later. Catalyst ink was either sprayed onto GDL or Teflon blank by a spray gun. Previous studies showed that the reproducibility of Mode 2 was very low. So, for all the experiments, Mode 1 MEA preparation technique was used.

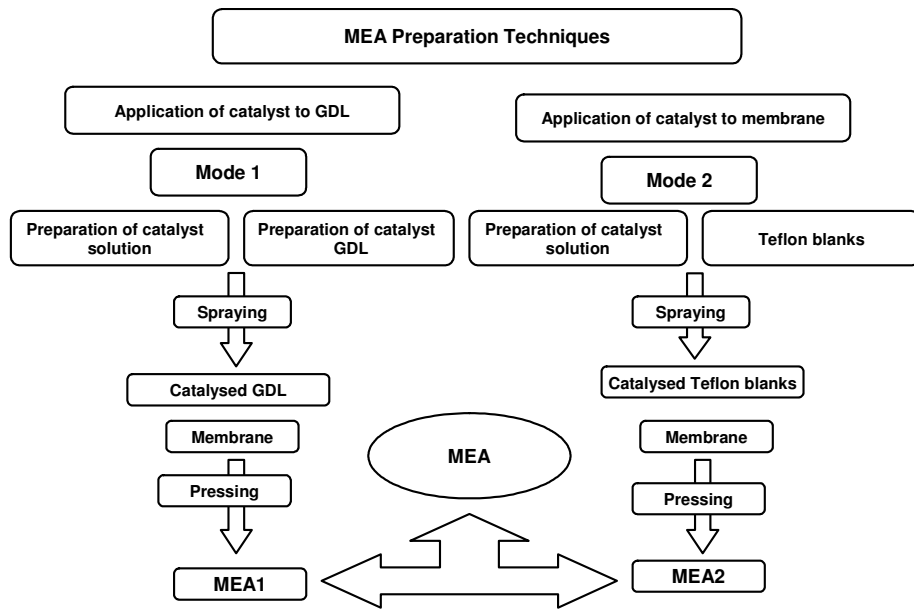


Figure 6.2 Flow chart for MEA preparation techniques

Then, this catalyst solution was sprayed onto the gas diffusion layer (GDL 31 BC, from SGL Carbon, Germany). After hot-pressing of these GDLs onto the Nafion 112 (50  $\mu\text{m}$  nominal thickness) membrane five layer MEA was obtained.



### *6.3.3 Single PEM Fuel Cell Construction*

The prepared MEA is placed into the commercially available PEM fuel cell hardware (Electrochem, FC05-01 SP REF) which had an electrode active area of 5 cm<sup>2</sup>. In this hardware the gas distribution plates were made of graphite with four channel serpentine flow channels and the current collection was achieved by using the coated metal. The MEA was placed between the two graphite plates and then they were covered by current collectors. The single PEM fuel cell sealing and the compression are very important. If sealing had failed hydrogen and oxygen gases would be mixed and since there is catalyst MEA could burn resulting in the burning of the MEA. Silicone (0.2 mm) gaskets are used to prevent the gas leakage. The torque was adjusted to 1.7 Nm diagonally on each bolt by a torque wrench.

### *6.3.4 Fuel Cell Test Station*

The fuel cell tests were performed in a home made fuel cell test station which is shown in Figure 6.3. The test station is suitable for testing single fuel cells and also short stacks. The reactant gas flow rates are adjusted with mass flow controllers (Aalborg GFC 171). There are four mass flow controllers in the system by which the flow rates of H<sub>2</sub>, O<sub>2</sub>, CO and CO<sub>2</sub> can be adjusted. So, by using the mass flow controllers, the simulated reformat gas composition can be prepared. Prior to entering the fuel cell, these gases were humidified by passing them through the water columns contained in stainless steel cylinders and heated with resistance heaters. The stainless steel gas lines were heated to prevent the condensation of the water in the lines. The temperature in the humidifiers, gas lines and fuel cell were controlled by PID temperature controllers (GEMO DT442) and K type thermocouples. The purge gases left through the water columns placed at the exit of the fuel cell.

The polarization curves were obtained by using a commercially available electronic load (Dynamload). Polarization curves were obtained after reaching the steady state by using a certain protocol (Appendix D). Briefly, due to this protocol, the fuel cell was operated overnight at 0.5 V. Then the data were collected at time intervals of 15 min until no more change was observed in the performance. In the performance tests, the flow rates of reactant gases were set to 0.1 slm for both gases by using mass flow controllers. Also the carbon dioxide percentage in the hydrogen was adjusted with mass flow controller.

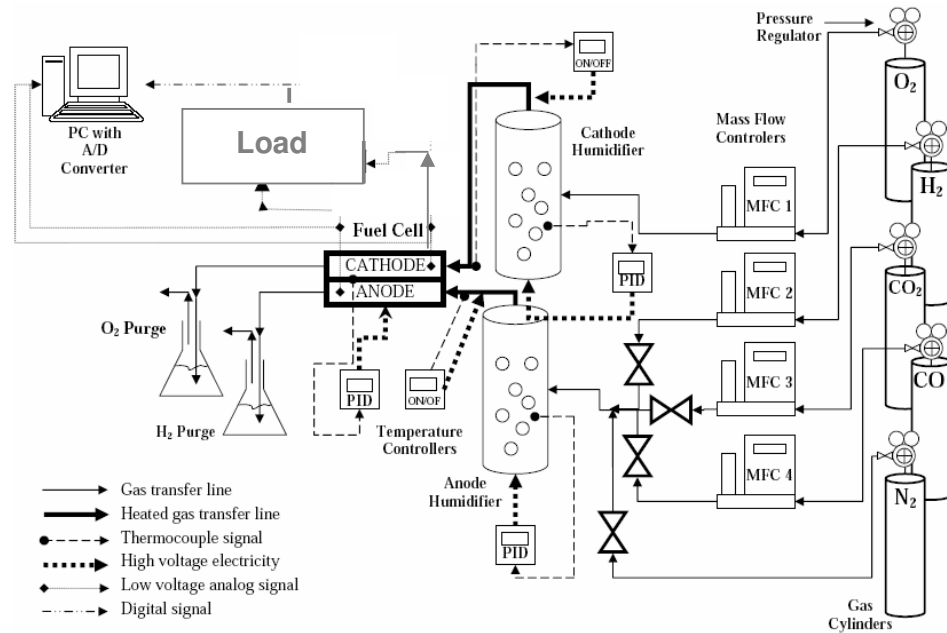


Figure 6.3 Flow chart for the fuel cell test station (modified version of Erkan, 2005)

## 6.4 Scope of the experiments

By using microwave irradiation method the Pt and PtRu based catalysts given in Table 6.1 were prepared by changing the microwave duration, carbon black, base concentration and surfactant/precursor (S/Pt) ratios.

Table 6.1 Catalysts prepared by microwave irradiation

Catalyst	Initial Pt (%)	BC (g/l)	Microwave duration (s)	S/Pt	Tests performed
Pt/VX	20	0.14	50	0	XRD, PEMFC
Pt/VX	20	0.27	50	0	XRD
Pt/VX	20	0.54	50	0	XRD, XPS, PEMFC
Pt/VX	20	0.14	30	0	XRD
Pt/VX	20	0.14	60	0	XRD, PEMFC
Pt/VX	20	0.14	90	0	XRD, PEMFC
Pt/VX	20	0.14	120	0	XRD, PEMFC
Pt/Regal	20	0.54	50	0	XRD, XPS, PEMFC
Pt/BP2000	20	0.54	50	0	XRD, XPS, PEMFC
PtRu/VX	30	0.54	50	0	XRD, PEMFC
Pt/VX (SB12)	20	0.54	50	10	XRD, PEMFC
Pt/VX (SB12)	20	0.54	50	40	XRD, PEMFC
PtRu/VX (SB12)	30	0.54	50	80	XRD, PEMFC

MEAs were prepared by using Pt based catalysts as cathode electrodes where the anode side was commercial ETEK catalyst (20% Pt/C). In case of prepared PtRu based catalyst, these prepared catalysts were used as anode electrode and the cathode was also commercial ETEK catalyst (20% Pt/C). It is known that the dilution of the input gases entering the fuel cell has an adverse effect on fuel cell performance. To eliminate this effect in carbon dioxide experiments,

the hydrogen flow rate was set to 0.1 slm and the percentage of CO<sub>2</sub> was varied by taking into account this value. To see the CO<sub>2</sub> effect on PEMFC performance a commercially available MEA was used (Electrochem MEA) and the amount of CO<sub>2</sub> was varied from 0 to 50%. For the testing of the binary PtRu/C catalysts the percentage of CO<sub>2</sub> gas was set to 30%. The cell temperature, and also the anode and cathode humidification temperatures were set to 70<sup>0</sup>C in all the experiments. To eliminate the condensation of the humidified gases, the inlet gas lines were heated to 72<sup>0</sup>C.

## CHAPTER 7

### RESULTS AND DISCUSSION OF THE CATALYSTS PREPARED BY SUPERCRITICAL CARBON DIOXIDE DEPOSITION

#### 7.1 Adsorption kinetics of Pt and Ru organometallic precursors on different carbon supports

Decoration of the support materials with either Pt or Ru nanoparticles were achieved by the dissolution of the organometallic precursors in the scCO<sub>2</sub> and then exposure to the carbon substrates. After reduction of the precursors to their metallic form, metal/support nanocomposites were obtained. In this aspect, the adsorption phenomenon is very crucial for the control of the metal loading onto the substrate. By changing the adsorption conditions and the amount of the precursor dissolved in scCO<sub>2</sub>, one can control the metal loading (Saquing et al., 2005). Pt based catalysts were prepared by dissolving Pt precursor in the scCO<sub>2</sub> and then exposure to the carbon supports of VXR, MWCNT and BP2000. For PtRu based catalysts, Ru precursor was dissolved in the scCO<sub>2</sub> and then exposure to the Pt/MWCNT and Pt/BP2000 catalysts. It was observed that the adsorption phenomena for the Pt and PtRu based adsorption show some differences.

The carbon supports used in the experiments had a wide range of surface area and pore size distributions. The surface area properties of carbon supports used in the scCO<sub>2</sub> deposition experiments are summarized in Table 7.1. The carbon supports of VXR, BP2000 and MWCNT were used in the experiments. As can

be seen from the table these carbon supports have different total surface areas, macro/meso and microporous areas.

Table 7.1 Surface area properties of carbon supports used in the present experiments and previous studies

Support	$S_{\text{tot}}$ (m <sup>2</sup> /g)	$S_{\text{meso/macro}}$ (m <sup>2</sup> /g)	$S_{\text{micro}}$ (m <sup>2</sup> /g)
BP2000 <sup>a</sup>	1450	515	935
MWCNT	300	--	--
VXR <sup>b</sup>	232	145	87
CA4 <sup>c</sup>	741	489	252
CA22 <sup>c</sup>	670	437	233

<sup>a</sup>Kruk et al,1996

<sup>b</sup>Yu, 2005

<sup>c</sup>Saquin et al., 2005

Kinetics of the the Pt/VXR is shown in Figure 7.1. Figure 7.1 illustrates the adsorption kinetics of Pt precursor on VXR. The experiments were conducted at 343 K and 24.2 MPa. This figure indicates that uptake reached to a steady state value after 6 hours. So, the adsorption experiments were performed for this time period.

An adsorption process is influenced by support-precursor interactions and adsorption conditions. The metal loading can be controlled by adsorption process, so that for catalyst preparation it is especially very crucial. The adsorption isotherm was obtained at 343 K and 24.2 MPa. The adsorption

isotherm for CODPtMe<sub>2</sub>, scCO<sub>2</sub> and different carbon supports is given in Figure 7.2. As can be seen from Figure 7.2 uptake of precursor strongly depends on the type of the supports which have different surface areas and pore size distributions, adsorption behavior and so the metal loading changed significantly. The higher the uptakes were, the higher the platinum loadings obtained. The platinum loadings were 9, 15 and 47.5% for Pt/VX, Pt/MWCNT and Pt/BP2000, respectively. The adsorption isotherm showed the partitioning of the Pt precursor between the carbon support and scCO<sub>2</sub>. These isotherms were fitted to Langmuir type model as given below:

$$q = \frac{K_1 Q_o c}{1 + K_1 c} \quad (7.1)$$

where  $K_1$  (g scCO<sub>2</sub>/mg precursor) is the Langmuir adsorption constant,  $Q_o$  (mg precursor/g support) is the adsorption capacity,  $c$  (mg precursor/g scCO<sub>2</sub>) is the solution concentration and  $q$  (mg precursor/g support) is the uptake by the adsorbent. After the regression, the Langmuir equilibrium constants obtained for this system are given in Table 7.2.

$Q_o$ , is the maximum number of the available sorption sites that the carbon supports can supply for the Pt precursor molecules in case of the Langmuir isotherm. The adsorption capacity of CODPtMe<sub>2</sub> on carbon support,  $Q_o$ , is increased by the increasing surface areas. Although the difference between the surface area of the VXR and MWCNT was not doubled as given in Table 7.1,  $Q_o$  value of MWCNT was twice of VXR. This indicates that available sorption sites of MWCNT are higher than that of VXR.  $K_1 Q_o$  value is a measure of the relative affinity of the solute towards the surface of the adsorbent. High  $K_1 Q_o$  values indicate that the CODPtMe<sub>2</sub> has more affinity for carbon supports than scCO<sub>2</sub>.

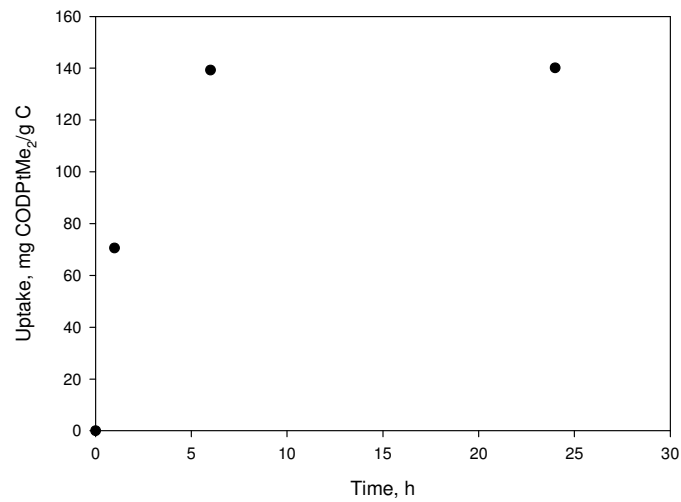


Figure 7.1 Equilibrium curve for Pt/VXR

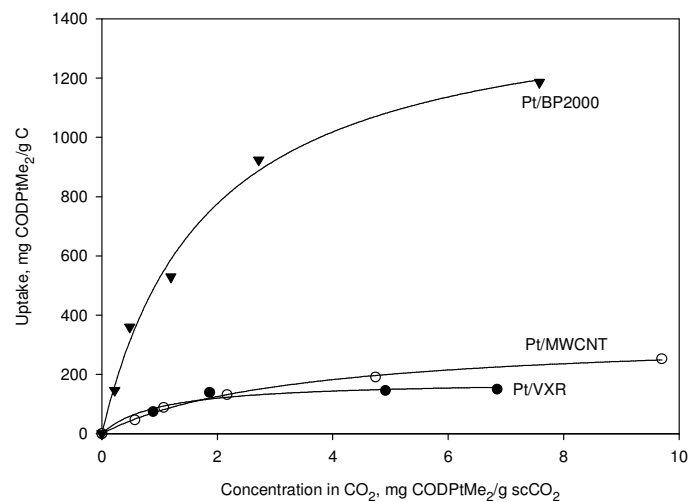


Figure 7.2 Adsorption isotherms of CODPtMe<sub>2</sub>, scCO<sub>2</sub> on different carbon supports in scCO<sub>2</sub> (lines represents Langmuir (Eqn 7.1) fits for the corresponding catalysts)



Table 7.2 Langmuir equilibrium constants for CODPtMe<sub>2</sub> on different carbon supports obtained in scCO<sub>2</sub> at 343 K and 24.2 MPa

Catalyst	$K_l$	$Q_o$	$K_l Q_o$	$R^2$
Pt/VXR (9%)	0.87	180	156	0.980
Pt/MWCNT (9.9%)	0.29	335	100	0.998
Pt/BP2000 (47.5%)	0.54	1481	801	0.993
Pt/CA4	0.79	1200	953	0.982
Pt/CA22	0.66	2000	1320	0.988

The adsorption isotherms for Ru(COD)(Tmhd)<sub>2</sub> in scCO<sub>2</sub> and different carbon supports are given in Figure 7.3 and also the Langmuir equilibrium constants of Eqn 7.1 of Ru catalysts are given in Table 7.3. A similar trend for adsorption of Ru(COD)(Tmhd)<sub>2</sub> on carbon support was observed. It has been found that  $Q_o$  values increase as the surface area increases. High  $K_l Q_o$  values also indicate that the affinity of Ru(COD)(Tmhd)<sub>2</sub> for carbon support is more than scCO<sub>2</sub>.

The aim of these adsorption studies was to determine the maximum metal loading that can be achieved on the carbon support under the adsorption conditions. It was observed that after the equilibrium was reached, dissolution of more organometallic precursor did not increase the metal loading on the support. So, platinum or ruthenium loading on the carbon supports is governed by thermodynamic control.

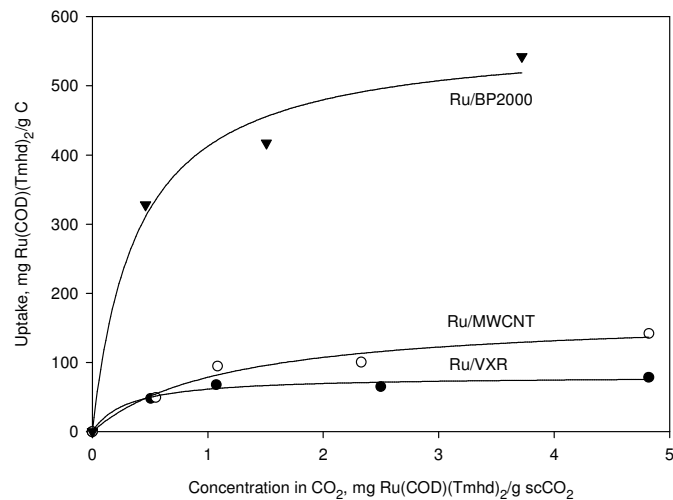


Figure 7.3 Adsorption isotherms for Ru(COD)(Tmhd)<sub>2</sub>, scCO<sub>2</sub> on different carbon supports at 343 K and 24.2 MPa (lines represents Langmuir (Eqn 7.1) fits for the corresponding catalysts)

Table 7.3 Langmuir equilibrium constants for Ru(COD)(Tmhd)<sub>2</sub> on different carbon supports in scCO<sub>2</sub> at 343 K and 24.2 MPa

Catalyst	$K_l$	$Q_o$	$K_l Q_o$	$R^2$
Ru/VXR	3.32	80	258	0.974
Ru/MWCNT	0.87	169	147	0.984
Ru/BP2000	2.58	572	1476	0.985
Ru/CA4	4.02	175	704	0.930
Ru/CA22	2.08	499	1039	0.981

The adsorption capacities for different carbon supports against the meso and macro surface area and total surface area are given in Figures 7.4 and 7.5, respectively.

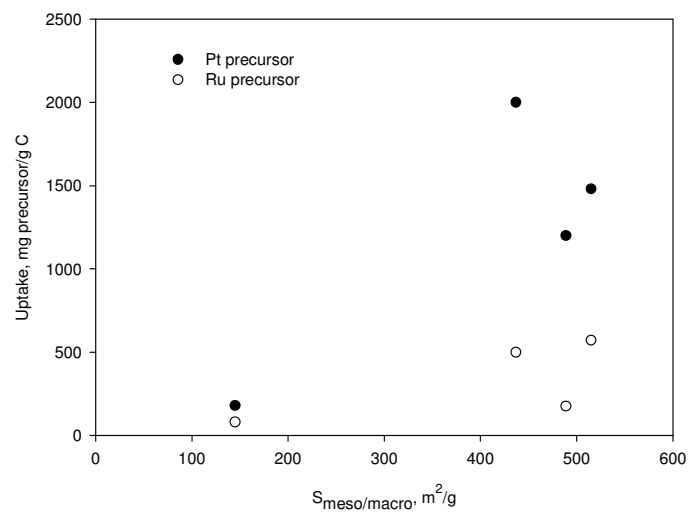


Figure 7.4 Uptake of Pt or Ru precursors on carbon supports with different mesoporous and macroporous surface area

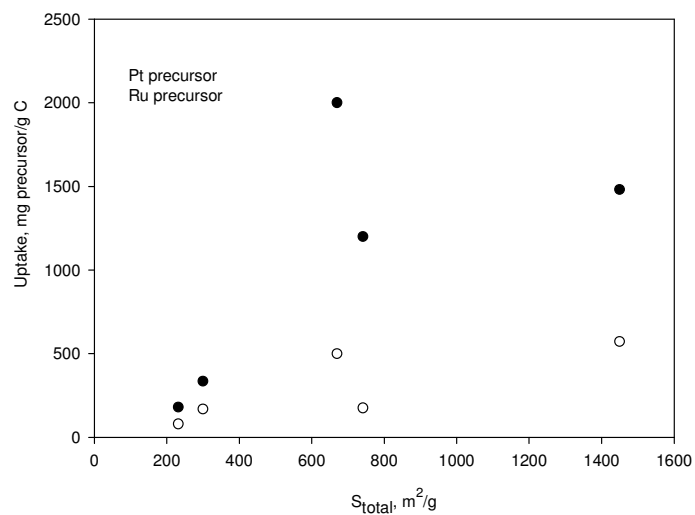


Figure 7.5 Uptake of Pt or Ru precursors on carbon supports with different total surface area

As can be seen from Figure 7.4 and 7.5 that uptake increases by increasing total surface area and the ratio of meso and macro surface area. But for CA22 (Saquing et al, 2005) it is seen that although it has a lower  $S_{\text{tot}}$  and  $S_{\text{meso,macro}}$  its uptake is higher than other carbon supports. This can be because of the accessibility of the total surface area of the CA22 is higher than others. To obtain higher uptakes and so higher metal loadings support properties and accessibilities of the pores are very critical.

The structure of the pores of the adsorbents and the molecular size of the adsorbate affect the accessibility of the sorption sites. If it is considered that the  $\text{CODPtMe}_2$  and  $\text{Ru(COD)(Tmhd)}_2$  precursor molecules are spherical and the diameters are 0.5 nm and 1 nm, respectively, the area covered by the precursors can be calculated by using Eqn (7.2):

$$S = Q_o A \pi r^2 \quad (7.2)$$

where  $S$  is the area covered by precursor,  $Q_o$  is the capacity,  $A$  is the Avogadro's number, and  $r$  is the radius of either Pt or Ru precursor (Zhang et al., 2005). The areas covered by either Pt or Ru organometallic precursors are given in Table 7.4. As can be seen from the table, the area covered by the precursor is increasing with the increase in the total surface area for all cases. The adsorptions of Ru precursor over Pt/MWCNT and Pt/BP2000 catalysts were also investigated. Figure 7.6 shows the adsorption behavior. Also, this isotherm was fitted to Langmuir adsorption isotherm and the Langmuir constants are summarized in Table 7.5.

Table 7.4 Area covered by Pt or Ru organometallic precursors on different carbon supports

Catalyst	$S_{Pt}$ (m <sup>2</sup> /g)	$S_{Ru}$ (m <sup>2</sup> /g)
Me/VXR	64	66
Me/MWCNT	119	139
Me/BP2000	525	470

Me represents either Pt or Ru

Table 7.5 Langmuir equilibrium constants for Ru(COD)(Tmhd)<sub>2</sub>, scCO<sub>2</sub> and Pt/BP2000, Pt/MWCNT

Catalyst	$K_l$	$Q_o$	$K_l Q_o$	$R^2$
PtRu/MWCNT	0.52	171	89	0.944
PtRu/BP2000	1.66	470	780	0.997

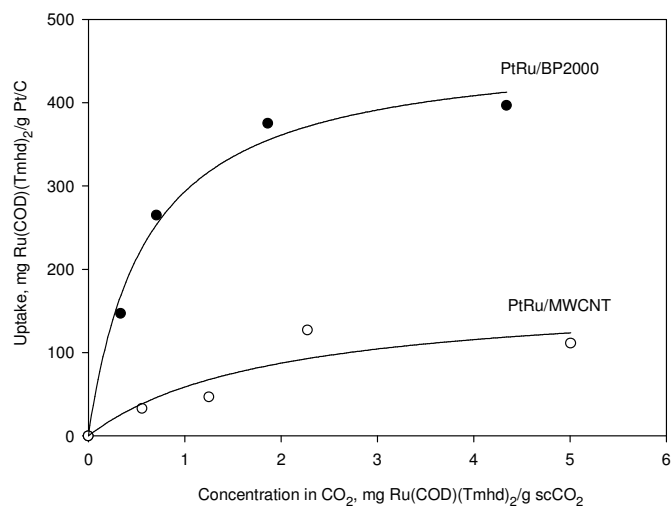
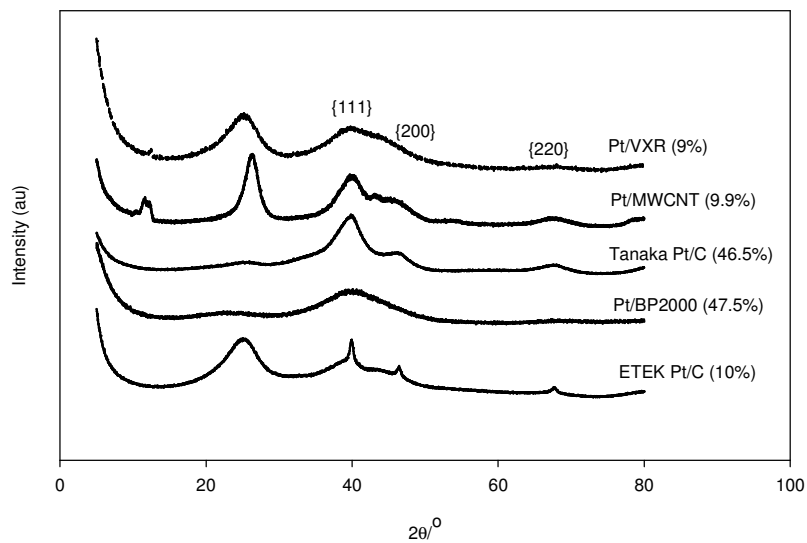


Figure 7.6 Adsorption isotherm for Ru precursor at 343 K and 24.2 MPa on Pt/C catalysts (lines represents Langmuir (Eqn 7.1) fits for the corresponding catalysts)

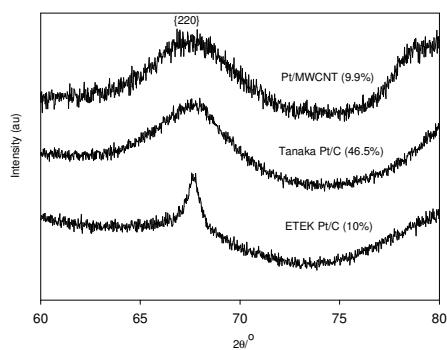
## 7.2 XRD and TEM results

The XRD spectra for the prepared and commercial catalysts are presented in Figure 7.7 (a). For all catalysts the characteristic {111}, {200}, {220} peaks for face-centered cubic (fcc) Pt were obtained. Since the {111}, and {200} Pt peaks overlapped, to produce the broad C peaks, the sizes of the Pt particles were calculated from the Scherrer equation using the half-full-width at half maximum of the {220} reflection (Zhao et al., 2006). Sample calculation is given in Appendix A. High-resolution XRD spectra obtained over the range  $2\theta = 60^\circ\text{-}80^\circ$  from the catalysts ETEK Pt/C, Tanaka Pt/C, Pt/MWCNT and Pt/BP2000, Pt/VXR are given in Figures 7.7 (b) and (c), respectively. The equivalent surface area (SA) of the metal phase (Pt) was determined using the mean particle sizes obtained from the XRD data (Pozio et al., 2002). The mean particle sizes are given in Table 1 and indicate that highly dispersed Pt catalysts with small Pt particle sizes were obtained by using the  $\text{scCO}_2$  deposition method.

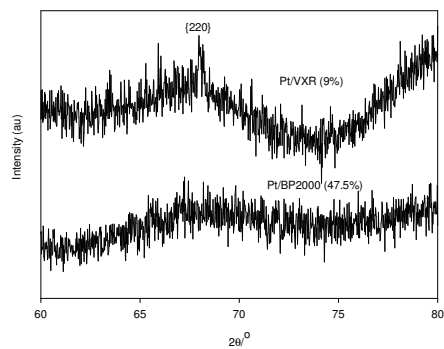
The HRTEM images of the synthesized and commercial catalysts are presented in Figures 7.8 for Pt/MWCNT (a),(b), Pt/VXR (c),(d), Pt/BP2000 (e),(f) and Figure 7.9 for ETEK Pt/C (a)-(d). In agreement with XRD data, it can be seen that a small Pt particle size of about 1-2 nm and uniform Pt distribution can be achieved using the  $\text{scCO}_2$  deposition method. The size of the Pt particles of ETEK catalyst Pt/C (10 wt %) was reported as 2-3 nm (Gloaguen et al., 1997 and the ETEK company). However, the calculations based on the XRD data resulted a particle size of 6 nm. The reason for this discrepancy might be due to the broad Pt particle size distribution in the ETEK catalyst as can be seen from the TEM data presented in Figure 7.9 (g)-(k). On the contrary, there is a good agreement between XRD and TEM data for the catalysts synthesized by the  $\text{scCO}_2$  deposition technique, indicating that they have a very narrow particle size distribution.



(a)



(b)



(c)

Figure 7.7 XRD patterns for the prepared and commercial catalysts a) whole scan for all catalysts b) narrow scan for Pt/MWCNT, Pt/C (Tanaka), Pt/C (ETEK) c) narrow scan for Pt/VXR and Pt/BP2000

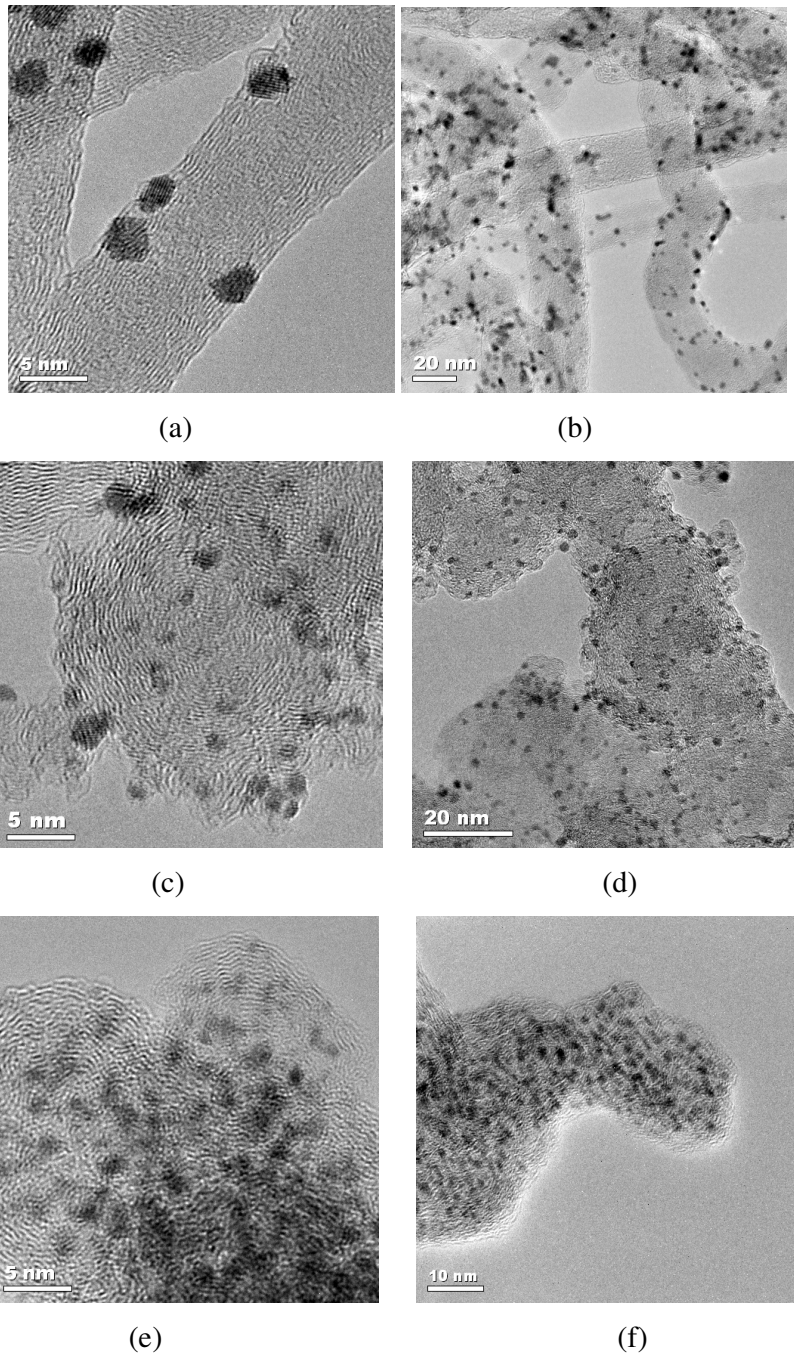


Figure 7.8 Bright field and HRTEM images for catalysts (a) and (b) Pt/MWCNT, (c) and (d) Pt/VXR, (e) and (f) Pt/BP2000



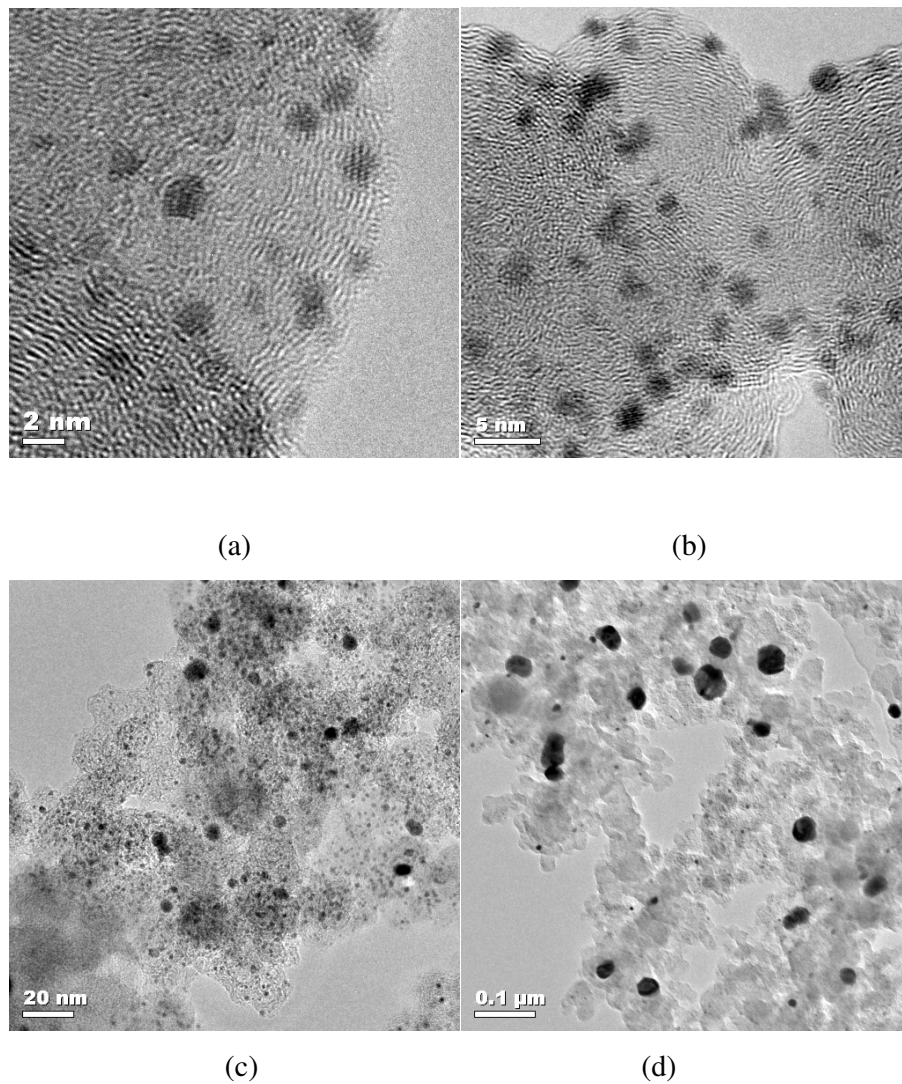


Figure 7.9 Bright field and HRTEM images for catalysts (a)-(d) Pt/C-ETEK

Among the carbon supports, the BP2000 has the highest surface area and it is this support on which the highest Pt loading was achieved in this work (47.5%). This is due to highest uptake of the Pt precursor due to the highest

surface area. However, for the Pt/BP2000 catalysts that have different Pt loadings, the ESA values obtained were approximately the same, presumably due to similar size of the Pt particles ( $\approx 1$  nm in diameter) which was confirmed by the XRD measurements.

### 7.3 CV results

CV results for the Pt/BP2000 catalysts which have 29 and 47.5 wt % Pt loadings are given in Figure 7.10. The ESA values for the Pt/BP2000 catalysts which have 29 and 47.5 wt % Pt loadings are  $110$  and  $102 \text{ m}^2 \text{ g}^{-1}$ , respectively. Similar ESA values at substantially different loadings indicate that ESAs are primarily governed by the platinum particle size for the same support. For comparison with other prepared catalysts Pt/BP2000 (47.5%) was used.

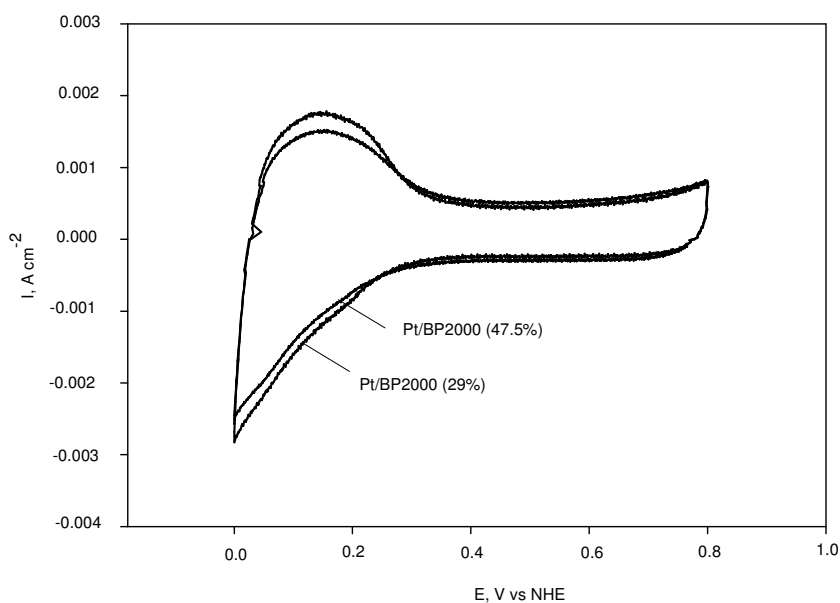


Figure 7.10 CV results for Pt/BP2000 catalysts with different Pt loadings

As demonstrated by the CV data (Figure 7.11), the catalytic activity of the Pt/VXR prepared by supercritical deposition method for the electrooxidation and reduction of hydrogen is substantially higher than the catalytic activity of the commercial Pt/C (EOTEK). Among the three different supports utilized in supercritical deposition, VXR has the highest catalytic activity. The particle size of the Pt/MWCNT and Pt/C (Tanaka) were 2 nm and the electrocatalytic activity of these catalysts showed similar results.

Electrochemical surface areas (ESAs) of the catalysts were calculated by using Eqn 7.3 taking into account the hydrogen reduction peak.

$$ESA = \frac{A}{K \cdot L \cdot S} \quad (7.3)$$

where  $A$  is the area under the curve for hydrogen reduction part excluding double layer capacitance up to second inflection point,  $K=0.21 \text{ mC/cm}^2$ ,  $S$  is the scan rate (50 mV/s) and  $L$  is the Pt loading on the electrode (Smirnova et al., 2005). The calculated SA and ESA values are given in Table 7.6.

Although Pt/VXR (scCO<sub>2</sub>) has the highest ESA and a low particle diameter (Table 7.6), the Pt utilization is only 74% (Appendix A). It can be assumed that in the case of small (~1 nm) Pt particles, the accessibility of the metal particles even in liquid electrolyte is more critical due to the partially hydrophobic nature of the carbon support. For Pt/MWCNT (scCO<sub>2</sub>) and Pt/C (Tanaka), which have larger Pt particles (2 nm), the utilization of Pt seems to be higher.

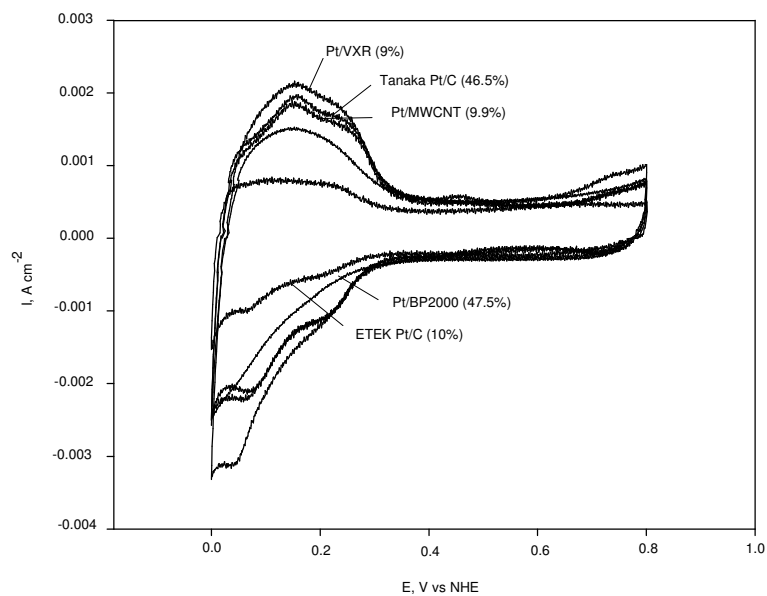


Figure 7.11 Cyclic voltammogram for the prepared catalysts in 0.1 M HClO<sub>4</sub> in H<sub>2</sub> atmosphere at a scan rate of 50 mV/s

Table 7.6 Electrochemical and total surface areas of the synthesized and commercial catalysts

Catalyst	Particle* (nm) size	SA (m <sup>2</sup> /g)	ESA (m <sup>2</sup> /g)	Pt (%)	Pt ut.
Pt/C (E TEK)	6	46.7	57	10	122
Pt/VXR (scCO <sub>2</sub> )	1.2	233.6	173	9	74
Pt/MWCNT (scCO <sub>2</sub> )	2	140.2	130	9.9	93
Pt/BP2000 (scCO <sub>2</sub> )	1	280.4	102	47.5	36
Pt/C (Tanaka)	2	140.2	128	46.5	91

\*From XRD and TEM data (Figures 7.7, 7.8 and 7.9)

Pt ut. is Pt utilization (see Appendix A)

Even though the particle size of Pt on VXR and BP2000 is approximately the same, the ESA of Pt/VXR is higher which results in a large difference in the Pt utilization for these two materials (Table 7.6). This could be due to differences in the structures of the carbon supports for these two catalysts, namely by the higher micropore volume of BP2000. Some of the platinum nanoparticles may be residing in the micropores and the electrolyte may not be contacting to these particles. The Pt utilization value of over 100% in the case of Pt/C (E-TEK) presumably arises because the Pt particle size is not uniform, as revealed in the HRTEM images for this material (Figures 7.8 g-k). We note, however, that Pt utilization values of over 100% have been reported elsewhere for E-TEK Pt/C (20%) catalyst (Shan and Pickup, 2000).

From this point forward the results are given for the high Pt loading catalysts which were prepared by reduction in supercritical carbon dioxide. To increase the platinum loading on the VXR carbon black, another reduction method was used. When reduction is carried out at atmospheric pressure in nitrogen atmosphere, the maximum loading is governed by the adsorption isotherm of the precursor between the carbon black phase and the scCO<sub>2</sub> phase. Higher loadings are possible when reduction is carried out in scCO<sub>2</sub>. In this case, after dissolving the organometallic precursor in scCO<sub>2</sub> at 343 K and 13.8 MPa for overnight, the reduction was achieved in the same vessel by increasing the temperature and pressure to 413 K and 31 MPa, respectively. By changing the conditions and reduction method, the Pt loading on the VXR was increased to 15 and 35%. This loading was controlled by the amount of the precursor put into the vessel.

The XRD spectra for the Pt/VXR (9%), Pt/VXR (15%) and Pt/VXR (35%) catalysts are given in Figure 7.12. For all catalysts characteristic patterns of Pt face-centered cubic (fcc) diffraction was obtained for {111}, {200}, {220} peaks. Because of the overlapped {111}, {200} Pt and carbon peaks, particle sizes of the catalysts were calculated by using Scherrer equation for the half-

full-width at half maximum of the {220} inflection (Appendix A). The surface area (SA) of the metal phase (Pt) was calculated from the particle sizes obtained from XRD data (Pozio et al., 2002). Particle size of Pt/VXR (35%) catalyst was obtained as 2 nm from the XRD data.

Figure 7.13 shows the bright field and high resolution TEM images for the Pt/VXR (15%) catalysts. As can be seen from the figure, by using the scCO<sub>2</sub> deposition method, not only small sized Pt particles can be obtained, but also a uniform and well Pt distribution can be achieved. Particle size was 1.3 nm for Pt/VXR (15%) catalyst. The particle sizes obtained from TEM were in good agreement with the ones obtained from XRD.

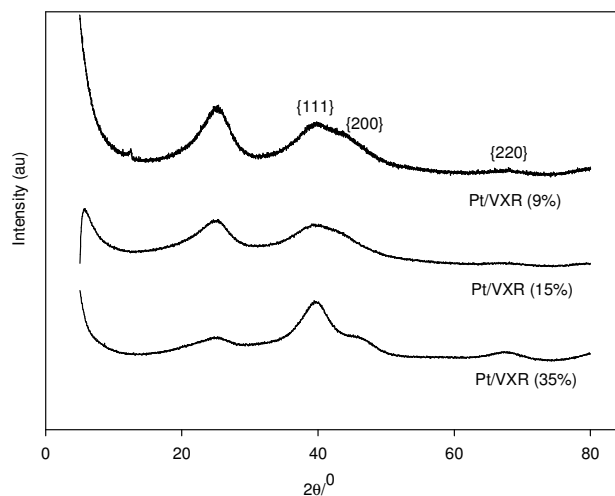


Figure 7.12 XRD pattern for high Pt loading Pt/VXR catalysts

The cyclic voltammograms for the prepared catalysts with different Pt loadings are given in Figure 7.14. As can be seen from the figure, the activity of the Pt/VXR (15%) for electrooxidation and reduction of the hydrogen is superior

to Pt/VXR (35%). Electrochemical and total surface areas of the Pt/VXR catalysts estimated from the XRD, TEM and CV data are tabulated in Table 7.7. ESAs for the 15 and 35% Pt/VXR catalysts were calculated by using Figure 12 as 125 and 87 m<sup>2</sup>/g, respectively. It was observed that when the platinum loading was increased, the particle size also increased. Although, the electrochemical surface area was higher than Pt/VXR (35%) catalyst, Pt/VXR (15%) had lower Pt utilization. High electrochemical surface area is an indication of more catalytic active sites on the catalyst.

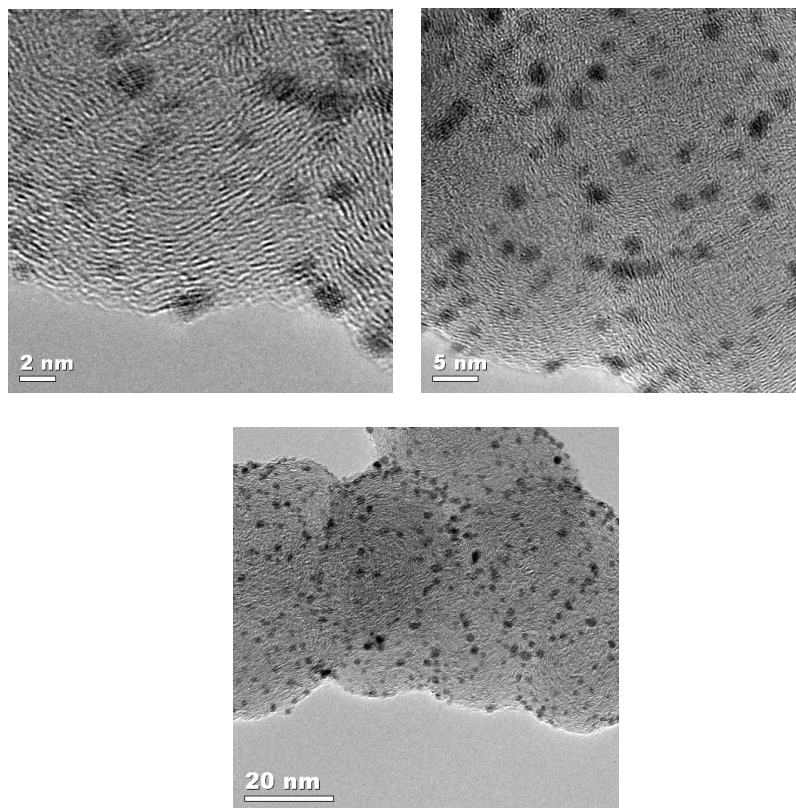


Figure 7.13 TEM images for 15% Pt/VXR

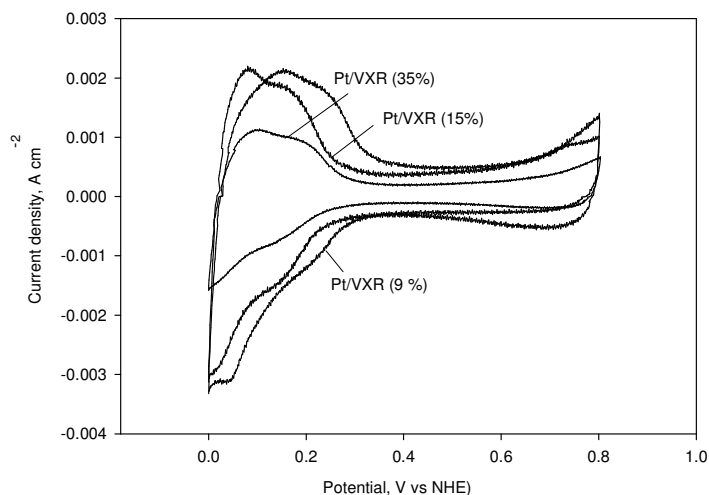


Figure 7.14 CV for high Pt loading Pt/VXR catalysts

Table 7.7 Electrochemical and total surface areas of the prepared high Pt loading catalysts

Catalyst	Particle (nm) size	SA (m <sup>2</sup> /g)	ESA (m <sup>2</sup> /g)	Pt (%)	% Pt ut.
Pt/VXR	1.3	215.7	125	15	58
Pt/VXR	2	140.2	87	35	62

But, utilization shows the active sites that are available for the reactions. In this case, the difference between the electrochemical surface areas of the Pt/VXR (15%) and Pt/VXR (35%) catalysts can be explained by the microporous structure of VXR. Pt/VXR (15%) catalyst has a particle size of 1.3 nm. Therefore, some of the Pt particles could be residing in the micropores and therefore are not accessible which causes the decrease in the utilization.



CV positive scans for O<sub>2</sub> reduction with rotation speeds varying between 100-2500 rpm at a 10 mV s<sup>-1</sup> sweep rate for the synthesized Pt/VXR, Pt/MWCNT and Pt/BP2000 catalysts are presented in Figures 7.15, 7.16 and 7.17, respectively. The CV data show similar trends to the ESA data. Thus, for Pt/MWCNT and Pt/VXR the current is higher than that for Pt/BP2000, and in all three cases the current increases gradually with the speed of rotation. The limiting current plateaus obtained for Pt/VXR and Pt/MWCNT indicate that the oxygen reduction is fast enough at high overpotentials and follows a trend (Shan and Pickup, 2000) similar to Pt/BP2000. If the electro-catalytically active sites are not distributed uniformly and the electrocatalytic reaction is slow, the current plateau becomes more inclined (Suárez-Alcantara et al., 2006).

Koutecky- Levich plots were obtained by using Eqn (7.4) and plotting  $i^{-1}$  vs  $w^{1/2}$  (Bron et al., 2002).

$$\frac{1}{i} = \frac{1}{Bw^{1/2}} + \frac{1}{i_k} \quad (7.4)$$

where  $i$  is the current,  $i_k$  is the kinetic current,  $w$  is the rotation speed and  $B$  is the Levich constant. The plots for Pt/VXR, Pt/MWCNT and Pt/BP2000 are presented in Figures 7.15(a), 7.16(a) and 7.17(a), respectively. The linearity of the plots indicate that the rotation speeds used in this study are large enough that the number of electrons transferred per oxygen molecule ( $n$ ) is independent of rotation speed. The Levich constants ( $B$ ) obtained from the slope of the Koutecky-Levich plots, were used to calculate the number of electrons transferred per O<sub>2</sub> molecule when  $w$  is expressed in revolutions per minute (González-Cruz et al., 2003; Dundar et al., 2006) using Eqn (7.5):

$$B = 0.2nFc_0D^{2/3}\nu^{-1/6} \quad (7.5)$$

where  $n$  is the number of electrons per  $O_2$  molecule,  $F$  is the Faraday constant ( $96485 \text{ C mol}^{-1}$ ),  $c_o$  is the oxygen bulk concentration ( $1.18 \cdot 10^{-6} \text{ mol cm}^{-3}$ ) (Zečević et al., 1997),  $D$  is the oxygen diffusion coefficient ( $1.9 \cdot 10^{-5} \text{ cm}^2 \text{ s}^{-1}$ ) (Zečević et al., 1997), and  $\nu$  is the viscosity of the electrolyte ( $9.87 \cdot 10^{-3} \text{ cm}^2 \text{ s}^{-1}$ ) (Mello and Ticianelli, 1997). By using the Levich constant obtained and Eqn (7.5), the number of electrons transferred was calculated as 3.5, 3.6 and 3.7 for Pt/BP2000 (1 nm), Pt/VXR (1.2 nm) and Pt/MWCNT (2 nm), respectively.

The oxygen reduction reaction is a multi-electron reaction which includes several elementary steps (Marković et al., 2001) and can follow either the  $2e^-$  or  $4e^-$  pathway, which leads to hydrogen peroxide formation or complete water formation reactions, respectively. The high number of electrons transferred per  $O_2$  molecule calculated here (close to 4) is an indication of low  $H_2O_2$  formation and an almost complete reduction of  $O_2$  to  $H_2O$ . Otherwise these values close to 2 indicate  $H_2O_2$  formation.

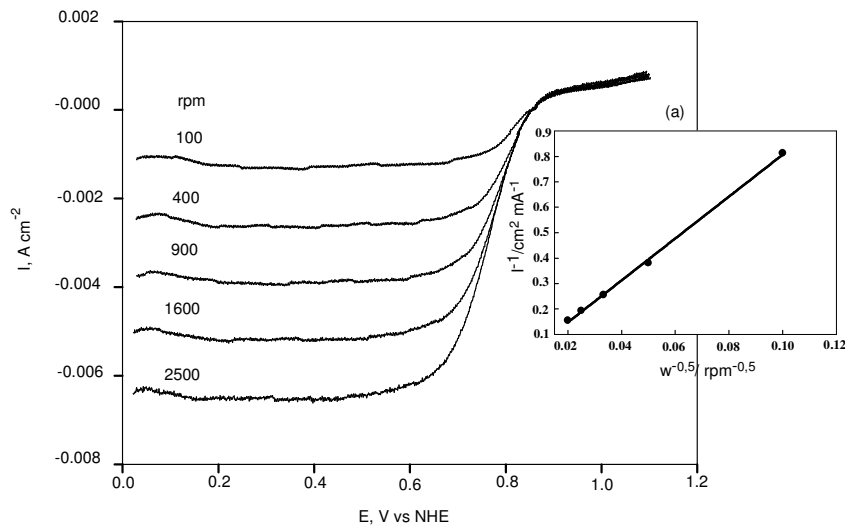


Figure 7.15 Hydrodynamic voltammograms of positive scans of Pt/VXR for  $O_2$  reduction in  $O_2$  saturated 0.1 M  $HClO_4$  (a) Koutecky-Levich plot at 0.2 V

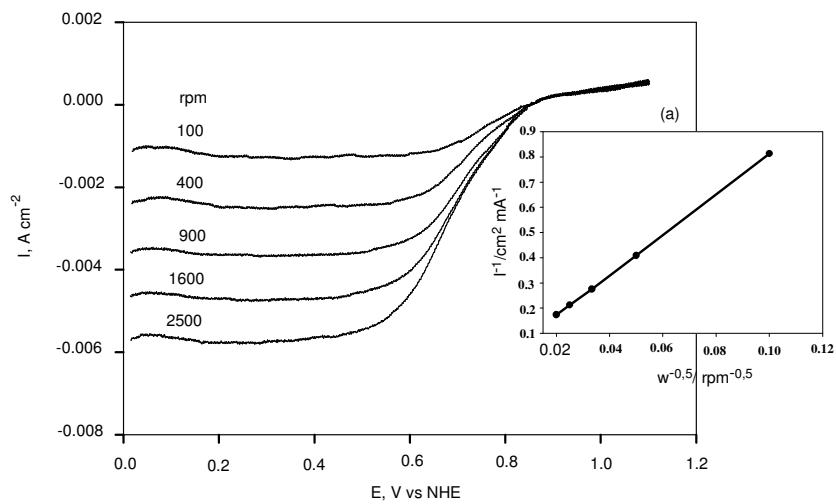


Figure 7.16 Hydrodynamic voltammograms of positive scans of Pt/MWCNT for O<sub>2</sub> reduction in O<sub>2</sub> saturated 0.1 M HClO<sub>4</sub> (a) Koutecky-Levich plot at 0.2 V

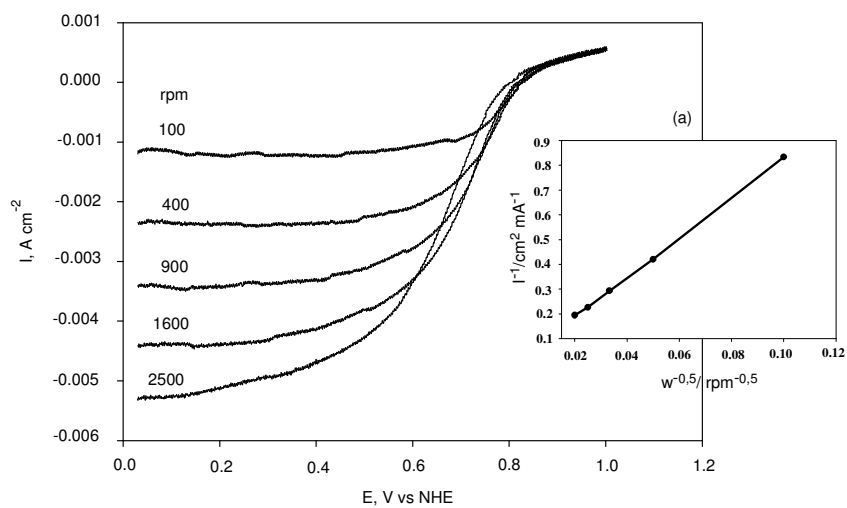


Figure 7.17 Hydrodynamic voltammograms of positive scans of Pt/BP2000 for O<sub>2</sub> reduction in O<sub>2</sub> saturated 0.1 M HClO<sub>4</sub> (a) Koutecky-Levich plot at 0.2 V

The Tafel plots of kinetic currents ( $i_k$ ) for oxygen reduction in positive sweep rates for the synthesized catalysts (Figure 7.18) show the same order as the ESA values, i.e. Pt/VXR>Pt/MWCNT>Pt/BP2000. For high potentials and low potentials, Tafel slopes were reported as 60 and 120 mV dec<sup>-1</sup> for carbon supported platinum catalysts, respectively (Antoine et al., 2001). However, there is a wide range of Tafel slopes reported in the literature for low potentials ranging between 120 and 200 mV dec<sup>-1</sup> (Yu et al., 2003). The higher values of Tafel slopes are possibly due low oxygen concentrations and due to a mixed activation/mass transport control (Antolini et al., 1999). The Tafel slopes obtained for the low overpotential and intermediate segment regions for Pt/MWCNT, Pt/VXR and Pt/BP2000 were 44, 36 and 40 mV dec<sup>-1</sup>; and 74, 54 and 50 mV dec<sup>-1</sup>, respectively. The Tafel slopes close to 40 mV dec<sup>-1</sup> in the low overpotential region indicates the dominance of the reduction of surface oxygen to OH. The Tafel slopes close to 70 mV dec<sup>-1</sup> in the intermediate region indicates that the oxygen reduction reaction kinetics can be explained with a mechanism of four electron transfer pathway involving a single electron transfer step yielding adsorbed O-containing species under Temkin adsorption conditions as the rate determining step (Jiang and Li, 2005).

By using scCO<sub>2</sub> deposition method it was seen that the catalysts which have very small particle sizes as small as 1-2 nm can be prepared. Adsorption studies showed that there is a maximum uptake value of the precursor on to the carbon support for the defined temperature and the pressure. The higher the carbon support's surface area the higher the uptake of the precursor obtained. Maximum Pt loading was achieved with BP2000 carbon support which has a surface area of 1500 m<sup>2</sup>/g. The XRD and TEM images of the catalysts indicated that the particle sizes of the catalysts were 1.2, 1 and 2 nm for Pt/VXR, Pt/BP2000 and Pt/MWCNT catalysts, respectively. To determine the electrocatalytic activity of the catalysts they were tested via a rotating disk electrode. The best electrocatalytic activity was obtained for Pt/VXR catalyst.

From the CV measurements it was concluded that the carbon support used is a very important parameter that affects the catalytic activity.

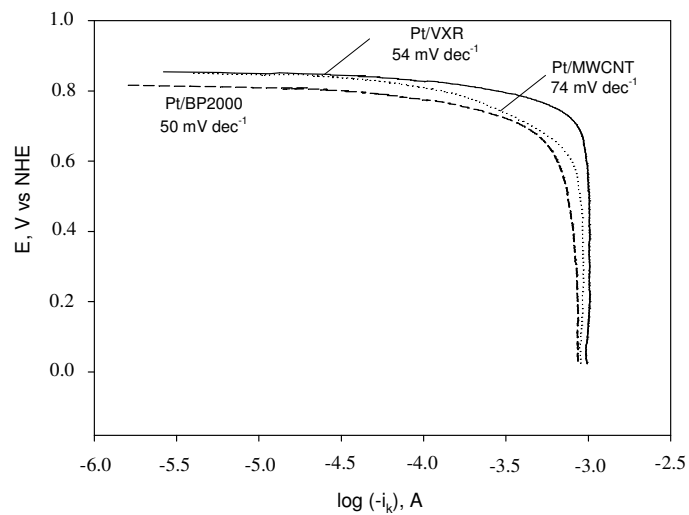


Figure 7.18 Tafel plots of  $i_k$  for  $O_2$  reduction in positive scans for synthesized catalysts in  $O_2$  saturated 0.1 M  $HClO_4$  for intermediate segment (0.85-0.75 V)

## CHAPTER 8

### RESULTS AND DISCUSSION OF THE CATALYSTS PREPARED BY MICROWAVE IRRADIATION

The aim of the utilization of the fuel cells in energy systems is for clean and efficient electricity production. The produced electricity has to be used in everywhere where the electricity is needed. By using single fuel cells to provide the required high powers one needs a fuel cell with a very high active area which is not feasible. So for generating high powers multiple cells can be electrically connected in series. By this way the required power is obtained with smaller active areas. By changing the active area the number of single cells can be arranged and vice versa. In fuel cell stacks it is needed to optimize the stack efficiency and size.

A stack with nominal cell voltage of 0.7 V requires about 40% larger active area than a stack sized at 0.6 V/cell. The stack size would be doubled when 0.8 V/cell nominal power is selected instead of 0.7 V/cell. However, higher cell voltage provides better efficiency and lower fuel consumption. Fuel cell developers mostly use between 0.7 and 0.6 V as voltage at nominal power (Barbir, 2005). By using microwave irradiation method it is aimed to prepare high power densities between the operating region of the fuel cell. The prepared catalysts were characterized physicochemically by XRD and XPS. Then they were tested in a PEM fuel cell. In this part the prepared catalysts were tested in PEM fuel cell full cell experiments to determine the performance of the catalysts.

## 8.1 Characterization of the catalysts

The prepared catalysts can be tested in fuel cell before the physicochemical characterization. But before fuel cell tests it will be meaningful to determine the catalyst properties which affect the catalytic performance of the catalysts. To determine whether the Pt crystals are obtained or not XRD was used. By using XRD the crystallite size which is given in this study as the particle size can be calculated. By using XPS the surface oxidation states were determined. By using both characterization techniques the catalyst properties were defined and it was searched for if the catalysts are suitable for fuel cell tests or not.

### 8.1.1 Characterization by XRD

The XRD spectra for the prepared and commercial catalysts for different conditions are given in the Figure 8.1. For all catalysts, the characteristic face-centered cubic (fcc) diffraction patterns for Pt were obtained for {111}, {200}, {220} peaks. Because of the overlapping of {111}, {200} Pt and carbon peaks, the particle sizes of the catalysts were calculated by using Scherrer equation (Appendix A) for the half-full-width at half maximum of the {220} inflection and also the surface areas (SAs) of the catalysts were calculated from the particle sizes obtained from the XRD data.

Firstly, the effect of microwave duration onto the particle size was investigated by varying the time between 30-120 s. From the XRD data in Figure 8.1, it was observed that the smallest particle size, where the broadening of {220} inflection was maximum, was obtained for 50 s. So, the other experiments were performed at these conditions. The microwave durations affect the temperature of the solution. So, at long microwave durations, 90 and 120 s, aggressive heating may occur and this will result in a rapid growth or

coalescence of Pt particles. But within 30 s the crystals did not occur yet. It was observed that microwave duration less than 40 s was not enough for the crystal formation. Particle sizes obtained from XRD spectra for different microwave durations and a comparison of the energy/gram data, when it is assumed to all energy is absorbed by the sample, for this study and the literature are given in Table 8.1.

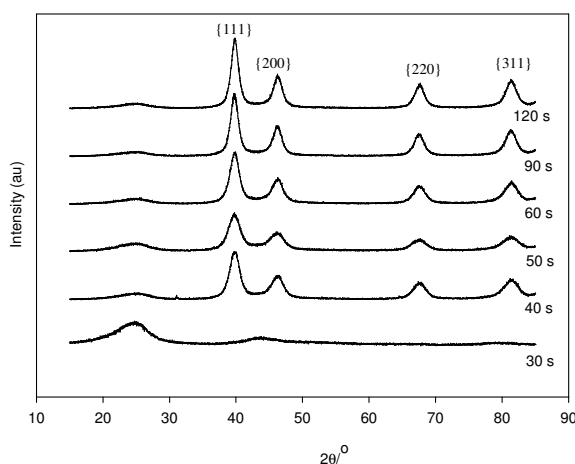


Figure 8.1 XRD pattern for the Pt/VX (20%) catalyst at base concentration of 0.14 g/l with different microwave durations

Table 8.1 Pt/VX (20%) catalyst prepared for different microwave durations

Microwave duration (s)	Particle size* (nm)	Input energy kJ/g*	Particle size** (nm)	Input energy kJ/g**
30	---	0.43	...	...
50	3.68	0.72	4	1.25 <sup>a</sup>
60	4.60	0.86	3.5-4	0.75 <sup>b</sup>
90	5.31	1.29	3-5	2.82 <sup>c</sup>
120	5.69	1.72	...	...

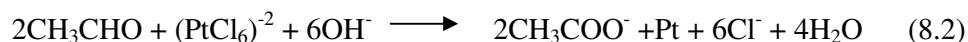
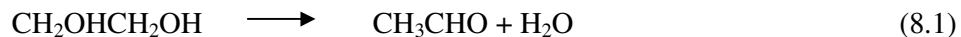
\* From this study

\*\* From the literature (<sup>a</sup> Song et al., 2007; <sup>b</sup> Tierney and Lidstrom, 2005; <sup>c</sup> Tian et al., 2006)



Effect of base concentration on the particle size of Pt/VX (20%) catalyst was investigated. For this purpose the base concentration was varied between 0.14 to 0.54 g/l. It was seen from Figure 8.2 that the peak of {220} inflection broadened when the base concentration increased.

Increasing the base concentration lead to smaller particle size. Therefore, by adjusting the base concentration in the solution, the particle size can be controlled. The reason for the effect of base concentration on the particle size is explained by the proposed mechanism (Li et al., 2005) given below:



The acetate formed in reaction (8.2) can serve as stabilizer for Pt colloids. So, at low base concentration values a low interaction between the acetate and Pt colloids occur. Poor stabilization at low base concentrations (BCs) resulted in high agglomeration and so large particle sizes. Effect of different carbon supports, which have various surface areas, on particle size of Pt was investigated and XRD spectrum is given in Figure 8.3.

The stabilizers are used in catalyst preparation to prevent the agglomeration of the metals by covering them. SB12 was used as the stabilizer in this study. Effect of different SB12/H<sub>2</sub>PtCl<sub>6</sub> (S/Pt) molar ratios on particle size of Pt was investigated and XRD spectrum is given in Figure 8.4, also the XRD pattern for commercial Pt/C (EOTEK) catalyst is given. The stabilization of the Pt nanoparticles provided by adding SB12 (CH<sub>3</sub>(CH<sub>2</sub>)<sub>11</sub>N(CH<sub>3</sub>)<sub>2</sub>(CH<sub>2</sub>)<sub>3</sub>SO<sub>3</sub>) surfactant via an electrosteric stabilization, i.e. the combination of electrostatic (SO<sub>3</sub><sup>-</sup>) and steric (-C<sub>12</sub>H<sub>25</sub>) stabilization. A stable electrosteric repulsion exist between the Pt particles covered by SB12: the positively charged part is adsorbed on the particle surface. The negatively charged part (SO<sub>3</sub><sup>-</sup>) and the

bulky alkyl chain ( $-C_{12}H_{25}$ ) are pointed away from the particles (Li and Hsing, 2006).

Binary PtRu/VX (30%) catalyst was prepared with and without surfactant and the XRD spectra is given in Figure 8.6. XRD spectra for commercial binary PtRu/C (Etek, 20 and 40%) catalysts are given in Figure 8.7. From the figure and the particle size calculation it was seen that as the Pt loading on the carbon support increases, the particles get larger and, as a consequence, the available Pt surface area is decreasing. So electrocatalysts with higher Pt-loadings yield thinner active catalyst layers in MEAs and electrodes which will enhance the accessibility of the metals, therefore they are gaining increased interest (Starz et al, 1999). The tabulated particle sizes of the prepared catalysts are given in Table 8.2 where the particle sizes were calculated by using the corresponding XRD patterns of the catalysts.

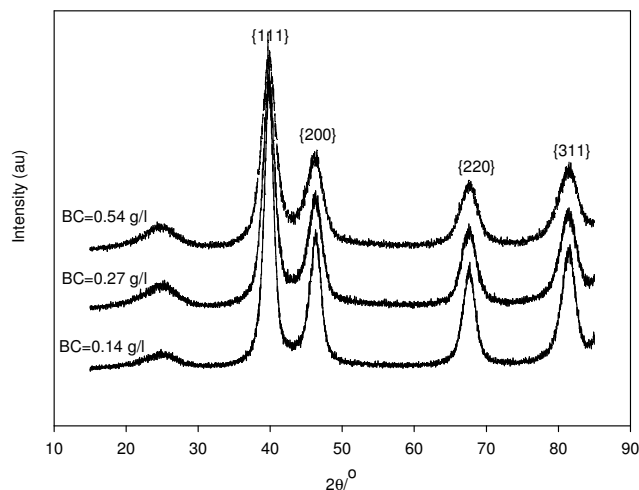


Figure 8.2 XRD pattern for the Pt/VX (20%) catalyst with different base concentrations (BCs), 50 s microwave duration

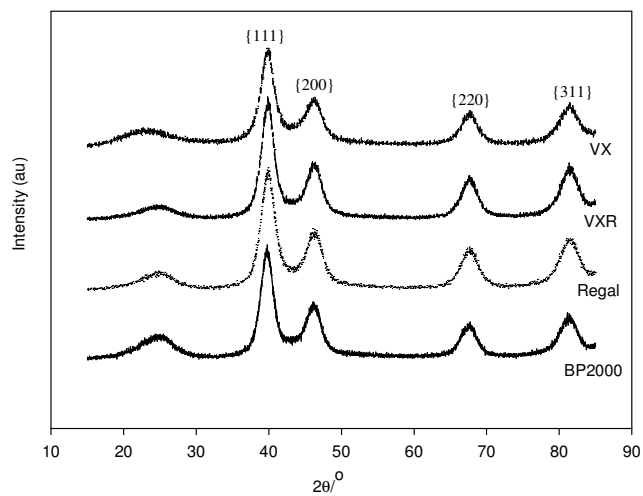


Figure 8.3 XRD pattern for the catalyst prepared with different carbon supports, 50 s microwave duration, Base concentration is 0.54 g/l

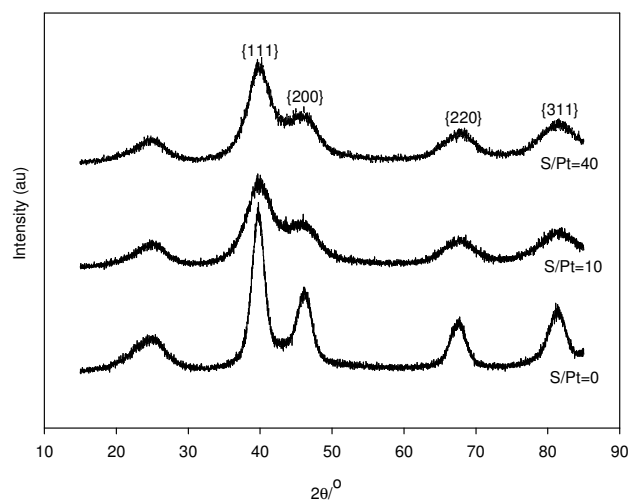


Figure 8.4 XRD pattern for the catalysts prepared with different SB12/ $H_2PtCl_6$  (S/Pt) molar ratios, 50 s microwave duration, BC=0.54 g/l

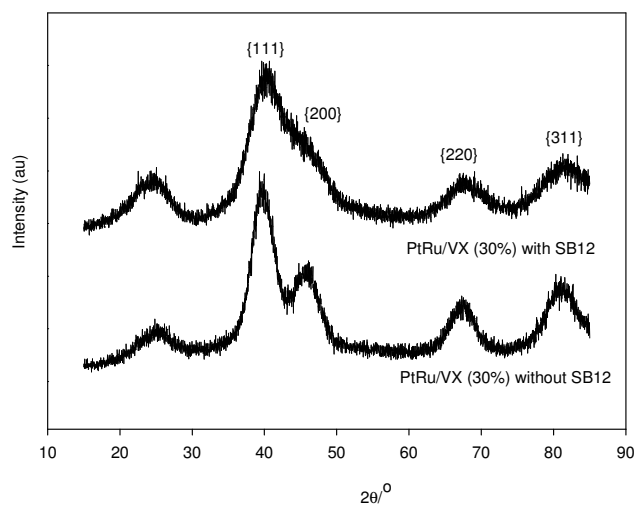


Figure 8.5 XRD pattern for PtRu/VX (30%) catalyst prepared with or without SB12 surfactant

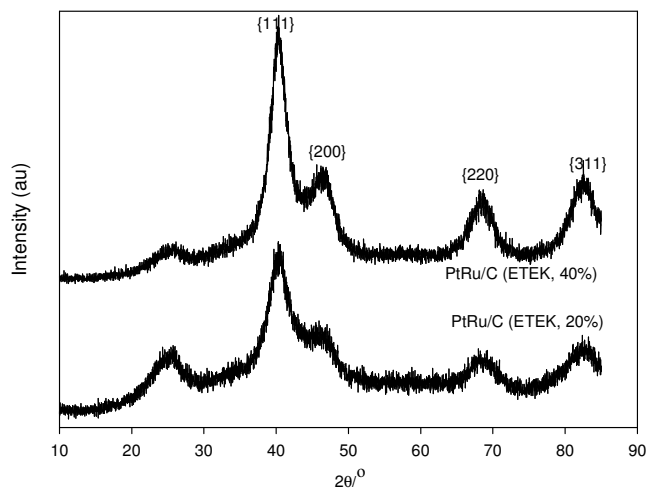


Figure 8.6 XRD pattern for binary commercial ETEK catalysts of PtRu/C 20% and 40%

Table 8.2 Particle sizes calculated for the commercial ETEK and the prepared catalysts by using XRD patterns

Catalyst	Initial Pt (%)	BC (g/l)	Microwave duration (s)	S/Pt	Particle size (nm)
Pt/VX	20	0.14	50	0	3.98
Pt/VX	20	0.27	50	0	3.85
Pt/VX	20	0.54	50	0	3.32
Pt/VX	20	0.14	30	0	...
Pt/VX	20	0.14	60	0	4.60
Pt/VX	20	0.14	90	0	5.31
Pt/VX	20	0.14	120	0	5.69
Pt/Regal	20	0.54	50	0	3.41
Pt/BP2000	20	0.54	50	0	3.68
PtRu/VX	30	0.54	50	0	2.39
Pt/VX (SB12)	20	0.54	50	10	2.52
Pt/VX (SB12)	20	0.54	50	40	2.28
PtRu/VX (SB12)	30	0.54	50	80	2.00
Pt/C (ETEK)	20	...	...	...	2.65
PtRu/C (ETEK)	20	...	...	...	2.67
PtRu/C (ETEK)	40	...	...	...	2.83

### 8.1.2 Characterization by XPS

XPS was used to determine the surface oxidation states of the catalysts prepared by microwave irradiation. Figures 8.7-8.10 represent the Pt 4f regions of the XPS spectrum of the Pt/C (ETEK), Pt/VX, Pt/Regal and Pt/BP2000 catalysts, respectively. The spectra show the doublets containing a low energy band (Pt 4f<sub>7/2</sub>) and a high energy band (Pt 4f<sub>5/2</sub>) in which the theoretical area ratio is 4/3 (Shao et al., 2006). For all the catalysts the Pt 4f signal consisted of three pairs of Pt peaks which correspond to Pt<sup>0</sup>, Pt<sup>+2</sup> and Pt<sup>+4</sup>.

The analysis of the Pt 4f doublet showed the presence of three different states of Pt, with Pt 4f<sub>7/2</sub> and 4f<sub>5/2</sub> bands located at 71.2, 72.6, 74.4 eV and 74.4, 76.1, 77.8 eV for Pt<sup>0</sup>, Pt<sup>+2</sup> and Pt<sup>+4</sup>, respectively (Liu et al., 2002). In Pt/C (E TEK) catalyst XPS spectra (Figure 8.7), the most intense peaks were observed at 71.2 and 74.5 eV binding energies which could be assigned to metallic Pt (Şen and Gökağaç, 2007). Second region which include the doublets at 72.6 and 76.1 eV were assigned to Pt<sup>+2</sup> which will be seen as PtO or Pt(OH)<sub>2</sub>. The third and the least intense peak at 74.4 and 77.8 eV binding energies were assigned to Pt<sup>+4</sup> in the form of PtO<sub>2</sub>. From the area under the curves the relative intensities of the ETEK catalysts were obtained. The catalyst has 62% Pt<sup>0</sup>, 25% Pt<sup>+2</sup> and 13% Pt<sup>+4</sup>. It is known that the surface functional groups affect the catalytic activity (Tian et al., 2006). The higher the metallic platinum (Pt<sup>0</sup>) present in the catalyst indicates the better the catalytic activity obtained.

Figure 8.8 represents the XPS spectra for Pt/VX catalyst. Similarly, the most intense peaks were observed at 71.2 and 74.4 eV binding energies. From the area under the curves the relative intensities of the catalyst was obtained as 60% Pt<sup>0</sup>, 27.5% Pt<sup>+2</sup> and 12.5% Pt<sup>+4</sup>.

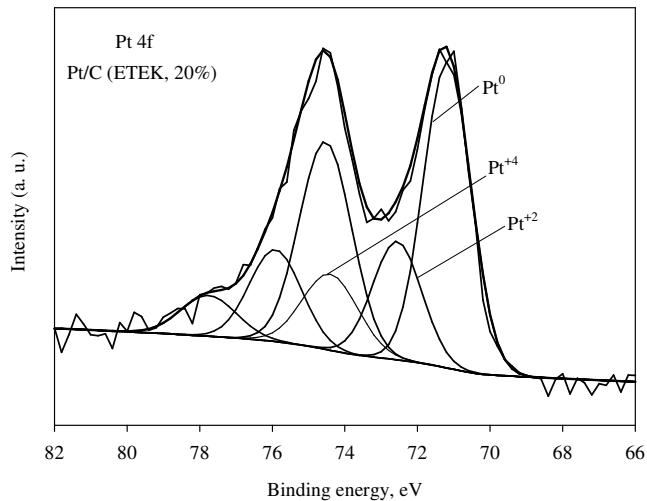


Figure 8.7 XPS core level spectra for Pt 4f for Pt/C (E TEK) catalyst

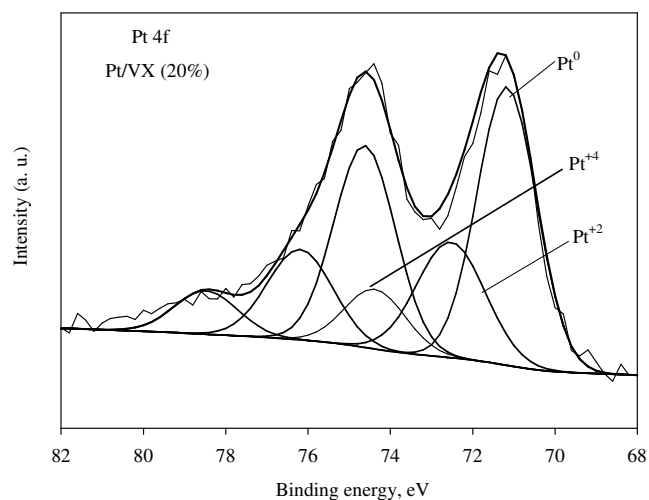


Figure 8.8 XPS core level spectra for Pt 4f for Pt/VX catalyst

Figure 8.9 represents the XPS spectra for Pt/Regal catalyst. Similarly, the most intense peaks were observed at 71.2 and 74.5 eV binding energies for metallic Pt. From the area under the curves the relative intensities of the catalyst was obtained as 61% Pt<sup>0</sup>, 28% Pt<sup>+2</sup> and 11% Pt<sup>+4</sup>.

From Figure 8.10 which shows the XPS spectra of Pt/BP2000, similar results for the binding energies of 71.45 and 74.8 were obtained that represents the metallic Pt. The corresponding relative intensities were 52% Pt<sup>0</sup>, 30% Pt<sup>+2</sup> and 18% Pt<sup>+4</sup>.

When the prepared and the commercial catalysts were compared, it was seen that the Pt/C (EOTEK), Pt/VX and Pt/Regal catalysts approximately have the same surface oxidation states related with Pt, whereas Pt/BP2000 has the highest oxide formation. While comparing the surface oxidation characteristic of these catalysts it will be meaningful to take into account the surface areas

and pore diameters of the carbon support used in the synthesis of the catalysts. The biggest surface area was belonging to the BP2000 carbon support which may lead to the surface oxidation because of having larger mesoporous area and pore volume may lead easy attack of oxygen atom onto the surface. Wang et al (2007) studied the carbon black support corrosion on the stability of Pt/C catalyst where they used the VX and BP2000 as the carbon supports. From their XPS results they also get the similar results for BP2000. They obtained the surface functional groups for Pt/VX as 59.4% Pt<sup>0</sup> and 40.6% Pt<sup>+2</sup> and for Pt/BP2000 as 50% Pt<sup>0</sup>, 35.6% Pt<sup>+2</sup>, 15.4% Pt<sup>+4</sup>. From this study, the results were for Pt/VX as 60% Pt<sup>0</sup>, 27.5% Pt<sup>+2</sup> and 12.5% Pt<sup>+4</sup> and for Pt/BP2000 as 52% Pt<sup>0</sup>, 30% Pt Pt<sup>+2</sup> and 18% Pt<sup>+4</sup>.

Figure 8.11 also shows the survey for the commercial and prepared catalysts. From the figure it is obvious that the O1s spectrum for the Pt/BP2000 catalyst is quantitatively higher than the others which clarify the results found from the Pt 4f spectra.

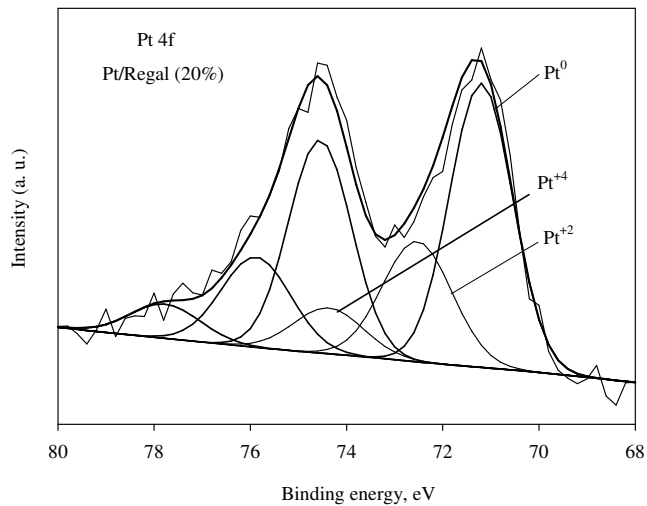


Figure 8.9 XPS core level spectra for Pt 4f for Pt/Regal catalyst



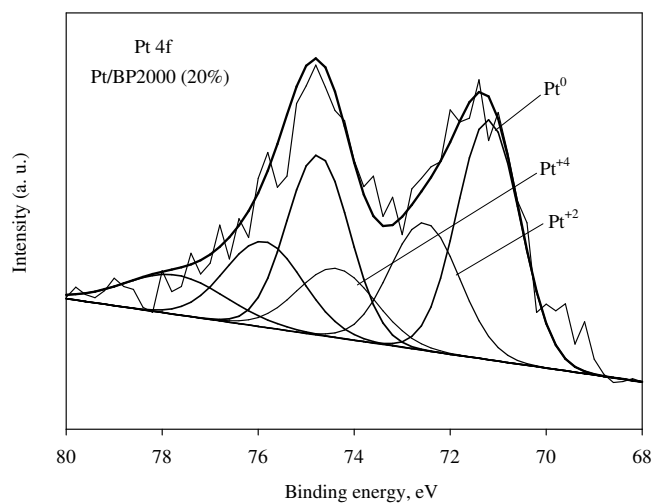


Figure 8.10 XPS core level spectra for Pt 4f for Pt/BP2000 catalyst

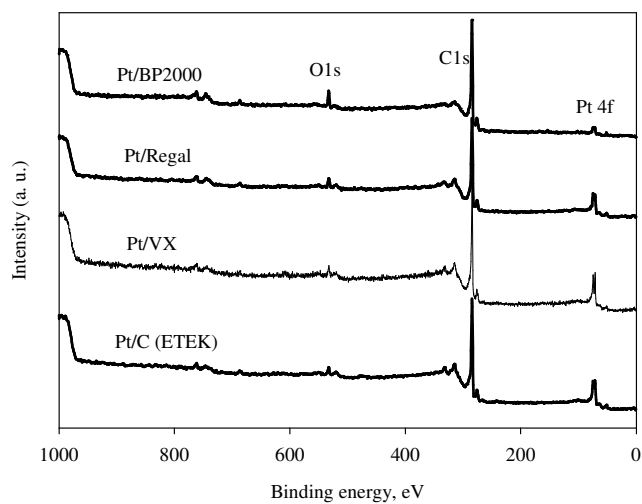


Figure 8.11 Survey XPS spectra for commercial and prepared catalysts

From the XPS core levels of C1s spectra the carbon oxidation was also investigated. From the literature it is known that the extent of graphitization affects the catalytic activity. The more graphitic carbon used the more catalytic activity obtained (Wang et al., 2007). The C1s spectrum obtained were composed of graphitic carbon (284.6 eV) and carbon with oxygen-containing functional groups (C-O: 286.1 eV, C=O: 287.6 eV) (Shao et al., 2006). The same results were obtained for the prepared catalysts and the higher oxygen-containing groups were obtained for BP2000 as given in Table 8.3.

Table 8.3 Results of the fits of the XPS spectra for carbon oxidation states (%)

Catalyst	C-C (284.6 eV)	C-O (286.1 eV)	C=O (287.6 eV)
Pt/C (EOTEK)	76	16	8
Pt/VX	78	15	7
Pt/Regal	76	18	6
Pt/BP2000	70	19	11

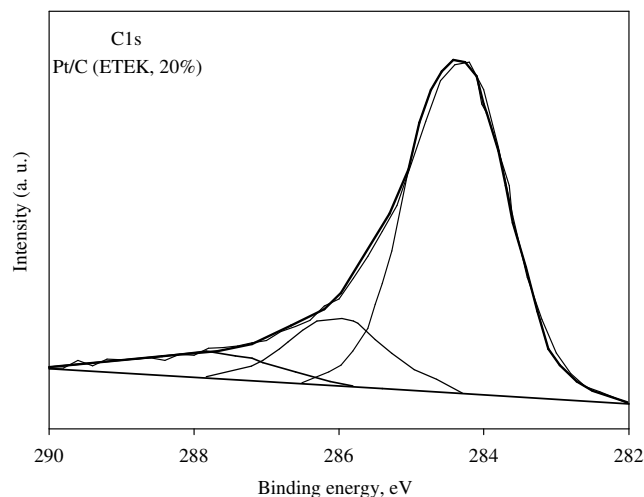


Figure 8.12 XPS core level spectra for C1s for Pt/C (EOTEK) catalyst

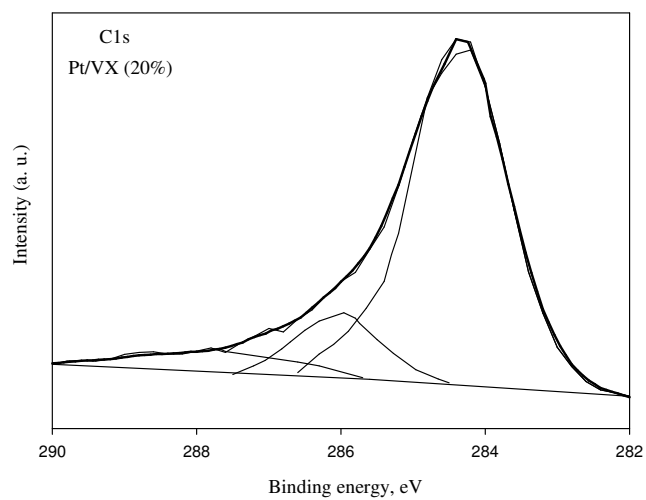


Figure 8.13 XPS core level spectra for C1s for Pt/VX catalyst

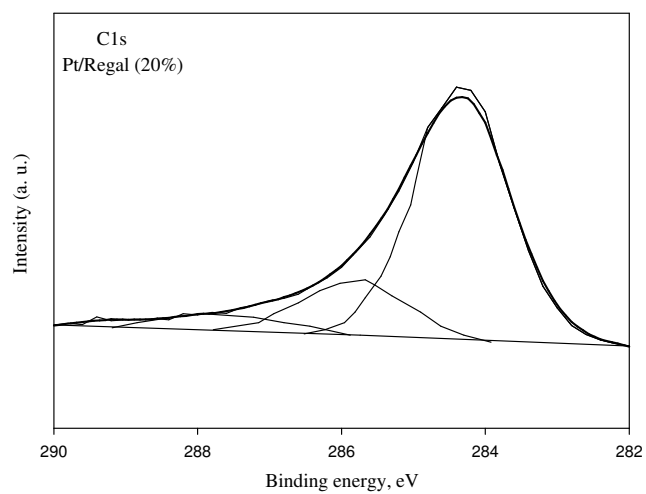


Figure 8.14 XPS core level spectra for C1s for Pt/Regal catalyst

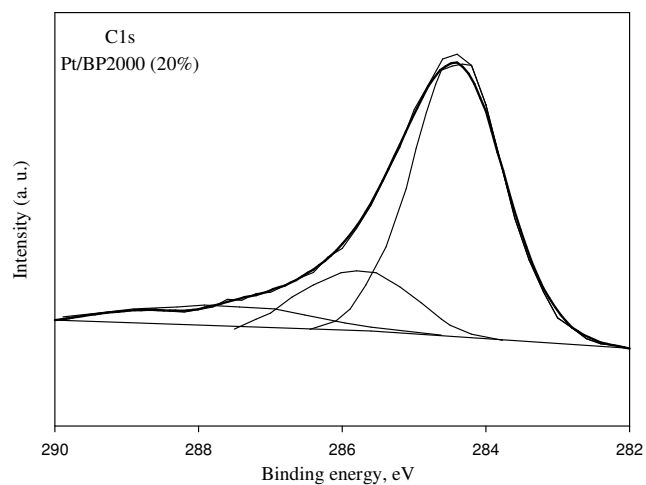
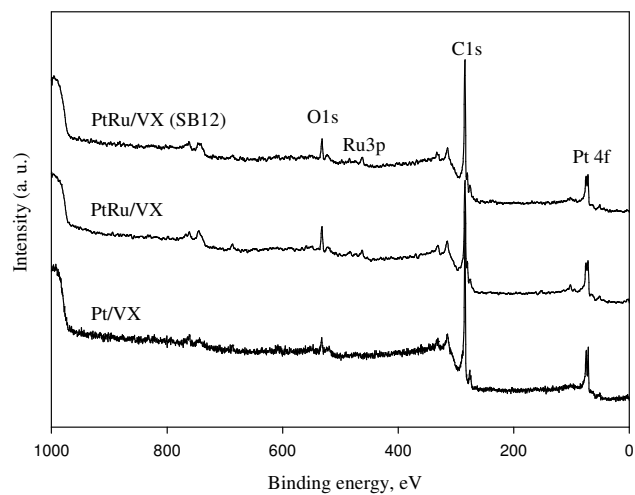
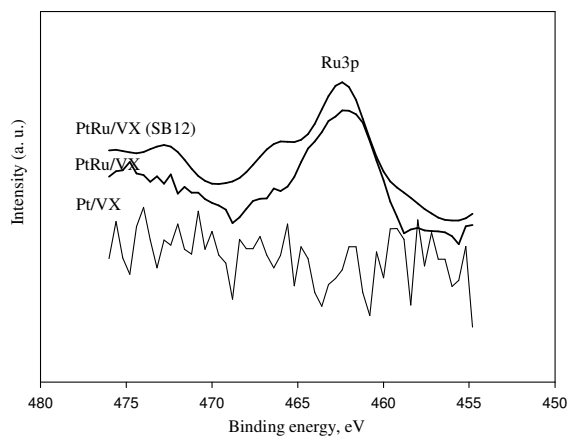


Figure 8.15 XPS core level spectra for C1s for Pt/BP2000 catalyst

Figure 8.16 showed the whole XPS spectra and core level spectra for Ru3p for PtRu based catalysts. From both figures it is obvious that the Ru is incorporated into the catalyst.



(a)



(b)

Figure 8.16 XPS for (a) whole and (b) core level spectra for Ru3p for PtRu based catalysts

## 8.2 PEMFC tests

### 8.2.1 Effect of base concentration on PEMFC performance

Two different base concentrations (0.14 and 0.54 g KOH/l solution) were used to prepare the Pt/VX (20%) catalyst for 50 s microwave duration. The PEMFC performance results for the MEAs prepared by these catalysts are given in Figure 8.17. In the experiments, the prepared catalyst was used as the cathode and commercial Pt/C (E-TEK, 20%) catalyst was used as the anode electrode. As can be seen from the figure there is a slight difference between the PEMFC performances of the catalysts prepared by different base concentrations. It is known that the base addition to the solution leads to the reaction of acetate

formation which behaves as a stabilizer, so when the amount of the base concentration is increased it helps to obtain smaller particle sizes.

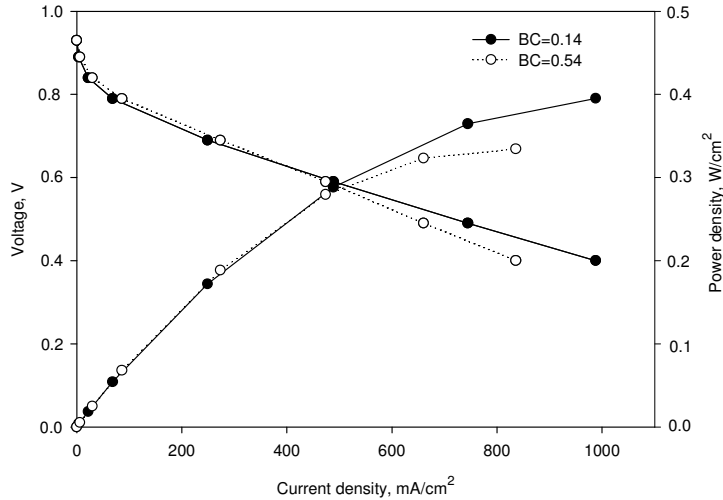


Figure 8.17 Effect of base concentration (BC) on PEMFC performance (Pt/VX, 20%, 50 s microwave duration)

At 0.6 V, current densities obtained for base concentrations 0.14 and 0.54 g/l were 489 and 474 mA/cm<sup>2</sup> with power densities of 0.29 and 0.28 W/cm<sup>2</sup>, respectively, whereas at 0.4 V these current density values altered to 988 and 836 mA/cm<sup>2</sup> with corresponding power densities of 0.4 and 0.33 W/cm<sup>2</sup>, respectively. For high current density region where the water formation increased, the catalyst prepared in the low base concentration gave better performance. At high current density region, the flooding in the pores that the Pt particles exist may affect the performance of the fuel cell especially for low particle sizes. The particle sizes for the catalysts prepared at the condition of 0.14 and 0.54 g/l base concentrations were 3.98 and 3.32 nm, respectively. Wikander et al (2007) prepared Pt/C nanoparticles by using colloidal methods

with particle sizes between 1.6 and 2.6 nm. And in the range of these nanoparticle diameters, no significant difference in catalytic performance for the ORR reaction was detected when normalized to the Pt-loading.

### 8.2.2 *Effect of microwave duration on PEMFC performance*

The effect of microwave duration to the PEMFC performance is given in Figure 8.18. The best performance was obtained for the microwave duration of 60 s where the particle size was 4.6 nm. It is known that the metal particle size increases when the temperature of the solution medium increased because of the agglomeration of the particles at high temperatures. The temperature of the solution put into the microwave oven is significantly changed with the microwave duration. In these experiments the microwave duration was changed between 50 to 120 s. By varying the microwave duration between 50 to 120 s, the particle sizes obtained ranged between 3.98 to 5.69 nm (see Table 8.2). Because the microwave duration affects the temperature of the solution in the microwave oven, and the higher the temperature is the higher the particles agglomerate. The corresponding current and power densities for the prepared catalysts with different microwave durations at 0.6 V and 0.4 V are tabulated in Table 8.4. The table indicates that especially at higher current density region the performance difference becomes more significant. Maximum power density was obtained for both 0.6 V and 0.4 V potentials for the 60 s microwave duration. The increase in the particle size had a positive effect on the performance up to an extent and after some point the performance started to decline. These results showed that smaller particle size does not mean that the performance will be high. In small particle sizes, other effects such as different lattice constants at smaller sizes, edge effects or different governing crystal planes for smaller particles may lower the activity when decreasing the size of the catalyst particles (Ekström, 2007). Also, Wikander et al (2007) emphasized that the particles lower than 3 nm are unstable and to make them stable it is needed to stabilize the particles from electrochemical sintering during the fuel

cell operation. Wang et al. (2007) also changed the microwave duration between 30-120 s and by using CV they obtained the best electrocatalytic activity for 90 s microwave duration with the particle sizes changing between 3-5 nm.

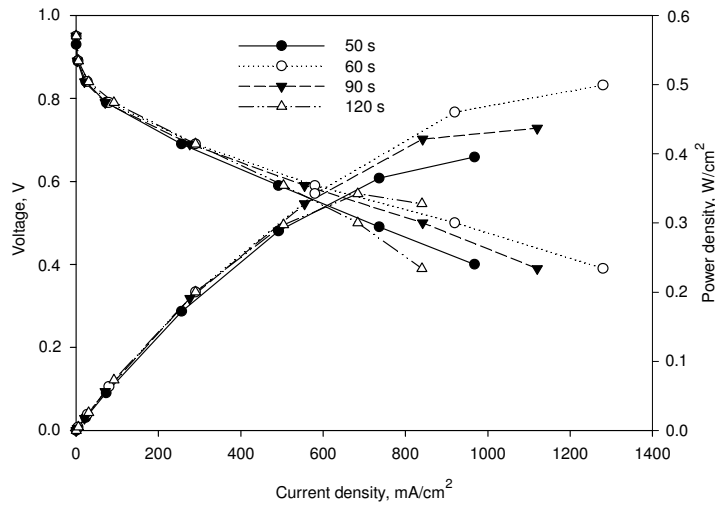


Figure 8.18 Effect of microwave duration on PEMFC performance (Pt/VX, 20%, Base concentration=0.14 g/l)

Table 8.4 Current and power densities for the catalysts prepared with different microwave durations (MDs)

MDs (s)	@0.6 V		@0.4 V	
	Current density (mA/cm <sup>2</sup> )	Power density (mW/cm <sup>2</sup> )	Current density (mA/cm <sup>2</sup> )	Power density (mW/cm <sup>2</sup> )
50	489	0.29	988	0.39
60	580	0.34	1280	0.50
90	555	0.33	1120	0.44
120	504	0.30	808	0.33



### 8.2.3 Effect of carbon support on PEMFC performance

The PEMFC performance of the catalysts prepared with different carbon supports is given in Figure 8.18. As can be seen from the figure, the VX carbon support gave the best performance when compared to Regal and BP2000. The particle size of the catalysts were not differing significantly, it was in the range of 3.32 and 3.68 nm, the performance showed an extreme difference either for low and high current density regions. Structural properties of the carbon supports and the functional groups formed on the support surface play an important role on the catalytic activity of the catalysts. The dispersion of the Pt metal on the support which affects the particle size, and also the accessibility of the metal on the support is very crucial in fuel cells to provide the good contact between the electrolyte and the Pt metal. VX, Regal and BP2000 carbon supports which have 235, 94 and 1500 m<sup>2</sup>/g surface areas, respectively, were used as the carbon supports.

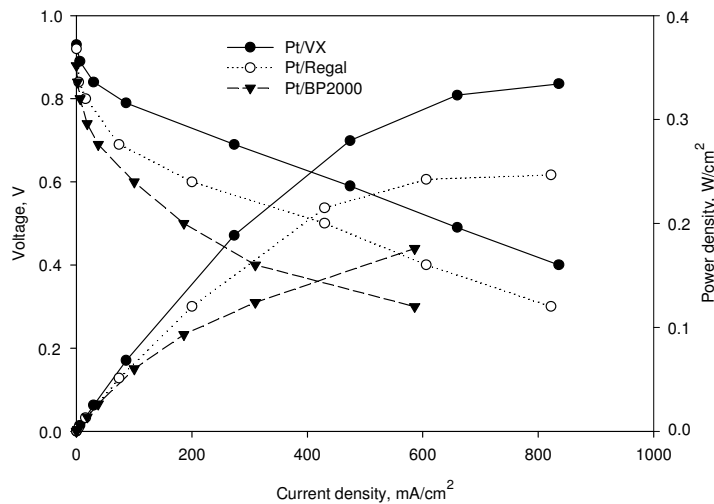


Figure 8.19 Effect of different carbon supports on PEMFC performance (50 s microwave duration, base concentration=0.54 g/l)

From Figure 8.19, at 0.6 V, the corresponding current densities were 474, 200 and 100 mA/cm<sup>2</sup> and power densities were 0.28, 0.12 and 0.06 mW/cm<sup>2</sup> for Pt/VX, Pt/Regal and Pt/BP2000, respectively. At 0.4 V, the corresponding current densities were 836, 606 and 310 mA/cm<sup>2</sup> and power densities were 0.33, 0.24 and 0.12 mW/cm<sup>2</sup> for Pt/VX, Pt/Regal and Pt/BP2000, respectively. It is observed that the carbon supports used do not affect the particle size but the performance. The probable surface functional groups formed on the carbon supports may vary significantly which may affect the performance. Also, the higher range of the surface areas of the carbon supports may affect the performance. As the carbon surface area increases, the available catalytic surface area increases while the support durability decreases because the extent of graphitization decreases as in the case of BP2000 (Stevens et al., 2005). The graphitization of the carbon supports plays a role in support stability, with more graphitic carbons being more thermally stable. VX has lower surface area than BP2000 and more graphitic in nature. The carbon support with high surface area is susceptible to corrosive conditions in PEMFC electrode (Wang et al., 2007). Pt may be lost from the support, if the support is oxidized. If the support is partially oxidized to surface oxide, this may weaken the platinum-support interaction resulted in the increase of Pt particle size, because the presence of surface oxides leading to a lower resistance to surface migration of Pt particles. From the XPS results, it is detected that the surface oxidation states of Pt/BP2000 catalyst are the highest and this might be explain their low performance in the fuel cell.

Tafel Equation is used to show the activation losses. Two Tafel slope regions were reported on bulk platinum in liquid electrolytes, one lower slope (around 60 mV/dec) at low current densities/high potentials, and one steeper, close to doubled, Tafel slope for high current densities/low potentials. The lower slope has been ascribed to ORR on a platinum oxide-covered surface, and the steeper slope to ORR on bare lpatinum (Hoare, 1968). Tafel slopes for the prepared catalysts at high potentials for Pt/VX, Pt/Regal and Pt/BP2000 were 52, 68 and

76 mV/dec, respectively (see Appendix A). Oxygen reduction reaction also occurs on carbon support, however the mechanism is different. In this reaction hydrogen peroxide is produced while two electrons are exchanged per oxygen molecule. Tafel slope in this case is 120 mV/dec. Thus, the larger the carbon BET active area (at fixed Pt area), the larger the Tafel slope (in the range 60 to 120 mV/dec). It is the case for VX and BP2000. But although Regal has a lower surface area its Tafel slope is more than VX. The higher Tafel slopes may arise from the non-negligible ORR activity of the carbon support. (Marie et al., 2004). The Tafel slopes close to  $70 \text{ mV dec}^{-1}$  in the intermediate region indicates that the oxygen reduction reaction kinetics can be explained with a mechanism of four electron transfer pathway involving a single electron transfer step yielding adsorbed O-containing species under Temkin adsorption conditions as the rate determining step (Jiang and Li, 2005).

#### *8.2.4 Effect of surfactant/Pt precursor ratio on PEMFC performance*

In order to decrease the agglomeration and obtain small particles various surfactants were used in catalyst preparation. SB12 is one of the surfactants that commonly used. The role of the surfactant is the prevention of the agglomeration by covering the Pt metal and not allowing Pt particles to coalesce. The S/Pt ratio in the experiments was varied between 0 to 40. The corresponding PEMFC performance results are given in Figure 8.20.

The addition of the surfactant decrease the particle size of the Pt as shown in Table 8.2 but that had an adverse effect on the performance. Further increase in the surfactant amount did not affect the performance significantly. Because the particle sizes for S/Pt ratios of 10 and 40 were very close to each 2.52 and 2.28 nm, respectively. At 0.6 V, current densities obtained for S/Pt ratios of 0, 10 and 40 were 474, 427 and 432  $\text{mA/cm}^2$  and corresponding power densities

were 0.28, 0.25 and 0.25 W/ cm<sup>2</sup>, respectively. But at 0.4 V, current densities obtained for S/Pt ratios of 0, 10 and 40 were 836, 932 and 890 mA/cm<sup>2</sup> and corresponding power densities were 0.33, 0.37 and 0.36 W/ cm<sup>2</sup>, respectively. It was observed that the performance of the surfactant stabilized catalysts gave better performance at high current densities. Although the particle sizes were smaller than 3 nm which make the catalyst unstable, at higher current density region the catalyst prepared with different S/Pt ratios show an increase in the performance. The stabilizer used in the experiments may improve the metal support interaction which resulted in lowering the platinum migration that would happen during the fuel cell operation.

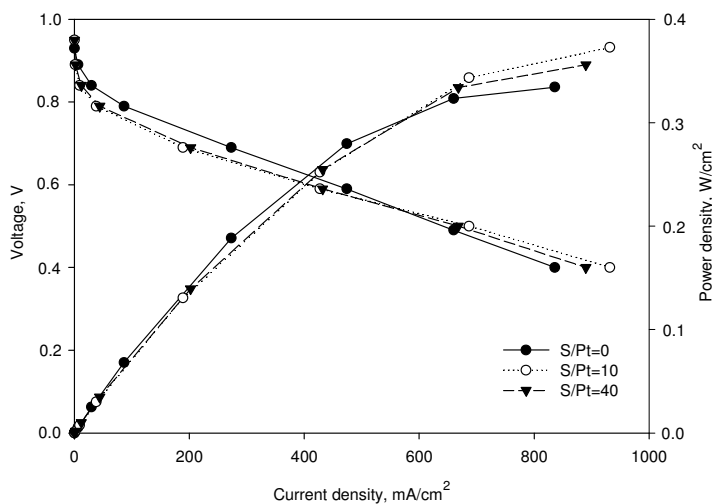


Figure 8.20 Effect of surfactant/Pt precursor (S/Pt) ratio on PEMFC performance (Base concentration=0.54 g/l, 50 s microwave duration)

### 8.2.5 Effect of catalyst properties on PEMFC performance

The Pt particle size change considerably with respect to different catalyst preparation conditions such as microwave duration, base concentration, surfactant/Pt precursor ratio, carbon support used. In Figure 8.21 current density versus the particle diameter at 0.6 V and 0.4 V is plotted. This figure shows that there is an optimum value for the particle size. A similar result was given in a study of Antoine et al. (2001). They proposed that the size effect appeared to be due to the stronger adsorption of oxygenated intermediate species on the smaller particles, which hinders the rate determining step. In another study, Wikander et al (2007) obtained the Pt nanoparticles on VX by a colloidal method by using alkylamine as the stabilizer. They investigated the particle size effects of the catalysts on PEMFC performance, and they found that nanoparticle diameters below 3 nm do not seem to be stable in the high potential electrochemical environment at the PEMFC cathode.

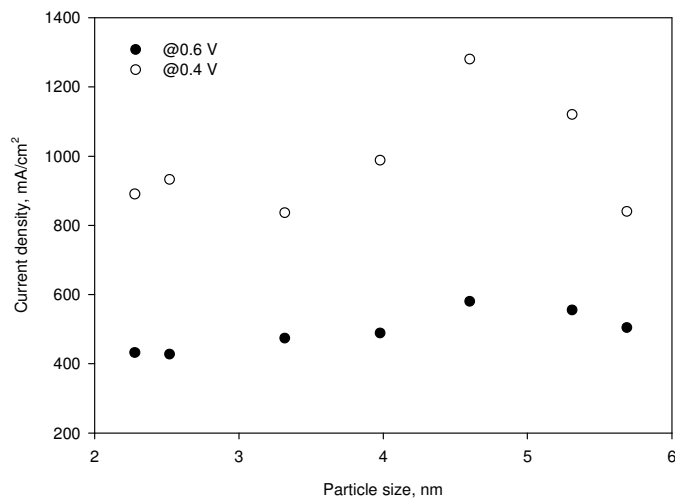


Figure 8.21 Current density versus the particle size for Pt/VX (20% ) with different conditions

In Figure 8.22 current density versus the particle size graph is given for the catalysts with different carbon supports of VX, Regal and BP2000 at 0.6 V and 0.4 V. From the figure it is obvious that the trend is different when compared to the same carbon support results.

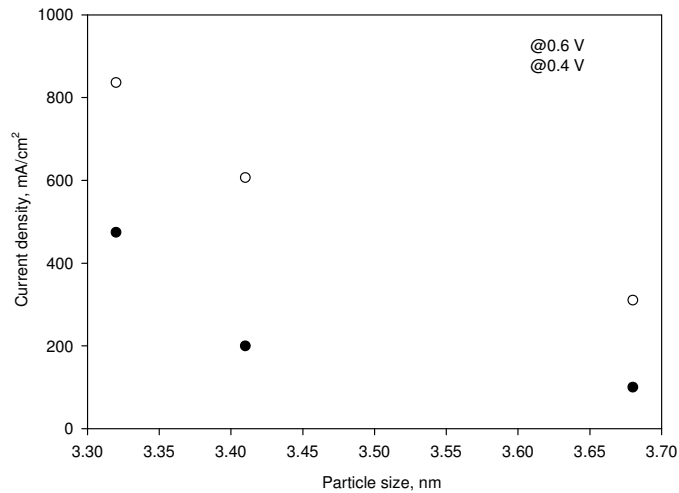


Figure 8.22 Current density versus the particle size for Pt/VX, Pt/Regal and Pt/BP2000 catalysts

### 8.3 PEMFC operated with CO<sub>2</sub> containing H<sub>2</sub>

It is important to evaluate the carbon dioxide effect on the performance. Because the CO<sub>2</sub> content in H<sub>2</sub> has a dilution effect which decreases the partial pressure of the H<sub>2</sub> which can be also observed with N<sub>2</sub>. To determine if CO<sub>2</sub> causes a further power loss, the fuel cell operated firstly with N<sub>2</sub> and then with CO<sub>2</sub>.

### 8.3.1 Effect of $N_2$ on PEMFC performance

Prior to the  $CO_2$  experiments, the effect of  $N_2$  on PEMFC performance was investigated. It is known that the dilution of the fuel at anode side has an adverse effect on the performance. To diminish this effect at the anode feed gas, the percentage of the second gas (either  $N_2$  or  $CO_2$ ) was arranged by keeping the hydrogen flow rate constant as 0.1 slm in all cases. A commercially available MEA was used in this experiment and  $N_2$  percentage was changed between 0 to 50%. The performance results are given in Figure 8.23. Although, the hydrogen flow rate was set to 0.1 slm in the gas composition to eliminate the dilution effect, from the figure it is clear that the performance still decreases as  $N_2$  percentage increases.

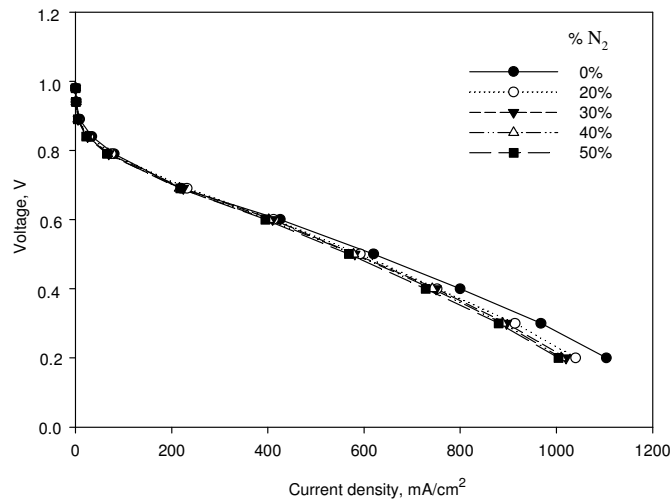


Figure 8.23 Effect of  $N_2$  percentage in the  $H_2$  gas fed to the fuel cell on PEMFC performance with commercial MEA (Electrochem)

It was calculated that under conditions of CO-free feed gas, the performance loss should not exceed 10% of full stack power with hydrogen concentrations as low as 40% (Bhatia et al, 2004). The current densities for the anode feed gas of H<sub>2</sub> including 0 and 50% N<sub>2</sub> at 0.6 V were 426 and 407 mA/cm<sup>2</sup>, respectively. The current loss for 50% N<sub>2</sub> at 0.6 V was 19 mA/cm<sup>2</sup>. Similarly at 0.4 V, the current densities for the anode feed gas of H<sub>2</sub> including 0 and 50% N<sub>2</sub> were 800 and 738 mA/cm<sup>2</sup>, respectively. The current loss was 62 mA/cm<sup>2</sup>. At 0.6 V and 0.4 V for 50% N<sub>2</sub> the percent power losses were % 6.2 and % 7.8, respectively.

### 8.3.2 *Effect of CO<sub>2</sub> on PEMFC performance*

The adverse effect of CO<sub>2</sub> on PEMFC performance is supposed to be because of either the reverse water gas shift reaction or electroreduction. In both mechanisms the reason for performance loss is resulted from CO formation which poisons the Pt electrode. The effect of CO<sub>2</sub>, ranging between 0 to 50%, on PEMFC performance is given in Figure 8.24. The current densities for the anode feed gas of H<sub>2</sub> including 0 and 50% CO<sub>2</sub> at 0.6 V were 426 and 395 mA/cm<sup>2</sup>, respectively. The current loss for 50% CO<sub>2</sub> at 0.6 V was 31 mA/cm<sup>2</sup>. Similarly at 0.4 V, the current densities for the anode feed gas of H<sub>2</sub> including 0 and 50% CO<sub>2</sub> were 800 and 728 mA/cm<sup>2</sup>, respectively. The current loss was 72 mA/cm<sup>2</sup>. At 0.6 V and 0.4 V for 50% CO<sub>2</sub> the percent power losses were % 8.8 and % 9.1, respectively. There is a small power loss difference between N<sub>2</sub> and CO<sub>2</sub> is observed. Also Divisek et al showed that with a 75% hydrogen, 25% CO<sub>2</sub>, and 100 ppm CO fuel feed, the steady state cell performance was lower than that with a 100% hydrogen, 100 ppm CO feed which shows that the addition of CO<sub>2</sub> cause further decrease in the performance. In another study, Bruijn et al (2002) found that diluting the hydrogen with CO<sub>2</sub> to H<sub>2</sub>/CO<sub>2</sub> ratio of 80:20 in the same set up led to a performance loss of 7% and further



addition of 10 ppm CO to H<sub>2</sub>/CO<sub>2</sub> mixture led to a performance loss 22%. Qi et al (2003) found that 70%H<sub>2</sub>/30%CO<sub>2</sub> gave similar results as pure H<sub>2</sub>, which indicates that the hydrogen concentration dilution by 30%CO<sub>2</sub> did not affect the performance, at least at a current density of 300 mA/cm<sup>2</sup> and from Figure 8.23 it is also seen that the CO<sub>2</sub> effect getting more important for current densities higher than about 400 mA/cm<sup>2</sup>.

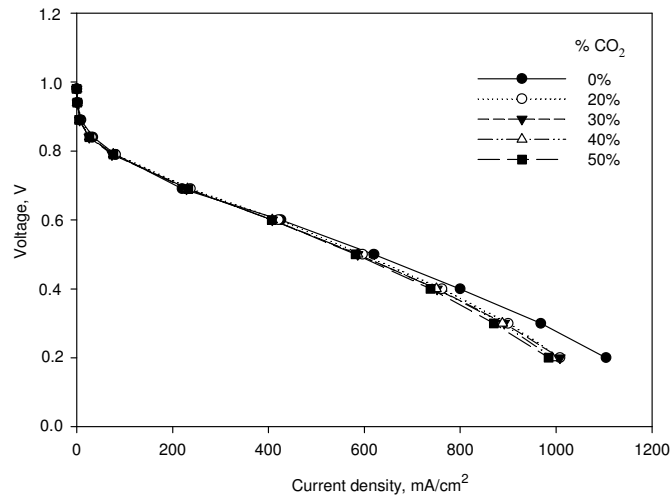


Figure 8.24 Effect of CO<sub>2</sub> percentage in the H<sub>2</sub> gas fed to the fuel cell on PEMFC performance with commercial MEA (Electrochem)

To determine whether the effect of carbon dioxide on PEMFC performance is temporary or not 30% CO<sub>2</sub> was firstly fed to the PEM fuel cell. And after reaching steady state conditions the voltage-current density data were recorded. To overcome the adverse effect of carbon dioxide after the deactivation process the carbon dioxide cut off and pure hydrogen fed to the system and waited for reaching the new steady state. As can be seen from Figure 8.25 the system approximately came back to its initial performance. This result showed that the

effect of carbon dioxide is temporary and could be overcome by removing the formed CO from the catalyst.

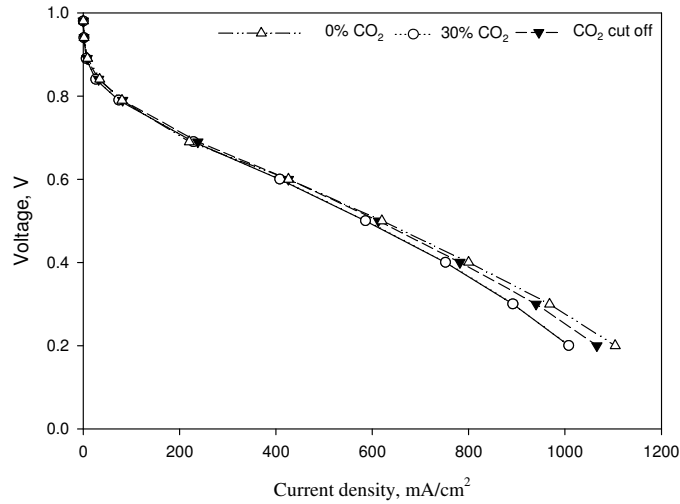


Figure 8.25 Effect of CO<sub>2</sub> cut off on PEMFC performance

### 8.3.3 Effect of 30% CO<sub>2</sub> on PEMFC performance when commercial PtRu/C anode (E TEK) is used

Before using binary PtRu/C catalyst as anode electrode the performance loss of the fuel cell was tested with single Pt/C catalyst. Effect of CO<sub>2</sub> on PEMFC performance when the anode and cathode electrodes were single commercial Pt/C (E TEK) catalyst is given in Figure 8.26. The percent power losses for 0.6 V and 0.4 V were obtained as 14.7 and 8.6%, respectively. In a model study, Janssen (2004) investigated the CO<sub>2</sub> poisoning and concluded that there is a stationary high coverage of the catalyst surface area by reduced CO<sub>2</sub>, e.g. CO,

this reduces the amount of surface area covered by hydrogen, which reduces both the hydrogen oxidation rate as well as the CO formation rate in the RWGS reaction. Binary catalysts are used to mitigate the poisoning effect. PtRu catalysts are used to mitigate the CO<sub>2</sub> poisoning effect and it is supposed that possibly the rate constant of the RWGS reaction is lower on PtRu.

Figures 8.27 and 8.28 are the PEMFC performances of the commercial PtRu/C (EOTEK) catalysts with 20 and 40% Pt loadings used as the anode electrode with 30% CO<sub>2</sub> containing hydrogen. XRD results showed that the particle sizes of these catalysts were 2.67 and 2.83 for 20 and 40% Pt loadings, respectively. The double increase in the Pt loading only caused small particle size increase. The percent power losses of the PtRu/C (EOTEK, 20%) at 0.6 and 0.4 V were 9.3 and 4.8%, respectively. For PtRu/C (EOTEK, 40%) these values for 0.6 and 0.4 V were 13.9 and 4.6%, respectively. These results showed that the power loss is decreased by using binary PtRu/C catalyst at the anode side.

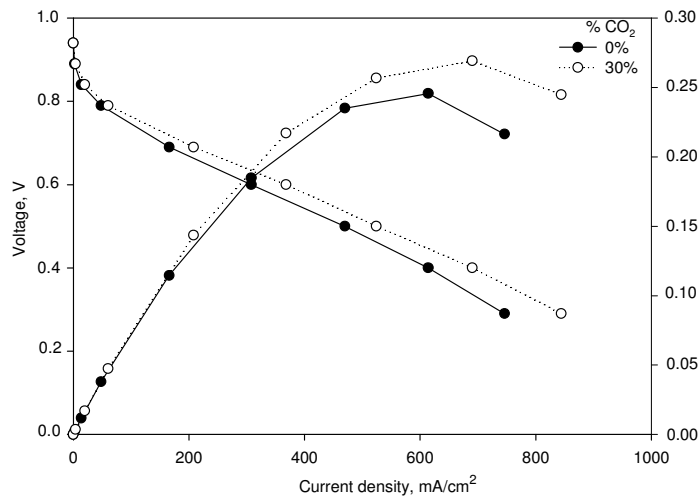


Figure 8.26 Effect of CO<sub>2</sub> on PEMFC performance (home made MEA with anode 20% Pt/C (EOTEK), cathode 20% Pt/C (EOTEK))

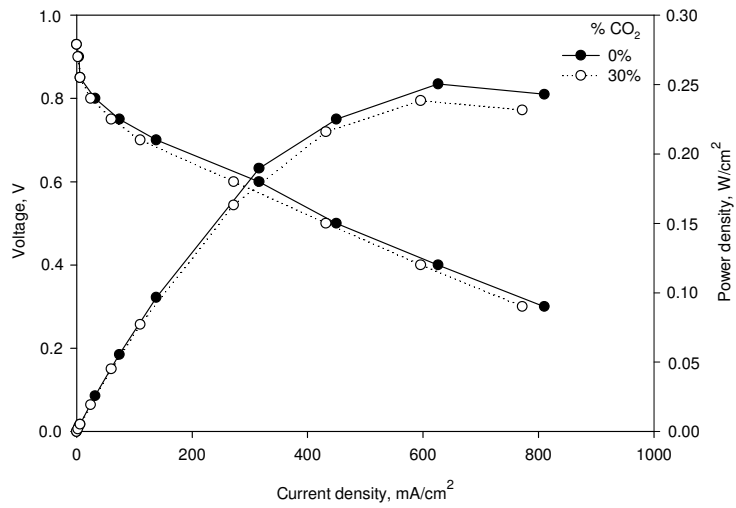


Figure 8.27 Effect of CO<sub>2</sub> on PEMFC performance (home made MEA with anode PtRu/C (ETEK, 40%), cathode 20% Pt/C (ETEK))

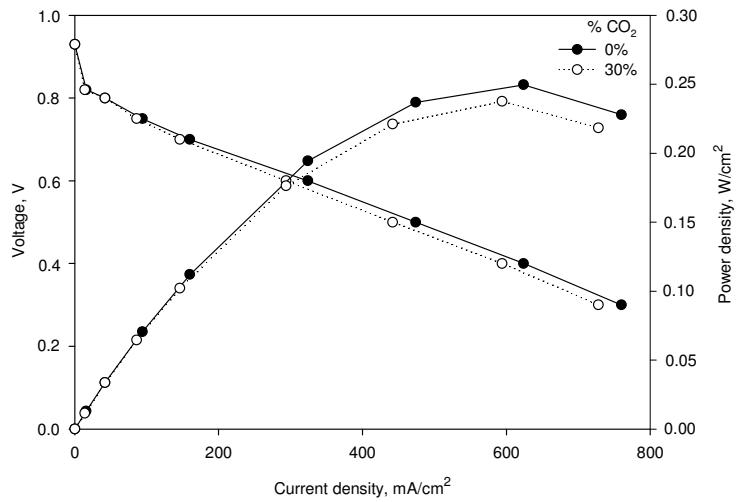


Figure 8.28 Effect of CO<sub>2</sub> on PEMFC performance (home made MEA with anode PtRu/C (ETEK, 20%), cathode 20% Pt/C (ETEK))

8.3.4 Effect of 30% CO<sub>2</sub> on PEMFC performance when PtRu/VX (microwave) anode is used

30% PtRu/VX catalysts were prepared with or without surfactant. Similar to single catalysts, the particle size was decreased when the surfactant used. Figures 8.29 and Figure 8.30 showed that also by using catalysts prepared in this study the tolerance of the fuel cell to CO<sub>2</sub> has improved. The power losses of the PtRu/VX (without S) at 0.6 V and 0.4 V were 12.9 and 2.7%, respectively. But for PtRu/VX (with S) the power losses at 0.6 V and 0.4 V were 14.4 and 6.6%, respectively. The comparison for the power losses at 0.6 and 0.4 V conditions for the commercial and prepared binary catalysts are summarized in Table 8.5.

Table 8.5 Percent power losses of the commercial and prepared PtRu/C catalysts with 30% CO<sub>2</sub>, cathode catalyst Pt/C (20%, ETEK) for all experiments

Catalyst	Power density (@0.6 V)			Power density (@0.4 V)		
	0% CO <sub>2</sub>	30% CO <sub>2</sub>	%Power loss	0% CO <sub>2</sub>	30% CO <sub>2</sub>	%Power loss
Pt/C (ETEK, 20%)	368	308	14.7	690	614	8.6
PtRu/C (ETEK, 20%)	324	294	9.3	624	594	4.8
PtRu/C (ETEK, 40%)	316	272	13.9	626	596	4.6
PtRu/VX (without S)	310	271	12.9	742	721	2.7
PtRu/VX (with S)	220	188	14.4	728	680	6.6

S represents the surfactant

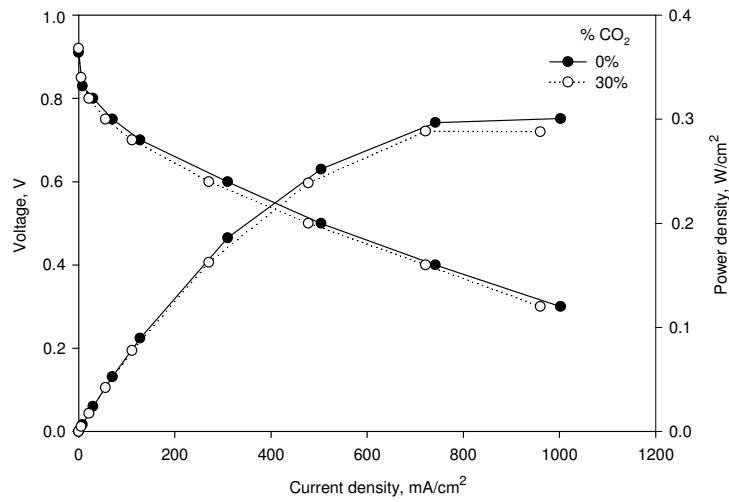


Figure 8.29 Effect of CO<sub>2</sub> on PEMFC performance (home made MEA with anode PtRu/VX (microwave, 30% PtRu), cathode 20% Pt/C (ETEK))

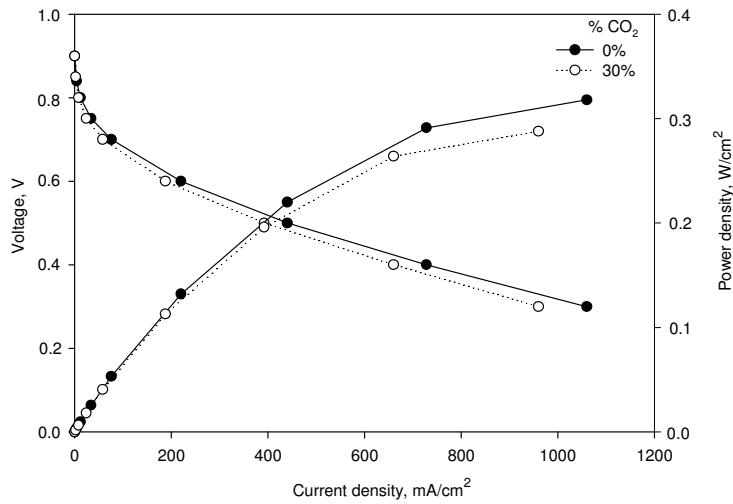
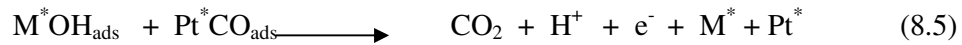
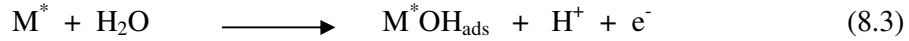


Figure 8.30 Effect of CO<sub>2</sub> on PEMFC performance (home made MEA with anode PtRu/VX (microwave with SB12, 30% PtRu), cathode 20% Pt/C (ETEK))

The improvement in the carbon dioxide tolerance can be explained by the mechanism given for the carbon monoxide oxidation with binary catalyst as follows:



M, metal has to provide water oxidation and then subsequent CO oxidation will result in carbon monoxide oxidation. M can be Pt or Ru (CO may be bonded to Pt or Ru) (Giorgi et al., 2001). A potential of only 0.2 V is required to adsorb water onto Ru, compared to 0.7 V for Pt due to the greater adsorption strength of OH<sub>ads</sub> onto Ru, which will ultimately lower the oxidation potential of CO to ~0.25 V.

#### 8.4 Comparison of the PEMFC performances of the prepared and commercial Pt and PtRu based catalysts

It will be worthy to compare the PEMFC performance results of the Pt based catalysts prepared in this study with commercial ETEK catalyst as shown in Figure 8.31. Two prepared catalysts were selected for comparison. One of the chosen catalysts had the particle size close to ETEK catalyst and the other was the catalyst that gave the best performance in fuel cell. It was observed that for low current density region the performance was similar whereas for high current density region commercial catalyst showed a performance decrease that may be due to the flooding. At 0.6 V the corresponding current densities were 580, 524 and 427 mA/cm<sup>2</sup> for microwave (60 s duration), ETEK and microwave (S/Pt=10) catalysts, respectively. Maximum power density obtained

for Pt/VX (60s microwave duration) was  $0.5 \text{ W/cm}^2$ . Microwave irradiation method seems to be a promising method that gave similar and higher performance when compared to the commercial catalyst. It was observed that the performance of the surfactant stabilized catalyst had higher performance than the commercial catalyst at high current density region.

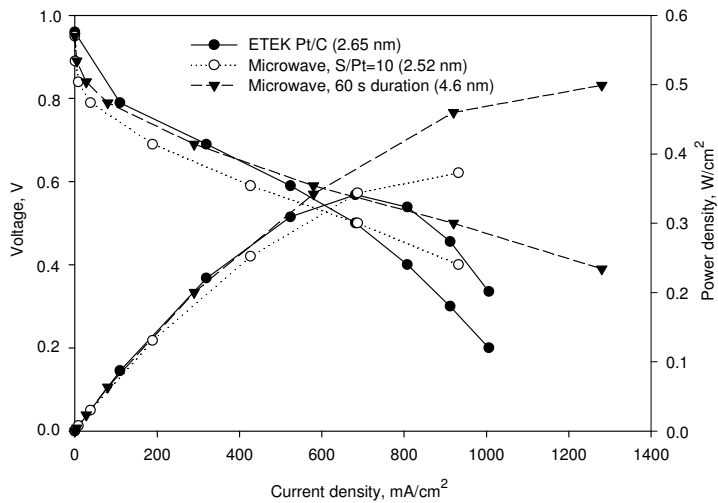


Figure 8.31 Comparison of PEMFC performances for commercial ETEK catalysts and the microwave irradiated catalysts with similar particle size and best performance

Figure 8.32 shows the PEMFC performances with pure hydrogen for the prepared and the commercial binary catalysts used in the experiments. Figure demonstrated that the performance of the PtRu/VX catalyst prepared by microwave irradiation had a better performance when compared to other catalysts. But for high current density region, the performance of the catalysts, prepared by microwave irradiation, increased with the help of the surfactant



and gave the best performance. In the case of the Pt based catalyst, similar results were obtained and the microwave irradiated catalyst treated with surfactant exhibited increased performance at high current densities and the performance surpassed the commercial catalyst's performance. Especially, for high current densities where the water formation increased, the water management becomes more important. So, the utilization of the surfactant in the catalyst preparation may enhance the hydrophobicity of the catalyst which diminish the flooding effects occurred at high current densities.

It was also observed that conditions for the catalyst preparation have an impact on the catalyst properties of the binary catalysts. Previously, the effect of the particle size on the current density has been shown and a trend has been obtained. Similarly, Figure 8.33 showed the current densities of the binary catalysts at 0.4 and 0.6 V potentials versus the particle size. As can be seen from the figure, particle diameter is one of the most important parameters that has to be taken into account to access the desired performances of a fuel cell.

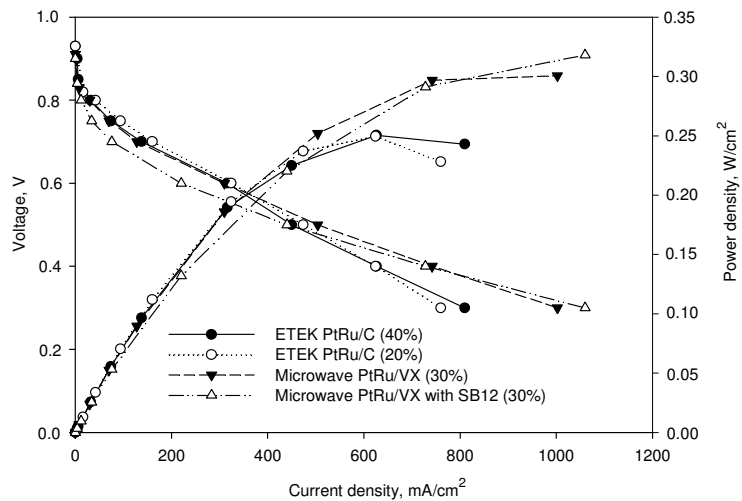


Figure 8.32 Comparison of commercial and microwave PtRu based catalysts

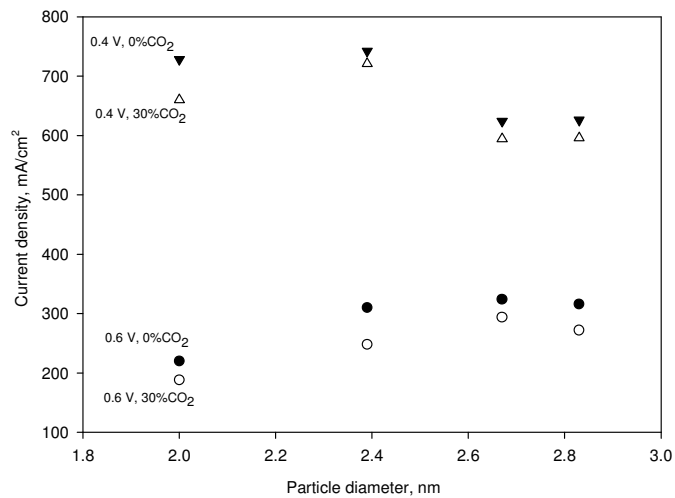


Figure 8.33 Current density versus the particle size for PtRu based catalysts

The experimental results showed that microwave irradiation method gave promising PEMFC performance results with the catalysts being either single or binary. It is concluded that the catalyst properties affect the catalytic activity significantly. Especially the particle size effect is a key parameter to obtain high performances in the fuel cell. The particle size of the prepared catalysts can be controlled by changing the catalyst preparation conditions.

## CHAPTER 9

### CONCLUSION AND RECOMMENDATION

The aim of this study was to prepare the catalytically highly active Pt and PtRu based catalysts by using two different catalyst preparation methods which were supercritical carbon dioxide deposition and microwave irradiation. Since two different preparation methods were used, the results were also separated into two parts.

In experiments described in the first part, the catalysts were prepared by the help of supercritical carbon dioxide deposition method. Adsorption phenomenon was very important for determining the maximum metal loading that can be achieved at the reaction medium conditions. The support properties were also very important which affect the properties of the metal deposited. Adsorption studies showed that the carbon support properties (total, macroporous and micro/mesoporous surface areas) affect the maximum loading.

The carbon supports used in the experiments of supercritical carbon dioxide deposition were VXR, MWCNT and BP2000. The adsorption experiments showed that the higher the total surface area of the support the higher is the Pt loading achieved. For the VXR and MWCNT supports, which have surface areas close to each other, the Pt loadings were 9 and 15%, respectively. But for the BP2000 Pt loading as high as 47.5% was achieved. Similar results were obtained for Ru catalyst, but the loadings for the supports were not as high as Pt catalyst. For binary catalyst preparation, the bare carbon supports and

Pt/MWCNT and Pt/BP2000 catalysts were used as the substrate. The Langmuir fits of the adsorption curves helped to understand the adsorption behavior.

The prepared Pt based catalysts were characterized by using XRD, TEM and CV. XRD results showed that in catalysts prepared by using supercritical carbon dioxide deposition method, the particle sizes could be as low as 1-2 nm. Also the TEM results supported the findings from the XRD data. After physical characterization of the catalysts they were subjected to electrochemical characterization by using cyclic voltammetry. The real electrochemical surface area of the catalysts can be determined by CV. From the CV results the electrochemical surface areas of the Pt/VXR, Pt/MWCNT and Pt/BP2000 were found to be 173, 130 and 102 m<sup>2</sup>/g, respectively. These catalysts were also compared with a commercial Pt/C (Tanaka, 46.5 %) catalyst. Besides the ESA values the Pt utilization is very important which represents the utilized parts of the catalytically active sites. Although the highest ESA was achieved for Pt/VXR, the highest utilization was achieved for Pt/MWCNT. Also, for similar particle sized catalysts Pt/VXR (1.2 nm) and Pt/BP2000 (1 nm), the Pt utilization differed too much, which can be explained by the difference of the carbon support properties such as total surface area, high microporous surface area etc. For all the experiments discussed up to now the reduction of the precursor was achieved by using thermal reduction in an inert nitrogen atmosphere. To pass through the high Pt loadings another in situ reduction method was tested. Pt loadings on the VXR carbon support were obtained as 15 and 35% with the particle sizes of 1.3 and 2 nm, respectively. But the ESAs of the catalysts prepared with thermal reduction in supercritical carbon dioxide gave lower performance when compared to the catalysts prepared by thermal reduction in nitrogen. CV measurements were also used to determine the oxygen reduction reaction performance of the catalysts. From these experiments number of electrons transferred per oxygen molecule was calculated as 3.5, 3.6 and 3.7 for Pt/BP2000, Pt/VXR and Pt/MWCNT, respectively. These values indicate that the oxygen reduction reaction is close

to the  $4e^-$  pathway, which results in an almost complete water formation reaction and negligible hydrogen peroxide formation.

In the second part, the experiments comprised the preparation and testing of the Pt and PtRu based catalysts that were prepared by using microwave irradiation. In other words the required thermal environment was achieved by using microwave heating. The carbon supports used in the experiments were VX, Regal and BP2000. The experiments revealed that the microwave duration, base concentration, carbon support used and surfactant/precursor ratio have a significant impact on the properties of the catalysts. The particle sizes of the catalysts were ranging between 2-6 nm. From the XRD results, it was observed that the base concentration did not affect the particle size significantly. But for different microwave durations the particle sizes varied. This result showed that as the microwave duration increases the temperature of the reaction medium increases which resulted in the agglomeration of the Pt metals. The XRD results also showed that the addition of the surfactant to the reaction environment lowers the particle size of the single and binary catalysts because of covering the Pt metal and inhibiting the coalescence. The XPS was used to determine the surface oxidation states of the catalysts. For all the catalysts the Pt 4f signal consisted of three pairs of Pt peaks which correspond to  $Pt^0$ ,  $Pt^{+2}$  and  $Pt^{+4}$ . From the XPS core levels of C1s spectra the carbon oxidation was also investigated. The C1s spectrum obtained were composed of graphitic carbon and carbon with oxygen-containing functional groups. The same results were obtained for the prepared catalysts and the presence of higher oxygen-containing groups were detected for BP2000.

Prepared Pt based catalysts were tested in PEMFC as cathode electrode to determine the oxygen reduction reaction performance. The performance results for the catalysts prepared by different base concentration showed very similar results. For the catalysts prepared with different microwave durations, the best performance was obtained for microwave duration of 60s which resulted in

4.65 nm particle size. The higher particle sizes caused performance losses. The huge performance difference was obtained for the catalysts prepared with different carbon supports. The performance was ordered as Pt/VX>Pt/Regal>Pt/BP2000. It was seen that the carbon supports used did not only affect the particle size but also the performance. From the XPS results, it was observed that the surface oxidation states of Pt/BP2000 catalyst were the highest and this may clarify the low performance in the fuel cell. The addition of the surfactant decrease the particle size of the Pt, but this behavior had an adverse effect on the performance. Further increase in the surfactant amount did not affect the performance significantly. It was observed that the performance of the surfactant stabilized catalysts gave better performance at high current densities.

The binary catalysts were used in the anode compartment to see if the carbon dioxide tolerance can be increased or not. Binary catalysts either commercial or prepared showed the better tolerance to CO<sub>2</sub> than Pt based catalysts. It can be concluded that the catalyst properties not only depend on the catalyst preparation method but also depended on the preparation conditions, carbon supports used, oxidation states that occurred on the support or metal. So, it is crucial to optimize the conditions for getting higher catalytic activities.

Recommendations:

- The prepared binary PtRu/VX catalysts which were carbon dioxide tolerant can be tested in the fuel cell stack.
- The prepared binary PtRu/VX catalysts can also be tested with carbon monoxide.
- The long term operation tests are important to determine the life time of the catalysts.
- In supercritical carbon dioxide deposition PtRu based catalysts were prepared by using sequential impregnation which may affect the

catalyst properties, so the co-impregnation can also be used to prepare PtRu based catalysts.

- CV tests can be performed to the catalysts prepared by microwave irradiation.
- In order to decrease the Pt amount at the cathode side a low cost metal such as Co, Ni can be added.
- Mesoporous carbon supports can be used to eliminate the pure accessibility of the metals in the micropores.
- The oxidation states of the catalysts can be controlled by either chemical or physical treatments.

## REFERENCES

Akay R. G., "Development and characterization of composite proton exchange membranes for fuel cell applications", PhD Thesis, METU, Ankara, 2008.

Amine K., Yasuda K., Takenaka H., "New process for loading highly active platinum on carbon black surface for application in polymer electrolyte fuel cell", *Ann. Chim. Sci. Mat.* 23 (1998) 31.

Antoine O., Bultel Y., Durand R., "Oxygen reduction reaction kinetics and mechanism on platinum nanoparticles inside Nafion", *Electroanal. Chem.* 499 (2001) 85-94.

Antolini E., Giorgi L., Pozio A., Passalacqua E., "Influence of nafion loading in the catalyst layer of gas-diffusion electrodes for PEFC", *J. Power Sources* 77 (1999) 136-142.

Arai Y., Sako T., Takebayashi Y., "Supercritical fluids: molecular interactions, physical properties, and new applications", Springer-Verlag Berlin Heidelberg New York, 2002.

Avcı A. K., Trimm D. L., Önsan Z. İ., "On-board fuel conversion for hydrogen fuel cells: comparison of different fuels by computer simulations", *Applied Catalysis A: General* 216 (2001) 243-256.

Avcı A. K., Trimm D. L., Önsan Z. İ., "Heterogeneous reactor modeling for simulation of catalytic oxidation and steam reforming of methane", *Chemical Engineering Science* 56 (2001) 641-649.

Avcı A. K., Trimm D. L., Önsan Z. İ., "Quantitative investigation of catalytic natural gas conversion for hydrogen fuel cell applications", *Chemical Engineering Journal* 90 (2002) 77-87.

Babić B.M., Vračar Lj.M., Radmilović V., Krstajić N.V., "Carbon cryogel as support of platinum nano-sized electrocatalyst for the hydrogen oxidation reaction", *Electrochimica Acta* 51 (2006) 3820-3826.

Barbir F., "PEM fuel cells: Theory and practice", Elsevier Academic Press, USA, 2005.



Baschuk J.J., Li X., "Modelling CO Poisoning and O<sub>2</sub> Bleeding in a PEM Fuel Cell Anode", International journal of Energy Research, 27 (2003) 1095-1116.

Bayrakçeken A., "Determination of the factors that affect the performance of proton exchange membrane fuel cells", Ms Thesis, METU, Ankara, 2004.

Bayrakçeken A., Erkan S., Türker L., Eroğlu İ., "Effects of membrane electrode assembly components on proton exchange membrane fuel cell performance", 33 (2007) 165-170.

Bhatia K.K., Wang C.Y., "Transient carbon monoxide poisoning of a polymer electrolyte fuel cell operating on diluted hydrogen feed", Electrochimica Acta 49 (2004) 2333-2341.

Bron M., Fiechter S., Hilgendorff, M., Bogdanoff, P., "Catalysis for oxygen reduction from heat treated carbon-supported iron phenantrolin complexes", J. Appl. Chem. 32 (2002) 211-216.

Bruijn F. A., Papageorgopoulos D. C., Sitters E. F., Janssen G. J. M., "The influence of carbon dioxide on PEM fuel cell anodes", Journal of Power Sources 110 (2002) 117-124.

Choi K.H., Kim H.S., Lee T.H., "Electrode fabrication for proton exchange membrane fuel cells by pulse electrodeposition", Journal of Power Sources, 75 (1998) 230-235.

Chu H.S., Yeh C., Chen F., "Effects of porosity change of gas diffuser on performance of proton exchange membrane fuel cell", Journal of Power Sources 123 (2003) 1-9.

Cirimile V., Kintz P., Majdalini R., Mangin P., "Supercritical fluid extraction of drugs in drug addict hair", Journal of Chromatography B 673 (1995) 173-181.

Cooper K. R., Ramani V., Fenton J. M., Kunz H. R., "Experimental methods and data analyses for polymer electrolyte fuel cells", Scribner Associates Inc., USA, 2005.

Copson D. A., "Microwave Heating: In freeze drying, electronic ovens and other applications", Westport, Connecticut-USA, The AVI publishing Company Inc., 1962.

Costamagna P., Srinivasan S., "Quantum jumps in the PEMFC science and technology from the 1960s to the year 2000: Part I. Fundamental scientific aspects", Journal of Power Sources 102 (2001) 242.

Danmarks Tekniske Universitet, www.kemi.dtu.dk last accessed at 13.01.2008.

Denis M.C., Lalande G., Guay D., Dodelet J.P., Schulz R., "High energy ball-milled Pt and Pt-Ru catalysts for polymer electrolyte fuel cells and their tolerance to CO", *Journal of Applied Electrochemistry* 29 (1999) 951-960.

Divisek J., Oetjen H.F., Peimecke V., Schmidt V.M., Stimming U., "Components for PEM Fuel Cell systems using hydrogen and CO containing fuels", *Electrochimica Acta* 43 (1998) 3811-3815.

Dundar F., Smirnova A., Dong X., Ata A., Sammes N., "Rotating disk electrode study of supported and unsupported catalysts for PEMFC application", *J. Fuel Cell Sci. Technol.* 3 (2006) 428-433.

Ekström H., "Evaluating cathode catalysts in the polymer electrolyte fuel cell", PhD Thesis, Stockholm, 2007.

Erdener H., "Development of organic-inorganic composite membranes for fuel cell applications", Ms Thesis, METU, Ankara, 2007.

Erkan S., "Synthesis of some metalphythalocyanines and their effects on the performance of PEM fuel cells", Ms Thesis, METU, Ankara, 2005.

Erkey C., "Supercritical carbon dioxide extraction of metals from aqueous solutions: a review", *Journal of Supercritical Fluids* 17 (2000) 259-287.

Eroğlu E., Eroğlu İ., Gündüz U., Türker L., Yücel M., "Biological hydrogen production from olive mill wastewater with two-stage processes", *International Journal of Hydrogen Energy* 31 (2006) 1527-1535.

Escudero M. J., Hontañón E., Schwartz S., Boutonnet B., Daza L., "Development and performance characterisation of new electrocatalysts for PEMFC", *Journal of Power Sources* 106 (2002) 206-214.

Gasteiger H. A., Panels J. E., Yan S. G., "Dependence of PEM fuel cell performance on catalyst loading", *J. Power Sources* 127 (2004) 162-171.

Ghadamian H., Saboohi Y., "Quantitative analysis of irreversibilities causes voltage drop in fuel cell (Simulation&Modelling)", *Electrochimica Acta* 50 (2004) 699-704.

Giorgi L., Pozio A., Bracchini C., Giorgi R., Turtù S., "H<sub>2</sub> and H<sub>2</sub>/CO oxidation mechanism on Pt/C, Ru/C and Pt-Ru/C electrocatalysts", *Journal of Applied Electrochemistry* 31 (2001) 325-334.

Gloaguen F., Leger J.M., Lamy C., "Electrocatalytic oxidation of methanol on platinum nanoparticles electrodeposited onto porous carbon substrates", *J. Appl. Electrochem.* 27 (1997) 1052-1060.

González-Cruz R., Solorza-Feria O., "Oxygen reduction in acid media by a Ru<sub>x</sub>Fe<sub>y</sub>Se<sub>z</sub>(CO)<sub>n</sub> cluster catalyst dispersed on a glassy carbon supported Nafion film", *J. Solid State Electrochem.* 7 (2003) 289-295.

Götz M., Wendt H., "Binary and ternary anode catalyst formulations including the elements W, Sn and Mo for PEMFCs operated on methanol or reformat gas", *Electrochimica Acta* 43 (1998) 3637-3644.

Grujicic M., Zhao C. L., Chittajallu K. M., Ochterbeck J. M., "Cathode and interdigitated air distributor geometry optimization in polymer electrolyte membrane (PEM) fuel cells", *Materials Science and Engineering B-108* (2004) 241-252.

Halseid R., Vie J. S. P., Tunold R., "Effect of ammonia on the performance of polymer electrolyte membrane fuel cells", *Journal of Power Sources* 154 (2006) 343-350.

Haji S., Zhang Y., Kang D., Aindow M., Erkey C., "Hydrodesulfurization of model diesel using Pt/Al<sub>2</sub>O<sub>3</sub> catalysts prepared by supercritical deposition", *Catalysis Today* 99 (2005) 365-373.

Hamann C. H., Hamnett A., Vielstich W., "Electrochemistry", 1<sup>st</sup> Edn., Wiley-VCH, Weinheim, 1998.

Hoare J. P., "The electrochemistry of oxygen", John Wiley and Sons, New York, 1968.

Hoogers G., "Fuel Cell Technology Handbook", CRC Press, USA, 2003.

Hou Z., Yi B., Yu H., Lin Z., Zhang H., "CO tolerance electrocatalyst of PtRu-H<sub>x</sub>MeO<sub>3</sub>/C (Me=W, Mo) made by composite support method, *Journal of Power Sources* 123 (2003) 116-125.

Hui C.L., Li X.G., H. I.M., "Well-dispersed surfactant stabilized Pt/C nanocatalysts for fuel cell application: Dispersion control and surfactant removal", *Electrochimica Acta* 51 (2005) 711-719.

Hyatt J. A., "Liquid and supercritical carbon dioxide a organic solvents", *J. Org. Chem.* 49 (1984) 5097-5101.

Isono T., Suzuki S., Kaneko M., Akiyama Y., Miyake Y., Yonezu I., "Development of a high-performance PEFC module operated by reformed gas", *Journal of Power Sources* 86 (2000) 269-273.

Janssen G. J. M., "Modeling study of CO<sub>2</sub> poisoning on PEMFC anodes", *Journal of Power Sources* 136 (2004) 45-54.

Jiang J., Yi B., "Thickness effects of a carbon-supported platinum catalyst layer on the electrochemical reduction of oxygen in sulfuric acid solution", *J. Electroanal. Chem.* 577 (2005) 107-115.

Jiang R., Zhang Y., Swier S., Wei X., Erkey C., Kunz H. R., Fenton J. M. "Preparation via supercritical fluid route of Pd-impregnated Nafion membranes which exhibit reduced methanol crossover for DMFC", *Electrochemical and Solid-State Letters* 8 (11) (2005) A611-A615.

Kappe O. C., "Controlled microwave heating in modern organic synthesis", *Angew. Chem. Int. Ed.* 43 (2004) 6250-6284.

Kawaguchi T., Sugimoto W., Murakami Y., Takasu Y., "Particle growth behavior of carbon-supported Pt, Ru, PtRu catalysts prepared by an impregnation reductive-pyrolysis method for direct methanol fuel cell anodes" *Journal of Catalysis* 229 (2005) 176-184.

Kemmere F. M., Meyer, T., "Supercritical carbon dioxide: in polymer reaction engineering", Wiley, Weinheim, 2005.

Kiran E., Brennecke J. F., "Supercritical fluid engineering science: Fundamentals and applications", American Chemical Society, California, USA, 1991.

King D. A., "From supersonic beams and single crystal microcalorimetry to the control of catalytic reactions", *Studies in Surface Science and Catalysis* 109 (1997) 79-89.

Korsgaard A. R., Refshauge R., Nielsen M. P., Banga M., Kær S. K., "Experimental characterization and modeling of commercial polybenzimidazole-based MEA performance", *Journal of Power Sources* 162 (2006) 239-245.

Kruk, M., Jaroniec, M., Berezniński, Y., "Adsorption study of porous structure development carbon blacks", *Journal of Colloid and Interface Science* 182 (1996) 282-288.

Kunimoto T., Inaba M., Nakayama Y., Ogata K., Umebayashi K., Tasaka A., Iriyama Y., Abe T., Ogumi Z., "Durability of perfluorinated ionomer

membrane against hydrogen peroxide”, *Journal of Power Sources* 158 (2006) 1222-1228.

Larminie J., Dicks A., "Fuel Cell Systems Explained", 2<sup>nd</sup> Edn., John Wiley&Sons, USA, 2003.

Lee H. K., Park J. H., Kim D. Y., Lee T. H., "A study on the characteristics of the diffusion layer thickness and porosity of the PEMFC", *Journal of Power Sources* 131 (2004) 200-206.

Lee S. J., Mukerjee S., McBreen J., Rho Y. W., Kho Y. T., Lee T. H., "Effects of nafion impregnation on performances of PEMFC electrodes", *Electrochimica Acta* 43 (1998) 3693-3701.

Lee W.K., Ho C.H., Zee J.W.V., Murthy M., "The effects of compression and gas diffusion layers on the performance of a PEM fuel cell", *Journal of Power Sources* 84 (1999) 45-51.

Leitner W., "Supercritical carbon dioxide as a green reaction medium for catalysis", *Acc. Chem. Res.* 35 (2002) 746-756.

Li W., Liang C., Zhou W., Qiu J., Zhou Z., Sun G., Xin Q., "Preparation and characterization of multiwalled carbon nanotube-supported platinum for cathode catalysts of direct methanol fuel cell", *J. Phys. Chem B* 107 (2003) 6292-6299.

Li X., Chen W. X., Zhao J., Xing W., Xu Z. D., "Microwave polyol synthesis of Pt/CNTs catalysts: Effects of pH on particle size and electrocatalytic activity for methanol electrooxidation", *Carbon* 43 (2005) 2168-2174.

Li X., Hsing I. M., "The effect of the Pt deposition method and the support on Pt dispersion on carbon nanotubes", *Electrochimica Acta* 51 (2006) 5250-5258.

Liang Y., Zhang H., Zhong H., Zhu X., Tian Z., Xu D., Yi B., "Preparation and characterization of carbon-supported PtRuIr catalyst with excellent CO-tolerant performance for proton-exchange membrane fuel cells", *Journal of Catalysis* 238 (2006) 468-476.

Lin Y., Cui X., Clive Y. H., Wai C. M., "PtRu/carbon nanotube nanocomposite synthesized in supercritical fluid: a novel electrocatalyst for direct methanol fuel cells", *Langmuir* 21 (2005) 11474-11479.

Lin Y., Cui X., Clive Y., Wai C. M., "Platinum/Carbon nanotube nanocomposite synthesized in supercritical fluid as electrocatalysts for low-temperature fuel cells", *J. Phys. Chem. B* 109 (2005) 14410-14415.

Liu Z., Lee J. Y., Han M., Chen, W., Gan L. M., "Synthesis and characterization of PtRu/C catalysts from microemulsion and emulsions", *J. Mater. Chem.* 12 (2002) 2453-2458.

Liu Z. L., Lin X., Lee J. Y., Zhang W., Han M., Gan L. M., "Preparation and Characterization of Platinum-Based Electrocatalysts on Multiwalled Carbon Nanotubes for Proton Exchange Membrane Fuel Cells", *Langmuir* 18 (2002) 4054-4060.

Liu Z. L., Lee J. Y., Chen W., Han M., Gan L. M., "Physical and electrochemical characterizations of microwave-assisted polyol preparation of carbon-supported PtRu nanoparticles", *Langmuir* 20 (2004) 181-189.

Liu Z., Gan L. M., Hong L., Chen W., Lee J. Y., "Carbon-supported Pt nanoparticles as catalysts for proton exchange membrane fuel cells", *Journal of Power Sources* 139 (2005) 73-78.

Liu Z., Guo B., Hong L., Lim T. H., "Microwave heated polyol synthesis of carbon-supported PtSn nanoparticles for methanol electrooxidation", *Electrochemistry Communications* 8 (2006) 83-90.

Liu Z. L., Hong L., Tham M. P., Lim T. H., Jiang H., "Nanostructured Pt/C and Pd/C catalysts for direct formic acid fuel cells", *Journal of Power Sources* 161 (2006) 831-835.

Londhe, V. P., Gupta, N. M., "Adsorption and microcalorimetric measurements on the interaction of CO and H<sub>2</sub> with polycrystalline Ru and Ru/TiO<sub>2</sub> catalyst", *Journal of Catalysis* 169 (1997) 415-422.

Luna A.M.C, Camara G.A., Paganin V.A., Ticianelli E.A., Gonzalez E.R., "Effect of thermal treatment on the performance of CO-tolerant anodes for polymer electrolyte fuel cells", *Electrochemistry Communications* 2 (2000) 222-225.

Ma L., Zhang H., Liang Y., Xu D., Ye W., Zhang J., Yi B., "A novel carbon supported PtAuFe as CO-tolerant anode catalyst for proton exchange membrane fuel cells", *Catalysis Communications* 8 (2007) 921-925.

Marie J., Berthon-Fabry S., Achard P., Chatenet M., Pradourat A., Chainet E., "Highly dispersed platinum on carbon aerogels as supported catalysts for PEM fuel cell-electrodes: comparison of two different synthesis paths", *Journal of Non-crystalline Solids* 350 (2004) 88-96.

Marković N. M., Gasteiger H. A., Ross P. N., "Oxygen reduction on Platinum low-index single-crystal surfaces in sulfuric acid solutions: rotating ring-Pt(hkl) disk studies", *Journal of Physical Chemistry* 99 (1995) 3411-3415.

Marković N. M., Gasteiger H. A., Grgur B. N., Ross P. N., "Oxygen reduction reaction on Pt(111): effects of bromide", *Journal of Electroanalytical Chemistry* 467 (1999) 157-163.

Marković N. M., Schmidt T. J., Stamenković V., Ross P. N., "Oxygen reduction reaction on Pt and Pt bimetallic surfaces: A selective review", *Fuel Cells* 1 (2001) 105-116.

Maruyama J., Abe I., "Application of conventional activated carbon loaded with dispersed Pt to PEFC catalyst layer", *Electrochimica Acta* 48 (2003) 1443-1450.

Mello R. M. Q., Ticianelli E. A., "Kinetic study of the hydrogen oxidation reaction on platinum and Nafion<sup>®</sup> covered platinum electrodes", *Electrochimica Acta* 42 (1997) 1031-1039.

Mulcahey L. J., Taylor L. T., "Supercritical extraction of active components in a drug formulation", *Anal. Chem.* 64 (1992) 981-984.

Nalawade S. P., Picchioni F., Janssen L. P. B. M., "Supercritical carbon dioxide as a green solvent for processing polymer melts: Processing aspects and applications", *Progress in Polymer Science* 31 (2006) 19-43.

Paddison S.J., "Proton Conduction Mechanism at Low Degrees of Hydration in Sulfonic Acid-based Polymer Electrolyte Membranes", *Annu. Rev. Mater. Res.* 33 (2003) 289-319.

Pan M., Tang H. L., Jiang S. P., Liu Z. "Self-assembled membrane-electrode-assembly of polymer electrolyte fuel cells", *Electrochemistry Communications* 7 (2005) 119-124.

Papageorgopoulos D.C., Keijzer M., De Bruijn F.A., "The inclusion of Mo, Nb and Ta in Pt and PtRu carbon supported 3electrocatalysts in the quest for improved CO tolerant PEMFC anodes", *Electrochimica Acta* 48 (2002) 197-204.

Passalacqua E., Lufrano F., Squadrito G., patti A., Giorgi L., "Nafion content in the catalyst layer of polymer electrolyte fuel cells: Effects on structure and performance", *Electrochimica Acta* 46 (2001) 799-803.

Passos R.R., Ticianelli E.A., "Effects of the operational conditions on the membrane and electrode properties of a polymer electrolyte fuel cell", *J. Braz. Chem. Soc.* 13 (2002) 483-489.

Pozio A., Francesco M. DE, Cemmi A., Cardellini F., Giorgi L., "Comparison of high surface Pt/C catalysts by cyclic voltammetry", *J. Power Sources* 105 (2002) 13-19.

Qi Z., Lefebvre M.C., Pickup P.G., "Electron and proton transport in gas diffusion electrodes containing electronically conductive proton-exchange polymers", *Journal of Electroanalytical Chemistry* 459 (1998) 9-14.

Qi Z., Kaufman A., "CO-tolerance of low-loaded Pt/Ru anodes for PEM fuel cells", *Journal of Power Sources* 113 (2003) 115-123.

Raghuveer V., Manthiram A., "Mesoporous carbon with larger pore diameter as an electrocatalyst support for methanol oxidation", *Electrochemical and Solid State Letters* 7 (2004) A336-A339.

Resources for electrochemistry, [www.consultrsr.com/resources](http://www.consultrsr.com/resources) last accessed at 13.01.2008.

Reubroycharoen P., Vitidsant T., Liu Y., Yang G., Tsubaki N., "Highly active Fischer–Tropsch synthesis Co/SiO<sub>2</sub> catalysts prepared from microwave irradiation", *Catalysis Communications* 8 (2007) 375-378.

Robinson J. P., Kingman S. W., Onobrakpeya O., "Microwave-assisted stripping of oil contaminated drill cuttings", *Journal of Environmental Management*, Article in press.

Rodríguez J. M. D., Melián J. A. H., Peña J. P., "Determination of the real surface area of Pt electrodes by hydrogen adsorption using cyclic voltammetry", *Journal of Chemical Education* 77 (9) (2000) 1195-1197.

Rohland B., Plzak V., "The PEMFC-integrated CO oxidation –a novel method of simplifying the fuel cell plant", *Journal of Power Sources* 84 (1999) 183-186.

Royal Society of Chemistry, <http://pubs.rsc.org> last accessed at 13.01.2008.

Saquin C. D., Cheng T. T., Aindow M., Erkey C., "Preparation of platinum/carbon aerogel nanocomposites using a supercritical deposition method", *J. Phys. Chem. B* 108 (2004) 7716-7722.

Saquin C. D., Kang D., Aindow M., Erkey C., "Investigation of the supercritical deposition of platinum nanoparticles into carbon aerogels", *Microporous and Mesoporous Materials* 80 (2005) 11-23.



Shao Y., Yin G., Wang J., Gao Y., Shi P., "Multi-walled carbon nanotubes based Pt electrodes prepared with in situ ion Exchange method for oxygen reduction", *Journal of Power Sources* 161 (2006) 47-53.

Shan J., Pickup P. G., "Characterization of polymer supported catalysts by cyclic voltammetry and rotating disk voltammetry", *Electrochimica Acta* 46 (2000) 119-125.

Shi W., Yi B., Hou M., Shao Z., "The effect of H<sub>2</sub>S and CO mixtures on PEMFC performance", *International Journal of Hydrogen Energy* 32 (2007) 4412-4417.

Smirnova A., Dong X., Hara H., Vasiliev A., Zammes N., "Novel carbon-aerogel supported catalysts for PEM fuel cell applications" *International Journal of Hydrogen Energy* 30 (2005) 149-158.

Song S., Wang Y., Shen P., "Pulse-microwave assisted polyol synthesis of highly dispersed high loading Pt/C electrocatalyst for oxygen reduction", *Reaction Journal of Power Sources* 170 (2007) 46-49.

Sperling D., Cannon J. S., "The hydrogen energy transition: Moving toward the post petroleum age in transportation", Elsevier Science and Technology Books, Academic Press 2004.

Spiewak B. E., Cortright R. D., Dumesic J. A., "Microcalorimetric measurements of differential heats of adsorption on reactive catalyst surfaces", *Thermochimica Acta* 290 (1996) 43-53.

Spiewak B. E., Dumesic J. A., "Microcalorimetric Studies of H<sub>2</sub>, C<sub>2</sub>H<sub>4</sub>, and C<sub>2</sub>H<sub>2</sub> Adsorption on Pt Powder", *Journal of Catalysis* 176 (1998) 405-414.

Spiewak B. E., Dumesic J. A., "Applications of adsorption microcalorimetry for the characterization of metal-based catalysts", *Thermochimica Acta* 312 (1998) 95-104.

Sridhar P., Perumal R., Rajalakshmi N., Raja M., Dhathathreyan K.S., "Humidification Studies on Polymer Electrolyte Membrane Fuel Cell", *Journal of Power Sources* 101 (2001) 72-78.

Starz K.A., Auer E., Lehmann Th., Zuber R., "Characteristics of Platinum-based Electrocatalysts for Mobile PEMFC Applications", *Journal of Power Sources* 84 (1999) 167-172.

Stevens D. A., Hicks M. T., Haugen G. M., Dahn J. R., "Ex situ and in situ stability studies of PEMFC catalysts: Effect of carbon type and humidification

on degradation of the carbon, *Journal of the Electrochemical Society* 152 (12) (2005) A2309-A2315.

Suárez-Alcantara K., Rodríguez-Castellanos A., Dante R., Solorza-Feria O., "Ru<sub>x</sub>Cr<sub>y</sub>Se<sub>z</sub> electrocatalyst for oxygen reduction in a polymer electrolyte membrane fuel cell", *J. Power Sources* 157 (2006) 114-120.

Subramaniam B., Rajewski R. A., Snively K., "Pharmaceutical processing with supercritical carbon dioxide", *Journal of Pharmaceutical Sciences* 86 (1997) 885-890.

Sun Z., Liu Z., Han B., An G. "Supercritical carbon dioxide assisted deposition of tin oxide on carbon nanotubes", *Materials Letters* 61 (2007) 4565-4568.

Şen F., Gökağaç G., "Different sized platinum nanoparticles supported on carbon: An XPS study on these methanol oxidation catalysts", *J. Phys. Chem. C* 111 (2007) 5715 -5720.

Şengül E., "Preparation and performance of membrane electrode assemblies with Nafion and alternative polymer electrolyte membranes", Ms Thesis, METU, Ankara, 2007.

Şengül E., Erkan S., Baç N., Eroğlu İ., "Development of gas diffusion electrodes for polymer electrolyte membrane fuel cells", Somer Symposium Series 1, Ankara-Türkiye, (2007).

Tian Z. Q., Wang X. L., Zhang H. M., Yi B. L., Jiang S. P., "Microwave-assisted synthesis of PTFE/C nanocomposite for polymer electrolyte fuel cells", *Electrochemistry Communications* 8 (2006) 1158-1162.

Tierney J. P., Lidström P., "Microwave assisted organic synthesis", CRC Press, USA and Canada, 2005.

Udomi, [www.udomi.de/images/fcm.gif](http://www.udomi.de/images/fcm.gif) last accessed at 13.01.2008.

Urian R.C., Gulla A.F., Mukerjee S., "Electrocatalysis of reformate tolerance in proton exchange membrane fuel cells:Part 1", *Journal of Electroanalytical Chemistry*, 554 (2003) 307-324.

Wang H. W., Dong R-X., Chang H-Y, Liu C-L, Chen-Yang Y-W., "Preparation and catalytic activity of Pt/C materials via microwave irradiation", *Materials Letters* 61 (2007) 830-833.

Wang J., Yin G., Shao Y., Zhang S., Wang Z., Gao Y., "Effect of carbon black support corrosion on the durability of Pt/C catalyst", *Journal of Power Sources* 171 (2007) 331-339.

Wang L., Liu H., "Performance studies of PEM fuel cells with interdigitated flow fields", *Journal of Power Sources*, 134 (2004) 185-196.

Weibel G. L., Ober C. K., "An overview of supercritical CO<sub>2</sub> applications in microelectronics processing", *Microelectronic engineering* 65 (2003) 145-152.

White A., Burns D., Christensen T. W., "Effective terminal sterilization using supercritical carbon dioxide", *Journal of Biotechnology*, 123 (2006) 504-515.

Wikander K., Ekström H., Palmqvist A. E. C., Lindbergh, G., "On the influence of Pt particle size on the PEMFC cathode performance", *Electrochimica Acta* 52 (2007) 6848-6855.

Williams M.V., Kunz H.R., Fenton J.M., "Operation of Nafion-based PEM fuel cells with no external humidification: Influence of operating conditions and gas diffusion layers", *Journal of Power Sources* 135 (2004) 122-134.

Xiong L., Manthiram A. "High performance membrane-electrode assemblies with ultra-low Pt loading for proton exchange membrane fuel cells", *Electrochimica Acta* 50 (2005) 3200-3204.

Yamada Y., Ueda A., Shioyama H., Kobayashi T., "High-throughput Screening of PEMFC Anode Catalysts by IR Thermography", *Applied Surface Science* 223 (2004) 220-223.

Yazaydın A. Ö, "Investigation of new horizons on H<sub>2</sub>/O<sub>2</sub> proton exchange membrane fuel cells", Ms Thesis, METU, Ankara, 2003.

Yu H., Hou Z., Yi B., Lin Z., "Composite anode for CO tolerance proton exchange membrane fuel cells", *Journal of Power Sources* 105 (2002) 52-57.

Yu E. H., Scott K., Reeve R. W., "Electrochemical reduction of oxygen on carbon supported Pt and Pt/Ru fuel cell electrodes in alkaline solutions", *Fuel Cells* 3 (2003) 169-176.

Yu K. M. K., Yeung C. M. Y., Thompsett D., Tsang S. C., "Aerogel-coated metal nanoparticle colloids as novel entities for the synthesis of defined supported metal catalysts", *J. Phys. Chem. B* 107 (2003) 4515-4526.

Yurdakul, A. Ö, "Acid-doped polybenzimidazole membranes for high temperature proton exchange membran fuel cells", Ms Thesis, METU, Ankara, 2007.

Zečević S. K., Wainright J. S., Litt M. H., Gojković S. LJ., Savinell R. F., J. "Kinetics of O<sub>2</sub> reduction on Pt electrode covered with a thin film of solid polymer electrolyte", *Electrochem. Soc.* 144 (1997) 2973-2982.

Zhang J., Wang X., Wu C., Wang H., Yi B., Zhang H., "Preparation and characterization of Pt/C catalysts for PEMFC cathode: effect of different reduction methods", *React. Kinet. Catal. Lett.* 83 (2004) 229-236.

Zhang, Y., Erkey, C., "Preparation of Platinum-Nafion-Carbon black nanocomposites via a supercritical fluid route as electrocatalysts for Proton Exchange Membrane Fuel Cells", *Ind. Eng. Chem. Res.* 44 (2005) 5312-5317.

Zhang Y., Kang D., Aindow M., Erkey C., "Preparation and characterization of ruthenium/carbon aerogel nanocomposites via a supercritical fluid route", *J. Phys. Chem. B* 109 (2005) 2617-2624.

Zhang Y., Kang D., Saquing C., Aindow M., Erkey C., "Supported platinum nanoparticles by supercritical deposition", *Ind. Eng. Chem. Res.* 44 (2005) 4161-4164.

Zhang Y., Erkey C., "Preparation of supported metallic nanoparticles using supercritical fluids: A review", *J. of Supercritical Fluids* 38 (2006) 252-267.

Zhao J., Wang P., Chen W., Liu R., Li X., Nie Q., "Microwave synthesis and characterization of acetate-stabilized Pt nanoparticles supported on carbon for methanol electro-oxidation", *Journal of Power Sources* 160 (2006) 563-569.

Zhao Z. W., Guo Z. P., Ding J., Wexler D., Ma Z. F., Zhang D. Y., Liu H. K., "Novel ionic liquid supported synthesis of platinum-based electrocatalysts on multiwalled carbon nanotubes", *Electrochem. Commun.* 8 (2006) 245-250.

## APPENDIX A

### SAMPLE CALCULATIONS

#### A.1 Calculation of particle size

The particle sizes of the catalysts were calculated by using Scherrer equation and the XRD spectra. The required parameters are given in Figure A.1.

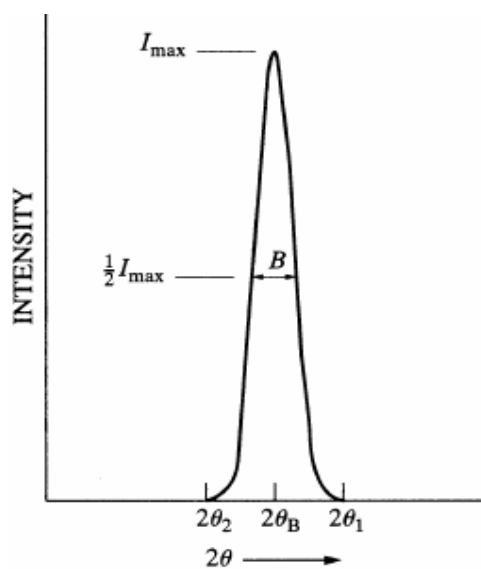


Figure A.1 XRD pattern

$$B \approx \frac{1}{2}(2\theta_1 - 2\theta_2) = \theta_1 - \theta_2 \quad (\text{A.1})$$

The Scherrer equation was as follows:

$$t = \frac{K \lambda}{B \cos \theta_B} \quad (\text{A.2})$$

where, K is the Scherrer constant,  $\lambda$  is the wavelength of radiation ( $\lambda_{\text{Cu,K}\alpha}=0.154$  nm), and B is the integral breadth of peak (in radians  $2\theta$ ) located at angle  $\theta_B$ . The particle size of the Pt/VX (50s microwave duration, BC=0.54 g/l) catalyst was calculated from the (220) plane.

For Pt/VX catalyst:

$$B = 2.88^\circ = 2.88^\circ \cdot 2 \cdot \pi / 360 = 0.0502 \text{ rad}$$

$$2 \theta_B = 67.6^\circ$$

$$K = 0.9$$

$$t = \frac{(0.9)(0.154)}{0.0502 \cos(67.6/2)} = 3.32 \text{ nm}$$

## A.2 Calculation of metal total surface area (SA)

If the metal particles are assumed to be spherical the surface area per mass can be expressed as:

$$SA = \frac{4\pi r^2}{\rho(4/3\pi r^3)} = \frac{3 \cdot 10^3}{\rho r} = \frac{6 \cdot 10^3}{\rho d} \quad (\text{A.3})$$

where  $\rho$  is the density of Pt ( $21.4 \text{ g/cm}^3$ ),  $d$  is the XRD particle size of Pt in nm. The total surface area was calculated by using the equation above and the Pt particle size obtained from the XRD data. SA for Pt/MWCNT which has a particle size of 2 nm is given below:

$$Pt/MWCNT; SA = \frac{6 \cdot 10^3}{(21.4)(2)} = 140.2 \text{ m}^2 \text{ g}^{-1}$$

### A.3 Calculation of electrochemical surface area (ESA)

Electrochemical surface areas (ESAs) of the catalysts were calculated by using the equation below taking into account the hydrogen reduction peak.

$$ESA = \frac{A}{K \cdot L \cdot S} \quad (\text{A.4})$$

where  $A$  is the area under the curve for hydrogen reduction part excluding double layer capacitance up to second inflection point,  $K=0.21 \text{ mC/cm}^2$ ,  $S$  is the scan rate ( $50 \text{ mV/s}$ ) and  $L$  is the Pt loading on the electrode. The ESA calculation for the prepared Pt/MWCNT catalyst is given below. The area under the curve of the hydrogen reduction peak from the figure was determined by using a computer program named Origin Lab 7.5. A sample graph for Pt/MWCNT is given in Figure A.2.

Pt/MWCNT;  $A=0.000382432 \text{ A.V/cm}^2$ ,  $K=0.21 \text{ mC/cm}^2$  ( $1 \text{ C}=1\text{A. 1s}$ )

$$L=28 \text{ }\mu\text{g/cm}^2, S=50 \text{ mV/s}$$

$$ESA = \frac{0.000382432}{(0.21)(28)(50)} 10^8 = 130 \text{ m}^2 \text{ g}^{-1}$$

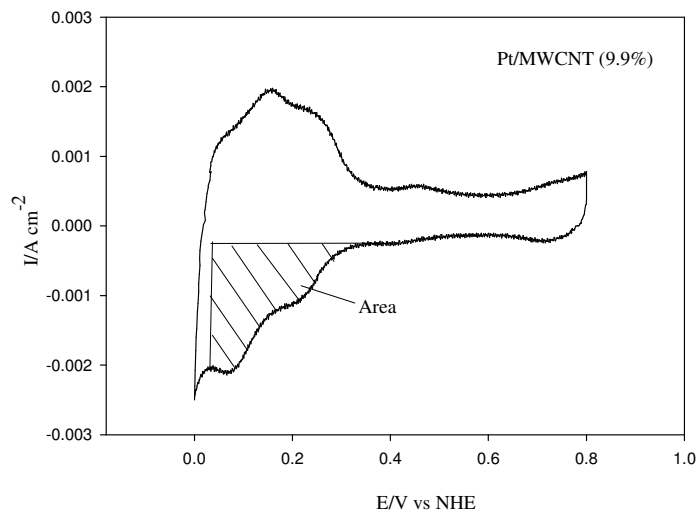


Figure A.2 Sample ESA graph for Pt/MWCNT

#### A.4 Calculation of Pt utilization

The Pt utilization is related with the contact of the metal and the accessibility of the metals with the electrolyte. It is expressed by the ratio of ESA to SA as given below:

$$Pt_{ut} (\%) = \frac{ESA}{SA} 100 \quad (A.5)$$

The Pt utilization for the prepared Pt/MWCNT is given below:

$$\text{Pt/MWCNT; } Pt_{ut} (\%) = \frac{130}{140.2} 100 = 93 \%$$



### A.5 Calculation of Tafel slope

By using the voltage-current density data and the formula given below the Tafel slope was calculated for Pt/Regal as given in Figure A3.

$$\Delta V_{act} = a + b \log(i) \text{ and } \Delta V_{act} = V_{rev} - V_{cell} \quad (\text{A.6})$$

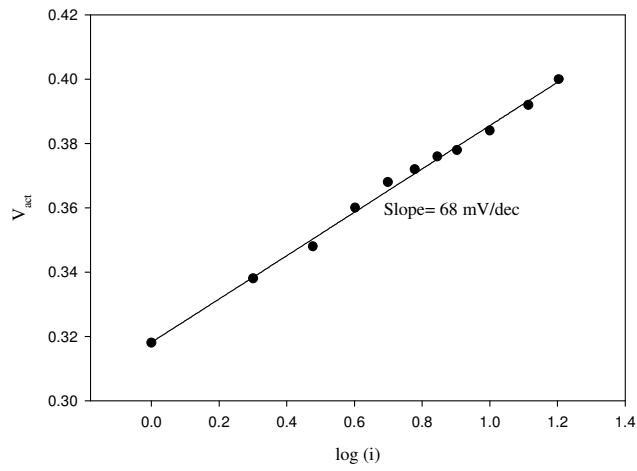


Figure A.3 Tafel slope for Pt/Regal

## APPENDIX B

### MEA PREPARATION PROTOCOL

1. Nafion 112 is cut into 5cm\*5cm dimensions.
2. GDL 31BC type gas diffusion layer is cut into 2.1cm\*2.1 cm dimensions and weighed with a balance (X=tare of the GDL).
3. Catalyst solution is prepared. The amounts of the chemicals given below are based on 20% Pt/C catalyst and 0.4 mgPt/cm<sup>2</sup> on the electrode.

$$\text{Pt/C amount} = (0.4 \text{ mgPt/cm}^2) * (5 \text{ cm}^2) * (100 \text{ mgPt/C} / 20 \text{ mgPt}) / 1000 \\ = 0.01 \text{ g Pt/C}$$

$$\text{Nafion amount} = (0.01) * (0.3) / (0.7) = 0.0043 \text{ g Nafion}$$

$$\text{Nafion solution amount} = (0.0043) * 100 / 5 = 0.0857 \text{ g Nafion solution}$$

3 times more than required amounts per 1 electrode to compensate the losses arised from spraying;

0.03 g Pt/C (20%)

0.2571 g Nafion solution (5%)

2 ml H<sub>2</sub>O

4 ml

This chemicals are mixed and then ultrasonicated for 1 hour and then sprayed onto the GDL by using spray gun and dried by a hot air gun.

4. After sprayed and dried the GDL weighed periodically to see if the weight of the GDL is reached to:  $X_{\text{final}}=X+(0.01)+(0.0043)$  g. If the weight is reached to  $X_{\text{final}}$  then the GDLs are ready for hot pressing.
5. Two electrodes are prepared in the same way and then they placed on two sides of the Nafion 112 membrane reciprocally. Then the MEA is hot pressed at 130°C and 250 psi.
6. After the hot press waited for a while for the MEA to cool down and then it is ready for use in fuel cell.

## APPENDIX C

### CYCLIC VOLTAMMETRY (CV)

By using rotating disk electrode electrochemical characterization of the catalysts can be made. By this technique some kinetic parameters such as Tafel slope, reaction orders, and apparent activation enthalpies can be determined in the absence of mass transport effects. To make the electrochemical characterization by using RDE mostly a three electrode cell configuration which includes counter, working and reference electrodes was used.

*Working electrode (WE):* The desired reaction takes place at the WE. Mostly a glassy carbon disk or ring electrode were used. The functions of the reference and counter electrodes are to ensure that the WE actually experiences the desired conditions, i.e. correct potential intended to be applied.

*Reference electrode (RE):* Function is to measure the potential at the interface of the WE and the sample as accurately as possible. In an ideal situation, no current passes through the RE. Ag-AgCl, Hg-HgSO<sub>4</sub> can be used.

*Counter electrode (CE):* function is to ensure that the correct potential difference between the RE and the WE is being applied. Platinum wire can be used as CE.

The potential difference between the WE and the RE is assumed to be the same as the desired potential at the WE. If the potential measured at the WE is not the potential desired at the WE, the potential that is applied between the CE

and WE is altered accordingly, i.e. the potential is either increased or decreased.

The reaction at the CE is also equal and opposite to the charge transfer reaction occurring at the WE, i.e. if an oxidation reaction is occurring at the WE then a reduction reaction will take place at the CE, thereby allowing the sample to remain electrically neutral.

A RE provides a reference for the voltage applied at the WE. The voltage applied must be sufficient to oxidize or reduce the species (molecule or ion) of interest at the surface of the WE. The voltage required is determined by the ease of removing or adding an electron to the species of interest. Because this voltage is applied externally (by means of potentiostat or battery), the reference point should be maintained at a constant value. If the value of the reference point changes with time, the external voltage applied should be varied accordingly. The three electrode cell configuration for CV measurements is given in Figure C.1.

As counter electrode mostly Pt wire is used because it is assumed to be an inert metal. In the WE desired oxidation or reduction reactions occur and if a reduction reaction occurs in WE in the CE oxidation reaction occurs and vice versa. The reaction at the WE needs to be examined to determine the relationship between the current and the voltage that is required to drive this reaction. Measurement of the potential between the WE and RE allows the change in potential of the WE needed to cause current to flow to be found. Normally the RE is separated from the WE with a compartment which is then connected with the WE with a salt bridge which contains the electrolyte. This permits separation of the bulk properties of the electrolyte from the interfacial properties. To minimize the additional resistance placed two as close as possible without disturbing the current flow to the WE.

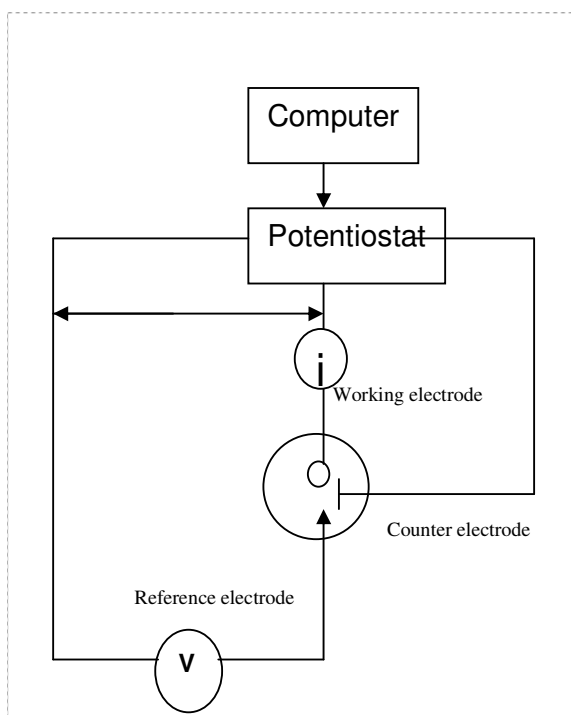
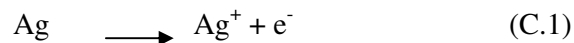


Figure C.1 Three electrode cell configuration

RE provides a standard redox reaction that will accept or give up electrons to the electrolyte. Ag/AgCl RE consists of a Ag metal wire and a AgCl salt. The basic reaction:



The Ag and  $\text{Ag}^+$  are surrounded by a solution of KCl which maintains electrical neutrality. When the reaction goes to the right then a  $\text{K}^+$  is released to the electrolyte through the salt bridge because salt bridge only allows ions to pass not electrolyte. When the reaction goes to the left then a  $\text{Cl}^-$  is released through the salt bridge.

Potentials for Ag/AgCl reference electrode is given below (<http://www.consultrsr.com/resources/ref/refpotls.htm#ssce> last accessed at 13.01.2008) in Table C.1.

Table C.1 Potentials for Ag/AgCl reference electrode

Potential @ 25°		
	vs. NHE	vs. SCE
Ag/AgCl, KCl (0.1M)	0.2881	0.047
Ag/AgCl, KCl (3M)	0.210	-0.032
Ag/AgCl, KCl (3.5M)	0.205	-0.039
Ag/AgCl, KCl (sat'd)	0.197	-0.045

## APPENDIX D

### FUEL CELL OPERATING PROTOCOL

After the fuel cell is connected to the home made test station the following procedure is followed:

- The humidifiers temperatures were set to 70°C.
- The fuel cell temperature was set to 70°C.
- The gas lines coming from humidifiers to fuel cell are heated to 75°C.
- Before the gases opened anode side of the fuel cell was purged with nitrogen.
- After the set temperatures were reached then the hydrogen and oxygen gases were opened with a flow rate of 0.1 slm.
- The fuel cell operated at 0.5 V overnight.
- The current density-potential data were recorded in the period of 15 min time intervals. When the steady state is reached the system closed.



## APPENDIX E

### REPRODUCIBILITY

To determine the reproducibility of the prepared catalysts a Pt/VX catalyst was prepared by microwave irradiation in different batches of experiments. Then the PEMFC test results were performed to see the reproducibility. The Figure E.1 shows the PEMFC performance results for 2 batches of the Pt/VX catalyst.

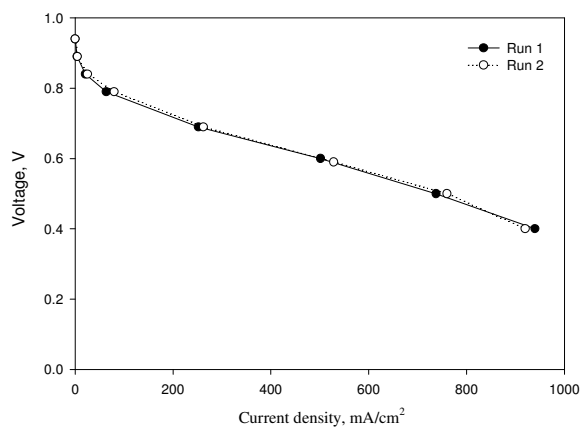


Figure E1 Reproducibility of the catalyst of Pt/VX (20%)

## CURRICULUM VITAE

Ayşe Bayrakçeken  
Middle East Technical University  
Department of Chemical Engineering  
06531 Ankara/Turkey

### PERSONAL INFORMATION

Nationality: Turkish (TC)  
Place of Birth: Erzurum  
Phone: +90 312 210 43 54  
Fax: +90 312 210 26 00  
E-mail: aybayrak@metu.edu.tr

### EDUCATION

Degree	Institution	Year of Graduation
Ph. D.	METU Chemical Engineering	2008
M. Sc.	METU Chemical Engineering	2004
B. Sc	Atatürk University Chemical Engineering	2000
High School	Erzurum Anatolian High School	1996

### WORK EXPERIENCE

Year	Place	Enrollment
1998 July	Erzurum Sugar Factory	Internship
1999 July	Doyasan Butter Factory	Internship

### MEMBERSHIPS

2006 - Catalysis Society of Turkey

## **FOREIGN LANGUAGES**

Fluent English, Beginner German

## **PROFESSIONAL**

2002- 2008, Research Assistant;  
Middle East Technical University (METU), Department of Chemical Engineering, Ankara, Turkey.

2006 January - August, Visiting Scientist;  
University of Connecticut, Department of Chemical, Materials and Biomolecular Engineering, Storrs, Connecticut, USA, "Preparation of Carbon Supported Platinum and Ruthenium Alloy Catalysts Using Supercritical Fluids".

## **PUBLICATIONS**

### **Refereed Journals:**

1. Bayrakçeken, A., Smirnova, A., Kitkamthorn, U., Aindow, M., Türker, L., Eroğlu, İ., Erkey, C., "Vulcan supported Pt electrocatalysts for PEMFCs by using supercritical carbon dioxide deposition", Chemical Engineering Communications, Article in press.
2. Bayrakçeken, A., Smirnova, A., Kitkamthorn, U., Aindow, M., Türker, L., Eroğlu, İ., Erkey, C., "Pt-based electrocatalysts for polymer electrolyte fuel cells prepared by supercritical deposition technique", Journal of Power Sources 179 (2008) 532-540.
3. Bayrakçeken, A., Erkan, S., Türker, L., Eroğlu, İ., "Effects of membrane electrode assembly components on proton exchange membrane fuel cell performance", International Journal of Hydrogen Energy, 33 (2008) 165-170.
4. Bayrakceken, A., Kitkamthorn, U., Aindow, M., Erkey, C., "Decoration of multi-wall carbon nanotubes with platinum nanoparticles using supercritical deposition with thermodynamic control of metal loading", Scripta Materialia 56 (2007) 101-103.

## National and International Conference Presentations

1. Bayrakçeken, A., Smirnova, A., Kitkamthorn, U., Aindow, M., Türker, L., Eroğlu, İ., Erkey, C., “High Pt loading Pt/Vulcan electrocatalysts for PEMFCs by Using Supercritical Carbon Dioxide technique”, Somer Symposium Series 1, Ankara-Türkiye, May 2007.
2. Bayrakçeken, A., Smirnova, A., Kitkamthorn, U., Aindow, M., Türker, L., Eroğlu, İ., Erkey, C., “Synthesis and Characterization of Pt Based Electrocatalysts by Supercritical Carbon Dioxide Deposition Method”, First National Catalysis Conference, Güzelyurt-Kıbrıs, January 2007.
3. Bayrakçeken, A., Smirnova, A., Kitkamthorn, U., Aindow, M., Türker, L., Eroğlu, İ., Erkey, C., “Preparation and Characterization of Pt-based Electrocatalysts for PEM Fuel Cells by Using Supercritical Carbon Dioxide Deposition”, International Hydrogen Energy Congress and Exhibition, İstanbul-Türkiye, July 2007.
4. Aindow, M., Kang, D., Kitkamthorn, U., Saquing, C.D., Zhang, Y.; Bayrakçeken, A., and Erkey, C. “Transmission Electron Microscopy Studies of Mesoporous Carbon Aerogels and Carbon/Metal Nanocomposites Produced using Supercritical Carbon Dioxide Based Processes”, Brazilian MRS Meeting, Florianopolis-Brazil, October 2006.
5. Eroğlu, İ., Erkan S., Bayrakçeken, A., Türker, L., “Utilization of Metal Phthalocyanines as Cathode Catalysts of Proton Exchange Membrane Fuel Cells”, AIChE Annual Meeting, San Francisco, CA-USA, November-2006.
6. Erkan, S., Bayrakçeken, A., Türker, L., Eroğlu, İ., “Synthesis of Metallophthalocyanines and Their Effects on the Performance of Fuel Cells”, Hydrogen is the Future Workshop, İstanbul-Türkiye, March 2005.
7. Bayrakçeken, A., Erkan, S., Türker, L., Eroğlu, İ., “Development of Membrane Electrode Assembly for Proton Exchange Membrane Fuel Cells”, Hydrogen is the Future Workshop, İstanbul-Türkiye, March 2005.
8. Erkan S., Bayrakçeken, A., Türker, L., Eroğlu, İ., “Utilization of Metallophthalocyanines as Cathode Catalyst of Proton Exchange Membrane Fuel Cells”, International Hydrogen Energy Congress and Exhibition, İstanbul-Türkiye, July 2005.
9. Bayrakçeken, A., Erkan, S., Türker, L., Eroğlu, İ., “Effect of Different Construction Materials on Proton Exchange Membrane Fuel Cell Performance”, International Hydrogen Energy Congress and Exhibition, İstanbul-Türkiye, July 2005.

10. Bayrakçeken, A., Türker, L., Erođlu, İ., “Proton Deđişim Zarlı bir Yakıt Hücresinin Performansı Üzerine Farklı Parametrelerin Etkisi”, Ulusal Kimya Mühendisliđi Kongresi 6, İzmir-Türkiye, September 2004.

#### **AWARDS:**

1. 2<sup>nd</sup> Rank Student Award, Faculty of Engineering, Atatürk University, 2000.
2. 2<sup>nd</sup> Rank Student Award, Department of Chemical Engineering, Atatürk University, 2000.

#### **SUMMER SCHOOLS:**

1. First Anatolian School on Catalysis (ASC-I), September 25 – October 6, 2006, Middle East Technical University, Ankara, Turkey, (Workshop I: *Master class Catalysis*. Workshop II: *Computational Catalysis*).

#### **RESEARCH PROJECTS:**

1. “Platinum and Platinum-Ruthenium based catalysts on various carbon supports prepared by different methods for PEM fuel cell applications”, METU Foundation, Researcher.
2. “Yüksek sıcaklıkta çalışabilen Proton Deđişim Zarlı Yakıt Hücresi geliştirilmesi”, TÜBİTAK, Researcher.
3. “Hidrojen gazı üretimi, depolanması ve yakıt hücrelerinde elektrik elde edilmesi”, DPT-YUUP, Researcher.